WASM: Minerals, Energy and Chemical Engineering

Effects of Water Quality on Rare Earth Phosphate Mineral Flotation

Moonchul Jung

0000−0002−8347−1312

This thesis is presented for the Degree of
Doctor of Philosophy
of
Curtin University

October 2023

Declaration

To the best of my knowledge and belief this thesis contains no material previously published by any other person except where due acknowledgement has been made.

This thesis contains no material which has been accepted for the award of any other degree or diploma in any university.

Signature: Moonchul Jung 

Date: 16.10.2023

Acknowledgement

I would like to express my sincere appreciation to the following individuals and organizations:

- Dr. Bogale Tadesse, whose expertise and guidance proved invaluable throughout my PhD journey.
- Dr. Boris Albijanic, Dr. Richard Alorro, and Dr. Laurence Dyer, who greatly enriched my academic experience through their encouragement.
- The Minerals Research Institute of Western Australia (MRIWA) and Lynas Rare Earths Ltd for their sponsorship and generous technical support.
- The technical staff at the Western Australian School of Mines (WASM), especially Mujesira Vukanic, Lahiru Basnayaka, Bernard Mwango, and Colin Tayler, for their consistent support in the laboratory.
- Dr. Hyongdoo Jang for his support and guidance, both within and beyond the academic realm.
- Dr. Kyoungkeun Yoo, whose invaluable guidance and mentorship played a crucial role in shaping my academic perspective and bringing me to this point in my journey.
- Finally, I extend my wholehearted gratitude to my family and friends for their unwavering support and encouragement throughout this endeavor.

Abstract

Rare earth elements (REEs), consisting of the lanthanide group of 17 elements, along with yttrium and scandium, are essential for a variety of high−tech applications. Their unique properties render REEs indispensable in advanced technologies, including electric vehicles, wind turbines, and military defence system. REE production primarily relies on a few commercially exploited minerals, notably monazite, a major rare earth (RE) phosphate mineral. Flotation, a widely used beneficiation technique, is vital for the beneficiation of RE minerals, particularly those from carbonatite deposits.

Water quality is a critical determinant of flotation efficiency. A recent challenge confronting the mineral processing industry is the limited availability of freshwater. This leads to the consideration of using alternative water sources for the mineral processing operation, especially flotation. Although impure water can hinder flotation efficiency, saline water has been effectively used in some sulfide mineral flotation projects. However, elevated salinity levels are detrimental to RE mineral flotation.

This PhD research aimed to assess the impact of water quality on the flotation efficiency of RE phosphate minerals obtained from a RE mine in Western Australia and to clarify the underlying mechanisms. To understand the primary mechanism of RE ore flotation, the flotation behavior of both valuable and gangue minerals was analyzed under varying conditions, such as solution pH, depressant concentration, and dissolved ions through microflotatation experiments. The study also evaluated the influence of water quality on ore samples, integrating techniques such as bench scale flotation, surface characterization, thermodynamic calculations, zeta potential measurements, and adsorption experiments.

The investigations into the monazite flotation mechanism using an oleate collector in the presence of ions such as Ca^{2+}, Mg^{2+}, Na^{+}, and K^{+} revealed that Ca^{2+} and Mg^{2+} negatively impacted monazite flotation. This was due to the formation of insoluble compounds with these ions, leading to reduced oleate ion adsorption on monazite surfaces and consequently, decreased flotation recovery. On the other hand, Na^{+} and K^{+} exhibited minimal impact on monazite flotation, due to their lack of affinity for oleate ions.

Subsequent studies highlighted the adverse effects of Ca^{2+} and Mg^{2+} on bench scale RE mineral flotation using ore samples. These ions disrupted the selectivity and recovery of RE minerals by interacting with the collector and depressant. The formation of insoluble compounds reduced the available collector concentration, resulting in decreased RE recovery. Notably, Mg^{2+} exhibited a more pronounced negative effect than Ca^{2+}, potentially due to its stronger affinity for the sodium silicate depressant. The introduction of divalent cations also elevated flotation pulp viscosity, likely due to changes in interparticle forces.

The presence of anions, namely Cl^{-}, SO_4^{2-}, and HCO_3^{-}, in the flotation pulp were found to reduce flotation efficiency, affecting the recovery of both RE and FeO minerals. The recovery of FeO gangue minerals increased significantly in their presence, decreasing the separation efficiency between RE and FeO minerals. Among these anions, Cl^{-} had the most substantial negative effect, while HCO_3^{-} had the least. The reduced separation efficiency was attributed to increased flotation pulp viscosity in the presence of these ions, leading to enhanced entrainment of FeO gangue minerals. Changes in the zeta potential of particles due to these ions influenced this viscosity change, a conclusion supported by particle settling experiments and DLVO theory calculations.

Furthermore, the flotation behavior of a primary gangue mineral, goethite, was examined in the presence of Ca^{2+} and Mg^{2+}, which were found to significantly reduce RE mineral recovery. The flotation recovery of goethite decreased with increasing ion concentration, primarily due to their reactions with the sodium oleate collector, as observed in the monazite single mineral flotation study. Notably, Ca^{2+} had a more pronounced negative effect than Mg^{2+}.

In conclusion, this PhD research highlighted the significant adverse effects on RE mineral flotation when water quality was altered by dissolved ions. Divalent cations interacted with flotation reagents, while anions in the flotation pulp altered pulp rheology, both leading to reduced separation efficiency between RE and FeO gangue minerals.

Table of contents

List of figures

List of tables

List of abbreviations

ATR−FTIR	Attenuated total reflection−Fourier transform infrared spectroscopy
CLD	Central lanthanide deposit
DAH	Dodecylamine hydrochloride
DLVO theory	Derjaguin−Landau−Verwey−Overbeek theory
EDL	Electric double layer
HIMS	High intensity magnetic separation
HREE	Heavy rare earth elements
ICP−OES	Inductively coupled plasma − optical emission spectroscopy
L.O.I	Loss of ignition
LIMS	Low intensity magnetic separation
LREE	Light rare earth elements
MIBC	Methyl isobutyl carbinol
NaOL	Sodium oleate
PMA	Particle mineralogical analysis
PZC	Point of zero charge
QEMSCAN	Quantitative evaluation of minerals by scanning
R/S	Rougher/scavenger
RE	Rare earth
REE	Rare earth elements
REO	Rare earth oxide
RPM	Revolutions per minute
S.E.	Separation efficiency
SDS	Sodium dodecyl sulfate
UV−Vis	Ultraviolet − visible
XPS	X-ray photoelectron spectroscopy
XRD	X-ray diffraction
XRF	X-ray fluorescence
ΔG_{HB}	Degree of hydrogen bonding of water structure

K^H	Dissociation constant
β_n	Cumulative stability constant
A_m	Hamaker constant of mineral particles
A_w	Hamaker constant of water (3.7×10^{-20} J) in vacuum
E_{edl}	Electrostatic forces
E_{tot}	Total interaction energy
E_{vdw}	van der Waals forces
N_A	Avogadro constant (6.023×10^{23} /mol)
R_g	Recovery of gangue minerals
R_m	Recovery of RE minerals
Z_i	Valence of the ion i
k_B	Boltzman constant (1.38×10^{-23} J/K)
n_i	Number of ions of type i per unit volume
ε_0	Dielectric constant in vacuum (8.854×10^{-12} C^2/Jm)
ε_r	Dielectric constant of medium (78.5 C^2/Jm)
$\tau_{B\,max}$	Maximum yield stress
τ_B	Yield stress
μ	Pulp viscosity
A	Effective Hamaker constant
C	Molar concentration
e	Elementary electric charge (1.602×10^{-19} C)
f	Parameter related to the shape of the plateau border
g	Gravitational acceleration
H	Distance between two particles
k	Constant for mono disperse spherical particles
K_{sp}	Solubility product
R	Universal gas constant (8.314 J/(molK))
R	Particle size
T	Temperature
x	Unit length of fluid cells
α	Reaction coefficient
γ	Tension of liquid surface
ΔG^θ	Standard gibbs free energy

ζ	Zeta potential
θ_c	Contact angle
ρ	Pulp density
κ	Thickness of electric double layer

Chapter 1. Introduction

1.1 Background

Rare earth elements (REEs) constitute a group of 17 elements that are essential in various high−tech applications due to their unique properties. These elements include the lanthanides, a series of 15 elements from lanthanum (La) to lutetium (Lu), as well as two additional elements, scandium (Sc) and yttrium (Y). Although referred to as rare, the name is somewhat misleading as REEs are not actually scarce in the Earth's crust. They are relatively abundant, with concentrations comparable to common metals such as copper, lead, zinc, and nickel (Gupta and Krishnamurthy, 2005). However, despite their abundance in the Earth's crust, REEs are not often found in concentrated deposits, making their extraction challenging and economically viable deposits relatively rare (Golev et al., 2014; Gupta and Krishnamurthy, 2005; Humphries, 2012). As a result, the global supply of REEs is heavily dependent on a few key producing countries and mines, with China being the dominant producer, accounting for approximately 70% of the world's total production (U.S. Geological Survey, 2023).

The unique properties of REEs make them indispensable in numerous cutting−edge technologies. For instance, neodymium, praseodymium, and dysprosium are crucial components of powerful permanent magnets used in electric vehicles, wind turbines, and various electronic devices. Cerium and lanthanum are employed in automotive catalysts, while europium and terbium are essential for phosphors in energy−efficient lighting and display technologies (Long et al., 2012). The increasing demand for REEs in advanced industries has sparked concerns about supply security and potential geopolitical implications.

Challenges on rare earth (RE) mineral mining and processing industry arise not only from the scarcity of economically viable deposits but also from the difficulty in separating REEs from each other (Gupta and Krishnamurthy, 2005). The similar chemical properties and ionic radii of these elements make their separation a complex and energy−intensive process (Humphries, 2012). As research and technological advancements continue, there is an ongoing effort to explore innovative methods for REE extraction, such as solvent extraction, ion exchange, and bioleaching, to enhance efficiency and minimize environmental impact (Balaram, 2019). Additionally, recycling, and urban mining (recovery of REEs from electronic waste and other

discarded products) have gained attention as potential solutions to supplement primary mining sources and reduce waste (Dang et al., 2021).

Flotation is the most widely used beneficiation technique to separate various types of valuable minerals including RE minerals, exploiting the differences in surface characteristics between minerals. Flotation is particularly vital for the beneficiation of RE minerals derived from carbonatite deposits, which are typically characterized by their fine−grained nature, with particle sizes ranging from 25 to 200 μm (W. Chen et al., 2017). The use of various reagents during flotation is necessary to increase the separation efficiency by enhancing hydrophobicity in the valuable minerals while maintaining the hydrophilicity of the gangue minerals. Flotation of RE minerals have been conducted using various collectors, including hydroxamic acid, phosphoric acid, and fatty acid collectors (Abaka-Wood et al., 2017a, 2018a, 2019; Espiritu et al., 2018a, 2018b; Espiritu and Waters, 2018; Wang et al., 2020a, 2020b; Zhang et al., 2017; Zhang and Honaker, 2018). It has been observed that hydroxamic acid exhibits superior selectivity towards RE minerals, due to the formation of highly stable complexes with RE metal cations on the mineral surface (Espiritu et al., 2018b; Pavez et al., 1996). Fatty acid collectors have gained wide usage in RE mineral flotation due to their affordability and low toxicity (Bulatovic, 2010). Additionally, achieving satisfactory selectivity can be facilitated by using high concentrations of depressants, such as sodium silicate, which effectively suppress oxide and silicate gangue minerals (Houot et al., 1991; Pavez and Peres, 1993; Pradip, 1981).

In recent times, the mineral processing industry has faced a significant challenge regarding the availability of fresh water, particularly in remote areas where water salinity is high (Luukkanen et al., 2022). Given that flotation processes require substantial amounts of water, extensive efforts have been made to reduce freshwater consumption by exploring alternative water sources, including internal process water, bore water, and seawater, either individually or in combination with fresh water (Castro and Laskowski, 2011; Ikumapayi and Rao, 2015; Nowosielska et al., 2023; Ozdemir et al., 2009; Peng and Bradshaw, 2012; Peng and Seaman, 2011; Wang and Peng, 2013). While impure water can adversely impact flotation efficiency due to factors such as salinity, dissolved ions, and microbes, saline water has been successfully utilized in numerous sulfide mineral flotation projects, such as nickel sulfide deposits in Australia and copper sulfide deposits in Las Luces and Sierra Gorda

in Chile (Laskowski and Castro, 2015; Peng and Bradshaw, 2012; Peng and Seaman, 2011). However, the high salinity levels in water significantly hinder RE mineral flotation. A limited number of studies have been conducted to investigate the effect of ionic species on the RE mineral flotation, but many of these studies were focused on the mechanism on the surface of pure single minerals (Cao et al., 2022; Espiritu et al., 2019; Wang et al., 2020a, 2020b; Zhang et al., 2017; Zhang and Honaker, 2018). Therefore, this study focused on investigating the influence of dissolved ions on the flotation of RE phosphate ore to understand possible mechanisms under the complex mineral composition.

1.2 Objectives of study

The main objectives of this study were to investigate the effect of water quality on the RE phosphate mineral flotation efficiency and to understand the underlying mechanisms. To understand the fundamental mechanism of RE ore flotation, the flotation behaviour of valuable and gangue single mineral must be primarily understood. The specific sub−objectives are as follows:

(1) Investigate the flotation behaviour of monazite and goethite single minerals, as a valuable and gangue mineral, respectively.

(2) Evaluate the effect of divalent cations on the flotation of RE ore.

(3) Evaluate the effect of various anions on the flotation of RE ore.

(4) Understand the underlying mechanisms involved by conducting experiments on the collector adsorption, zeta potential measurement, rheology analysis, solution chemistry studies, and thermodynamic calculations.

1.3 Significance of study

The significance of this study lies in the potential cost−saving and environmentally sustainable benefits that it offers to the mining industry. The high expenses associated with water purification for mineral processing operations, especially in removing dissolved ions such as Na^+, K^+, Ca^{2+} and Mg^{2+} through methods such as reverse osmosis, can reach millions of dollars annually for mining companies (Nativ et al.,

2021). Adopting process water with minimal treatment could lead to substantial economic advantages in various mineral processing operations, particularly in techniques such as flotation. Considering that mining, manufacturing, and related industries consume around 20% of Australia's water, the need for efficient water management strategies is evident (Prosser et al., 2011). Moreover, mining operations often share water sources with multiple users, necessitating the reduction of water usage in remote areas with water scarcity to minimize environmental and community impact (Rao and Finch, 1989).

This study aims to contribute to more water−efficient practices, cost−saving, and reduced environmental impact in the mining sector by finding ways to use recycled process water in mineral processing without compromising the value recovered. Although the study was carried out using a RE phosphate mineral from specific mine site, the findings could potentially be applied to numerous mining operations, creating positive ripple effects throughout the industry.

1.4 Thesis overview

This thesis is organized into eight chapters, as outlined in the following sections:

Chapter 1 includes a general introduction, presenting the main−objectives and sub−objectives and the structure of this thesis.

Chapter 2 provides a literature review on RE minerals, froth flotation, and the impact of water quality on the flotation process. It discusses global distribution, major deposits, mineralogy, and flotation principles. Furthermore, the chapter conducts an extensive literature review, investigating how water quality affects the flotation process, considering perspectives related to solution, surface, froth, and rheological aspects.

Chapter 3 presents information about the materials and experimental equipment used in the study, along with detailed descriptions of the experimental procedures.

Chapter 4 (Jung, M., Tadesse, B., Dick, C., Logan, A., Dyer, L., and Albijanic, B., 2022. Influence of Monovalent and Divalent Cations on Monazite Flotation. *Colloids and Surfaces A: Physicochemical and Engineering Aspects* 653: 129975) investigates

the effect of divalent and monovalent cations on the monazite flotation using sodium oleate collector and sodium silicate depressant.

Chapter 5 (Jung, M., Tadesse, B., Dick, C., Logan, A., Dyer, L., Albijanic, B., 2022. Understanding the role of water quality in separation of rare earth minerals from iron oxide minerals in a flotation circuit. *Minerals Engineering*, 205, 108461) discusses the effect of cations dissolved in the flotation pulp on the flotation performance of the RE ore. Moreover, the detailed mechanism about the chemical interactions between flotation reagents and dissolved cations was suggested through the measurement of dissolved collector ions in the flotation pulp and the solution chemistry studies.

Chapter 6 (Jung, M., Tadesse, B., Dick, C., Logan, A., Dyer, L., Albijanic, B., 2023. Rheological properties of rare earth minerals flotation pulp in the presence of anions. *Journal of Rare Earths*, In press. https://doi.org/10.1016/j.jre.2023.10.006) describes the flotation behaviour of RE ore samples in the presence of various anions such as Cl^-, SO_4^{2-} and HCO_3^-, which are common constituents in the impure waters.

Chapter 7 discusses the effect of dissolved cations such as Ca^{2+} and Mg^{2+} on flotation behaviour of major gangue minerals in the RE phosphate ore sample.

Chapter 8 concludes the study, summarizing key findings and their significance. Furthermore, it offers suggestions for future research on flotation for RE phosphate minerals, particularly in the context of using impure water sources.

Chapter 2. Literature review

2.1 Introduction

Chapter 2 provides a brief overview of REEs and RE minerals, covering their types, applications, and occurrences. It also explores the principles of froth flotation, discussing its theories, reagents, and equipment. Moreover, this chapter emphasizes the significance of water quality in RE mineral flotation. It provides a literature review on factors that can be influenced by water quality, which in turn can impact flotation performance through changes in solution, mineral surface, rheological, and froth properties.

2.2 Rare earth elements and minerals

2.2.1 Rare earth elements and its applications

REEs denote a group of 17 elements, including lanthanides ranging from lanthanum (La, atomic number 57) to lutetium (Lu, atomic number 71), as well as scandium (Sc, atomic number 21) and yttrium (Y, atomic number 39). These elements are categorized into two groups based on the presence of paired or unpaired electrons within their 4f subshell, giving rise to the distinction between light rare earth elements (LREEs) and heavy rare earth elements (HREEs) (Gupta and Krishnamurthy, 2005). The LREEs consist of lanthanum to europium, while the HREEs encompass gadolinium to lutetium and yttrium. Yttrium, due to its similar atomic size and chemical characteristics, is included within the HREE group. In contrast, scandium does not possess the required chemical similarities to be classified within either the LREE or HREE groups (Gupta and Krishnamurthy, 2005).

The proportion of REE in the Earth's crust is not as rare as the name suggests. The abundance of REEs in the Earth's crust is higher than precious metals such as gold (5×10^{-7} wt.%) and silver (1×10^{-5} wt.%), and they are present in comparable amounts to elements such as copper, lead, zinc, and nickel (Golev et al., 2014; Haxel et al., 2002). Figure 2−1 illustrates the relative abundance of lanthanide elements in the Earth crust, showing significant variations in the storage of individual REEs, even within the group of REE. However, REEs do not exist in pure form in nature but are dispersed in various minerals. The scarcity of commercially viable minerals containing REEs has led to dependence on a few large−scale mines for their supply, making REEs even

rarer (Humphries, 2012). Furthermore, REEs have similar ionic radii, which makes their separation challenging within mineral lattices (Gupta and Krishnamurthy, 2005).

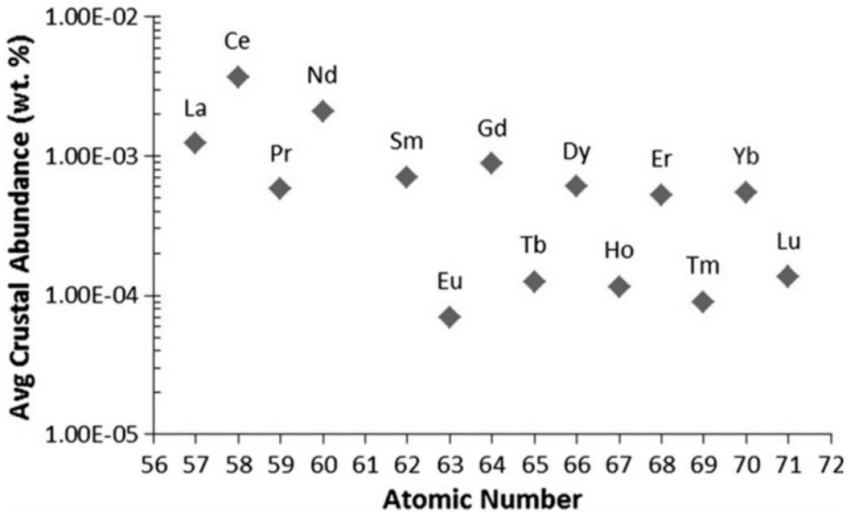

Figure 2−1. Crustal abundance of lanthanide group elements (Jordens et al., 2013; Trifonov, 1963).

Due to advancements in cutting−edge technologies, the demand for REEs has been increasing across various industrial sectors. REEs are considered indispensable in advanced industries due to their unique properties. Industries utilizing REEs include permanent magnets, batteries, metal alloys, petroleum refining, automotive catalysts, ceramics, and display technologies. Table 2−1 presents the types of REE elements used in each industry and their respective proportions within the overall REE consumption (Long et al., 2012). As shown in Table 2−1, a significant portion of the total REE demand is concentrated in LREEs, except for the phosphors and ceramics industry. According to (Alonso et al., 2012), over 80% of the total REE demand in 2007 was attributed to LREEs.

Table 2−1. Application of rare earth elements and its requirement on each industry (Long et al., 2012).

Applications	La	Ce	Pr	Nd	Sm	Eu	Gd	Tb	Dy	Y
Magnets			23.4	69.4			2.0	0.2	5.0	
Battery alloys	50.0	33.4	3.3	10.0	3.3					
Metal alloys	26.0	52.0	5.5	16.5						
Auto catalysts	5.0	90.0	2.0	3.0						
Petroleum refining	90.0	10.0								
Polishing compounds	31.5	65.0	3.5							
Glass additives	24.0	66.0	2.0	3.0						2.0
Phosphors	8.5	11.0				4.9	1.8	4.6		69.2
Ceramics	17.0	12.0	6.0	12.0						53.0

(Unit. %)

2.2.2 Rare earth minerals

Over 250 minerals containing REEs have been identified, encompassing various types such as oxides, halides, carbonates, silicates, and phosphates (Bulatovic, 2010). These REE bearing minerals are typically categorized into those rich in either light or heavy REEs. Table 2−2 provides a list of minerals containing both light and heavy REEs, along with their corresponding chemical formulas (Haque et al., 2014; Jordens et al., 2013). Despite their abundance, most REE−bearing minerals have low concentrations, ranging from 10 to 300 parts per million (ppm), which poses challenges in economically extracting them. Currently, the commercially viable minerals for REE recovery are limited to bastnäsite, monazite, xenotime, and ion−adsorption clay (Ito et al., 1991; Jordens et al., 2013).

Table 2−2. Rare earth minerals and its chemical composition.

LREE		
Type	Name	Chemical Formula
Halide	Fluocerite	$(Ce,La)F_3$
Silicate	Allanite	$(Ce,Ca,Y,La)_2(Al,Fe^{+3})_3(SiO_4)_3(OH)$
	Stillwellite	$(Ce,La,Ca)BSiO_5$
Carbonate	Bastnaesite	$(REE)CO_3F$
	Ancylite	$Sr(Ce,La)(CO_3)_2(OH)\cdot H_2O$
	Parasite	$Ca(Nd,Ce,La)_2(CO_3)_3F_2$
	Lanthanite	$(Ce,Nd,La)_2(CO_3)_3\bullet 8(H_2O)$
Oxide	Loparite	$(Ce,Na,Ca)_2(Ti,Nb)_2O_6$
	Cerianite	$(Ce^{4+},Th)O_2$
Phosphate	Monazite	$(Ce,La,Nd,Th)PO_4$
		$(Nd,La,Ce)PO_4$
		$(Sm,Gd,Ce,Th)PO_4$
	Chevkinite	$(Ce,Ca,Th)_4(Fe,Mn)_2(Ti,Fe)_3[Si_2O_7]_2O_8$
	Britholite	$(Ce,Ca)_5(SiO_4)_3OH$
HREE		
Type	Name	Chemical Formula
Silicate	Yttrialite	$Y_2Si_2O_7$
Oxide	Gadolinite	$Y_2Fe^{2+}Be_2Si_2O_{10}$
	Samarskite	$YFe^{3+}Nb_2O_8$
	Euxenite	$(Y,Ca,Ce,U,Th)(Nb,Ta,Ti)_2O_6$
	Fergusonite	$(Ce,La,Nd)NbO_4$
	Yttrotantalite	$(Y,U^{4+},Fe^{2+})(Ta,Nb)(O,OH)_4$
	Yttrotungstite	$YW_2O_6(OH)_3$
Phosphate	Xenotime	YPO_4

2.2.2.1 Bastnaesite

Bastnäsite is a fluoro−carbonate mineral with the chemical formula $(Ce,La)CO_3F$, which predominantly contains REEs such as cerium and lanthanum. It typically has a high rare earth oxide (REO) content, accounting for approximately 70% of its composition. The formation of bastnäsite has been reported to occur in various deposit

types, including vein deposits, contact metamorphic deposits, pegmatite deposits, and carbonatite deposits (Gupta and Krishnamurthy, 2005). The primary source of bastnäsite is the Bayan Obo mine in China, which accounts for a significant portion of global RE production. Another major mine, the Mountain Pass mine in the United States, is a prominent carbonatite deposit that predominantly yields bastnäsite as the primary RE mineral (Kanazawa and Kamitani, 2006). Froth flotation is an essential process in bastnäsite ore beneficiation, and it is employed in most large−scale mines, including Mountain Pass and Bayan Obo, to obtain the final concentrate through flotation separation.

2.2.2.2 Ion-adsorption clay

Ion−adsorption clay is a major mineral for the recovery of HREEs, along with xenotime. It typically contains a low REO content, ranging from 0.03% to 0.2% (Kanazawa and Kamitani, 2006; Yang et al., 2013). Ion−adsorption clay is formed through the continuous chemical and biological weathering of granite and granite porphyry, which contains a certain amount of REEs (Yang et al., 2013). During the weathering process, the REEs are dissolved and, as the solution moves, they undergo continuous adsorption and concentration on the surfaces of clay minerals. This results in the formation of ion−adsorption clay. This type of clay is exclusively found in certain regions of southern China, including Jiangxi, Guangdong, Fujian, Zhejiang, Hunan, Guangxi, and Yunnan (Yang et al., 2013). In UK, the kaolin deposit “St Austell”, formed by weathering of granite has been also proved as a potential source of RE mineral production (Dehaine et al., 2015; 2019). Although the grade of REEs in ion−adsorption clay is lower compared to major REEs found in ore deposits, it offers the advantage of being amenable to open pit mining, allowing the recovery of REEs without the need for beneficiation processes.

2.2.2.3 Xenotime

Xenotime is a phosphate mineral with the chemical formula YPO_4. It is an important mineral for the recovery of the HREEs. It typically contains approximately 67% total REO content, including yttrium oxide as the main element, as well as small amounts

(~8.4%) of LREE contents such as cerium, lanthanum, praseodymium, and neodymium (Gupta and Krishnamurthy, 2005). Xenotime is formed in various geological settings, ranging from igneous to sedimentary and metamorphic rocks. It is commonly recovered as a byproduct in the beneficiation process of heavy minerals, such as monazite, ilmenite, and gold, which are the major minerals in placer deposits (Chelgani et al., 2015a). Xenotime is reported to be distributed in several regions, including northern Europe (such as Finland and Norway) and Southeast Asia (such as Malaysia, Sri Lanka, and Thailand) (Pradip and Fuerstenau, 1991). It is typically co−recovered with monazite at a ratio of approximately 0.5−5% (Gupta and Krishnamurthy, 2005). The recovery of xenotime is commonly achieved through physical separation processes from placer deposits, with gravitational and other physical methods used for its concentration. However, in cases where physical separation methods are not suitable, flotation is usually employed for the beneficiation of this mineral.

2.2.2.4 Monazite

Monazite is a phosphate mineral with the chemical formula $(Ce,La,Th)PO_4$. It is known for its excellent chemical stability and is primarily found in placer deposits such as beach sands. The total REO content in monazite can vary depending on the region and mineral composition, but it is generally around 70% (Gupta and Krishnamurthy, 2005). It is mainly composed of lanthanum (approximately 40%) and cerium (approximately 30%), along with other REEs (Houot et al., 1991). Monazite also contains thorium (Th), a radioactive material, with a concentration ranging from 4% to 12% (Gupta and Krishnamurthy, 2005). In the past, monazite was mined for the recovery of thorium, but its significance has shifted to being a major mineral for the recovery of REEs due to the increasing demand for these elements (Abaka-Wood et al., 2017b).

In the late 1980s, monazite accounted for 40% of global RE production. However, due to difficulties in waste disposal caused by its radioactive nature and the increased supply of bastnäsite from large−scale RE mines such as Bayan Obo and Mountain Pass, the importance of monazite as a RE raw material decreased (Gupta and Krishnamurthy, 2005). Monazite is primarily recovered as a byproduct in heavy

mineral sands and is typically found alongside minerals such as ilmenite, magnetite, gold, garnet, and quartz. The processing of monazite involves a combination of gravity separation, magnetic separation, and electrostatic separation. However, if the particle size of monazite is small, flotation separation is efficient for its beneficiation (Ferron et al., 1991).

2.2.3 Global distribution and major deposits

RE minerals are widely distributed across approximately 34 countries, as shown in Figure 2−2 (Chen, 2011). The total global reserves of RE minerals are approximately 130 million tons based on the most recent USGS estimates in 2022 (U.S. Geological Survey, 2023). Table 2−3 shows the detailed RE mineral production by countries around the globe (U.S. Geological Survey, 2019; 2020; 2021; 2022; 2023). China dominates these reserves, holding approximately 35% of the global total. Furthermore, countries such as Russia, India, Vietnam, Australia, and Brazil are also significant players in RE mineral reserves and are expected to become major contributors in the future, given their estimated reserves.

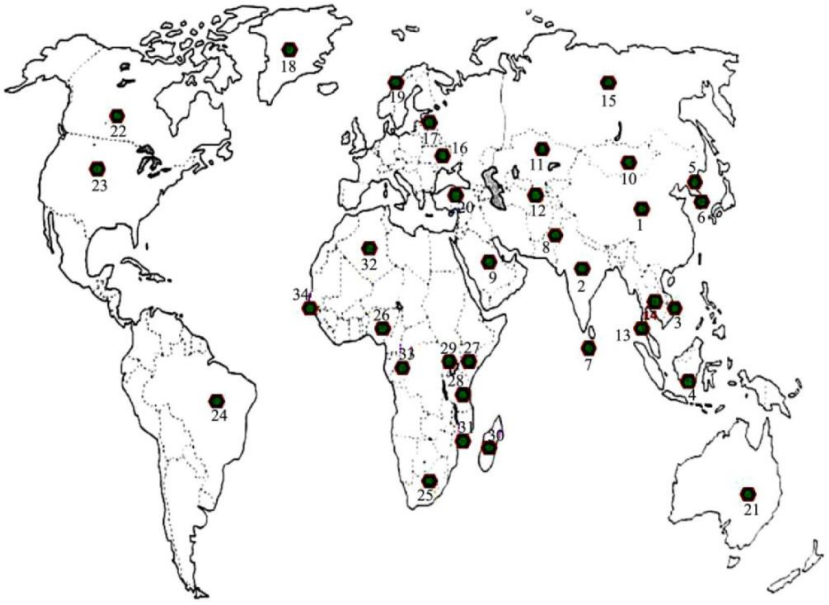

Figure 2−2. Global RE mineral deposits (Chen, 2011).

Unlike the global distribution, the primary production of RE minerals is concentrated in a few countries, namely China, USA, Australia, and Myanmar, as seen in Table 2−3.

According to the report from USGS in 2023, the total mine production of RE minerals in the listed 4 countries take charge of 94% of global production (U.S. Geological Survey, 2023). China is the dominant supplier of RE minerals, contributing significantly to the global supply with about 70% of the total production. The Bayan Obo deposit located in Inner Mongolia, China, stands as the world's largest RE mine and serves as a major source of REEs. While the United States, Australia, and Myanmar are also significant countries in RE mineral production, their output remains relatively smaller compared to China. Both the United States and Australia are notable for their substantial RE reserves and production capabilities, whereas Myanmar is believed to possess promising RE mineral resources in its southern regions.

Table 2−3. World mine production of RE minerals (U.S. Geological Survey, 2023, 2022, 2021, 2020, 2019).

	Mine production (ton)					Reserves (ton)
	2018	2019	2020	2021	2022	
United States	18,000	28,000	39,000	42,000	43,000	2,300,000
Australia	21,000	20,000	21,000	24,000	18,000	4,200,000
Brazil	1,100	710	600	500	80	21,000,000
Myanmar	19,000	25,000	31,000	35,000	12,000	NA
Burundi	630	200	300	200		NA
Canada						830,000
China	120,000	132,000	140,000	168,000	210,000	44,000,000
Greenland						1,500,000
India	2,900	2,900	2,900	2,900	2,900	6,900,000
Madagascar	2,000	4,000	2,800	6,800	960	NA
Russia	2,700	2,700	2,700	2,600	2,600	21,000,000
South Africa						790,000
Tanzania						890,000
Thailand	1,000	1,900	3,600	8,200	7,100	NA
Vietnam	920	1,300	700	400	4,300	22,000,000
Other countries	60	66		60	80	280,000
World total	190,000	220,000	240,000	290,000	300,000	130,000,000

2.2.3.1 Bayan Obo

The Bayan Obo deposit, the largest REE deposit globally, is a critical hub for global REE supply. Situated in Inner Mongolia, China, the Bayan Obo deposit stretches about 18 km east to west and varies in width from 0.5 to 5 km (Shimazaki et al., 2008). It has several orebodies, with the East and Main orebodies being predominant for Nb−REE−Fe. The ores are categorized into three main types based on mineralization, and the deposit contains over 190 different mineral species (Fan et al., 2016). In the past few years, Bayan Obo has contributed to over half of annual REEs production in China (Bai et al., 2022).

The mineralogical diversity of Bayan Obo is a distinctive feature. The primary REE bearing minerals found here are bastnaesite and monazite. This deposit also contains significant amounts of magnetite, dolomite, and fluorite (Sun et al., 2013). Additionally, it is enriched with niobium, thorium, and fluorine, which contribute to the complexity of its mineralogical assemblage (Voncken, 2015). Notably, the distribution of REEs in Bayan Obo shows a clear preference for LREEs over HREEs, which distinguishes it from many other REE deposits (Fan et al., 2016; Zhan et al., 2023).

The processing of Bayan Obo ores combines magnetic separation with froth flotation. Both low intensity magnetic separation (LIMS) and high intensity magnetic separation (HIMS) methods extract magnetite and haematite from the raw materials. Following that, RE minerals and fluorite are obtained through the multi−stage flotation processes (Cheng et al., 2023).

2.2.3.2 Mount Pass

Mountain Pass is characterized predominantly by a carbonatite hosted ore body rich in bastnaesite with a grade of 7.7% REO (Gupta and Krishnamurthy, 2005). The ore is composed of 60% carbonates (mainly calcite), 20% barite/celestite, 10% RE fluocarbonates (bastnaesite), and the remaining 10% consists of other minerals, such as silica (Pradip and Fuerstenau, 2013). Mountain Pass mining, once the world's leading REE producer since the 1950s, stopped operations in 2022 due to low REE prices (Mariano and Mariano, 2012). With a surge in REE demand, Mountain Pass

resumed production and achieved an output of 39,000 tons of RE concentrate in 2020 (Zhao et al., 2023).

The concentration of RE minerals such as bastnaesite at Mountain Pass is primarily achieved using flotation to separate them from sparingly soluble gangue minerals. The ore undergoes initial crushing and grinding before being directed to the flotation circuit, which includes six stages of conditioning. The rougher concentrate possesses a grade of 30% REO, and after undergoing four cleaning stages, it yields a final concentrate with a 63% REO grade (Pradip and Fuerstenau, 2013).

2.2.3.3 Mount weld

Mount Weld is recognized as one of the world's most significant RE deposits, renowned for its richest REO grade in the world. Located approximately 250 km northeast of Kalgoorlie in Western Australia, this deposit has gathered considerable attention from both academia and the mining industry due to its vast economic potential.

The distinctive geological setting of the Mount Weld deposit can be attributed to the carbonatite intrusion stretching across three kilometers in diameter as seen Figure 2−3 (Jaireth et al., 2014). The primary deposits are found within the soil/regolith layer, which consistently overlays the entire carbonatite. These deposits appear as superficial lenses and sheets, seldom extending beyond 60 meters beneath the surface (Gupta and Krishnamurthy, 2005). Central to this vast carbonatite is the central lanthanide deposit (CLD), where LREEs are predominantly enriched. The Duncan REE deposit, situated southeast of the CLD, holds a lower−grade relative to the CLD, comprising about 25% of the total REO resource. However, it distinguishes itself by having a larger proportion of the valuable HREE in comparison to the CLD (Jaireth et al., 2014).

The dominant RE minerals in the deposit are secondary REE phosphate minerals, notably monazite. These RE minerals are typically dispersed finely within iron oxide, hydroxide, and oxyhydroxides, including limonite and goethite, which are the primary gangue minerals in this deposit (Cook et al., 2023). Other identified gangue minerals at Mount Weld include calcite, dolomite, barite, magnetite, ilmenite, rutile, and various silicates, among others.

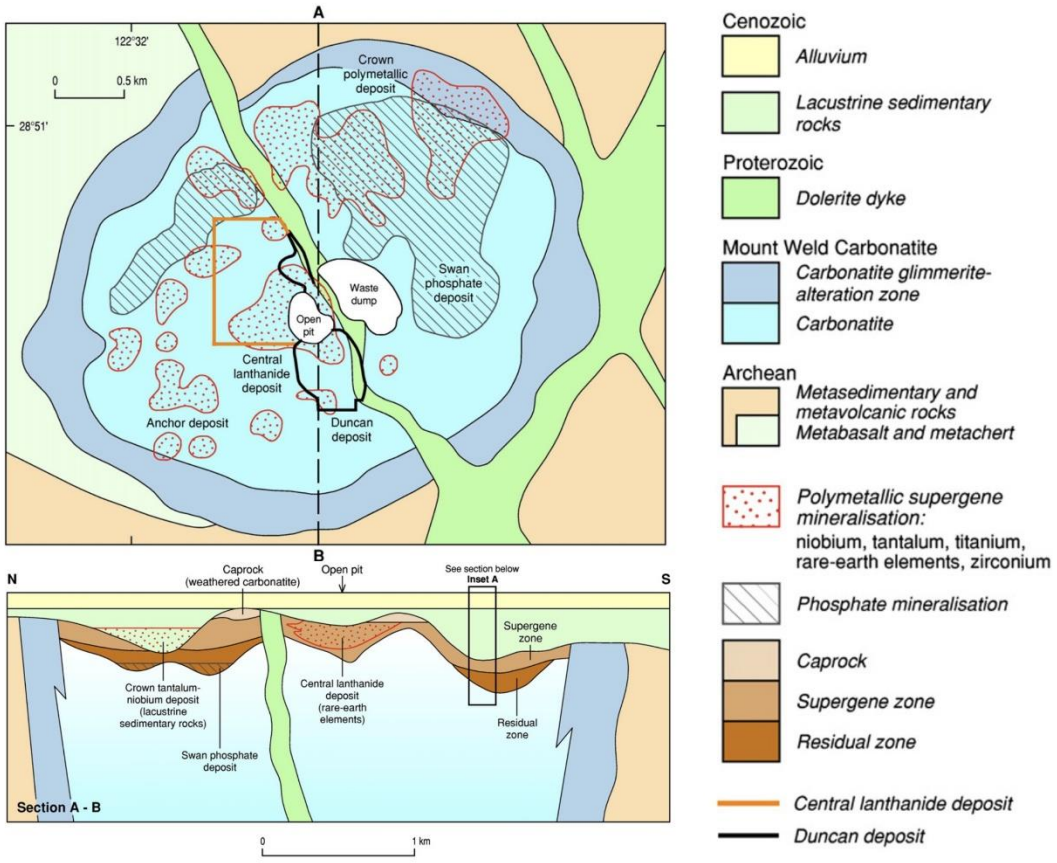

Figure 2−3. Geological layout and cross−section of Mount Weld deposit (Jaireth et al., 2014).

The Mt. Weld deposit is mined through an open−cut mining operation. The primary focus of mining activities is the CLD, which has an average grade of 15% REO (Haque et al., 2014). This positions it as one of the globe's premier high−grade RE deposits. The mine's total REO production capacity was approximately 16,000 tons of REO in 2022 (Lynas, 2022).

2.3 Froth flotation

2.3.1 Principles of froth flotation

Froth flotation is the most widely used beneficiation technique for separating valuable minerals from gangue minerals. This process utilizes the distinct surface properties of mineral particles, namely their hydrophobicity or hydrophilicity. The flotation mechanism comprises essential subprocesses such as bubble−particle collision, attachment, and detachment (Albijanic et al., 2010). Mineral particles with hydrophobic properties, upon colliding with air bubbles, may attach to the air bubbles and rise to the surface of flotation cell. These mineral particles then accumulate in a mineralized froth layer, which is subsequently skimmed off as concentrate as shown in Figure 2−4. In contrast, particles with hydrophilic surfaces tend to remain in flotation pulp because of the lack of affinity for air bubble attachment. After a specified particle collection time, any material remaining in the pulp of the flotation cell proceeds to the tailings of the flotation process.

The wettability of mineral surface, which refers to the degree to which a liquid maintains contact with a solid surface, is an important factor which can determine the hydrophobicity of particles (Rao, 2013). The wettability can be quantitatively described by the contact angle (θ_c), which is the angle formed between a liquid droplet and the solid surface as seen in Figure 2−5. If the contact angle is less than 90°, it means the liquid effectively wets the mineral's surface. Such minerals are described as hydrophilic, meaning they have an affinity for water and do not readily adhere to air bubbles in flotation processes. Conversely, when the contact angle is greater than 90°, the mineral surface repels the liquid, which indicates that the mineral is hydrophobic.

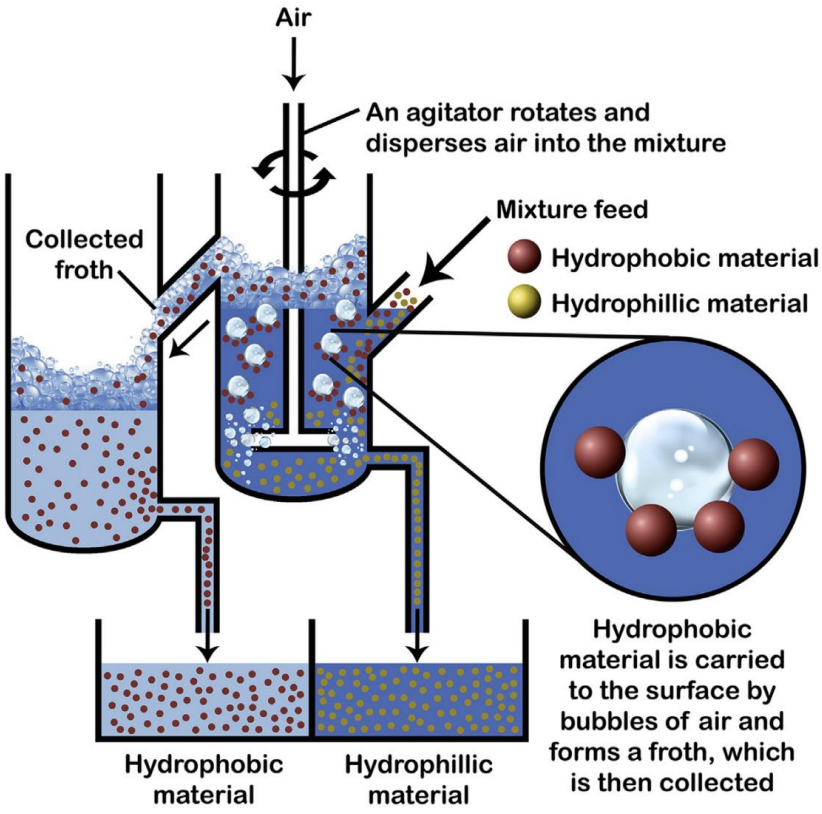

Figure 2−4. Schematic diagram of froth flotation (Crawford and Quinn, 2016).

Numerous studies have extensively explored its underlying mechanism, yet the flotation process remains not completely understood. This is because it takes place in a mixture of three distinct phases (solid−water−air), with numerous underlying subprocesses and interactions (Wills, 1988). Notably, the effectiveness of this flotation process is influenced by several factors. These include the feed particle size, degree of liberation, exposure of the mineral surface, reagent scheme and concentrations, distribution of residence time, and operational parameters such as agitation, impeller speed, and aeration speed (Klimpel, 1984). Therefore, examining the effects of a single factor in isolation becomes challenging, and any slight changes in factors can result in unexpected the outcome.

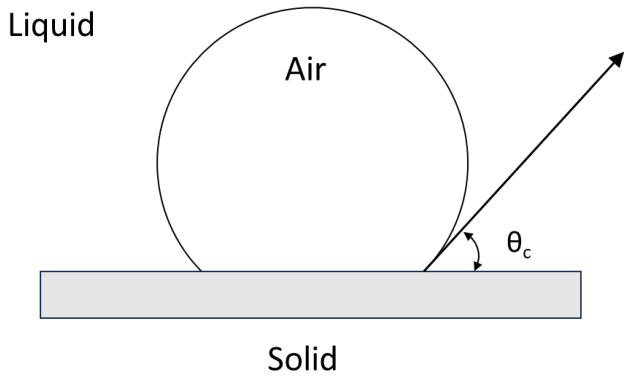

Figure 2−5. Schematic diagram of contact angle in solid−air−liquid phase.

2.3.2 Reagents for rare earth mineral flotation

The introduction of flotation reagents to the pulp is essential for the flotation process. While certain minerals such as sulfide minerals tend to be naturally hydrophobic, reagents are still employed to enhance the separation efficiency between valuable and gangue minerals. In RE mineral froth flotation, a range of reagents is employed to enhance flotation performance. Depending on their role, these reagents can be categorized as collectors, depressants, or modifiers (Wills, 1988).

2.3.2.1 Collectors

A collector is a chemical compound used in the froth flotation process to selectively render the surface of a target mineral hydrophobic, thus facilitating its separation from other minerals present in the ore. The structure of collectors consists of a polar and a non−polar functional group. Generally, the polar head attaches to the mineral surfaces and the non−polar long chain hydrocarbon is exposed to the aqueous phase, thus the attachment of collectors make the mineral surfaces more hydrophobic (Bradshaw et al., 1998).

Flotation studies on the RE minerals have been carried out using different types of collectors such as hydroxamate, phosphoric acid esters, and carboxylate collectors as seen in (Abaka-Wood et al., 2019; Espiritu et al., 2018a; Espiritu and Waters, 2018; Jung et al., 2022; Wang et al., 2020a, 2020b; Zhang et al., 2017; Zhang and Honaker, 2018). Hydroxamic acids and their corresponding salts, often referred to as hydroxamates, are generally regarded as the leading collectors for the flotation of RE minerals such as bastnasite and monazite (Marion et al., 2020). Many studies have

shown that the binding of hydroxamate with metal ions on the mineral lattice involves the substitution of the hydrogen atom within the hydroxyamide part with a metal cation. This binding process is subsequently finalized by forming a ring closure with the oxygen atom found in the carbonyl group (Espiritu et al., 2018b; Pavez et al., 1996).

Phosphoric acid collectors interact with RE mineral surface through chemisorption, such as hydroxamates and carboxylates. The adsorption mechanism of phosphoric acid ester on minerals was suggested that the two hydroxyl groups in the collector molecule forms a bidentate chelate complex with metal cations on the mineral surface (Espiritu et al., 2018a; Gupta and Krishnamurthy, 2005; Stark et al., 2017). Unlike hydroxamates, they are usually less selective toward RE minerals because it shows the high affinity to other gangue minerals as well (Li et al., 2021). This selectivity is explained by the polarity of oxygen atoms in these interactions. Nitrogen in hydroxamates is the most electronegative, followed by carbon in carboxylates, and phosphorous in phosphoric acids. Thus, the oxygen in hydroxamates is less available to interact with metal cations, whereas the oxygen in phosphoric acids is more available, making them typically less selective (Espiritu et al., 2018).

Carboxylate collectors are traditionally employed in the flotation of RE minerals, including not only RE minerals such as bastnasite and monazite but also various oxide minerals and non−sulfide minerals. Their application in RE mineral flotation is well−studied and commonly observed in various industrial processing facilities for these minerals. These collectors have a benefit in use such as low cost and low toxicity due to its origination (Bulatovic, 2010). Carboxylate collectors possess long hydrocarbon chains with a terminal carboxyl group (RCOOH) derived primarily from natural sources. Examples of these naturally occurring fatty acid collectors include oleic acid ($C_{18}H_{34}O_2$), linoleic acid ($C_{18}H_{32}O_2$), stearic acid ($C_{18}H_{36}O_2$) and palmitic acid ($C_{16}H_{32}O_2$), which are typically extracted from animal fats and plant oils. While a single type of acid is typically used for laboratory scale experiments, commercial plants generally utilize a mixture of carboxylic acids known as tall oil fatty acid. Sylfat2 is a renowned commercial fatty acid collector derived from tall oil fatty acid, which consists of predominant amounts of oleic and linoleic acids, with lesser amount of stearic and palmitic acids.

Even though carboxylate collectors have many advantages, the low selectivity is the main challenge of carboxylate collectors because these collectors also tend to easily bind to other gangue minerals such as calcite, dolomite, barite, and quartz (Wills, 1988). Improving low selectivity can be achieved by conditioning or conducting flotation at higher temperatures. This improvement might be attributed to the increased solubility of the fatty acid collector or possibly because the mineral surface becomes cleaner at elevated temperatures (Pradip and Fuerstenau, 1991; Xu et al., 2016).

The adsorption of the collectors can be achieved as either physisorption or chemisorption (Rao, 2013). Physisorption refers to the mechanism by which the collector binds to the mineral surface via forces such as electrostatic interactions or Van der Waals forces (Parfitt and Rochester, 1983). Physisorption is recognized as a less selective process because adsorption can happen whenever there's a matching electrical charge or hydrophobic property, irrespective of the specific traits of the mineral surface. On the other hand, chemisorption involves the collector binding to the mineral surface through chemical bonds, specifically between the collector's functional group and the mineral's lattice ions (Somasundaran and Wang, 2006). The process of chemisorption occurs between the surfactant's polar head group (either cationic or anionic) and the corresponding anionic or cationic sites on the mineral surface. This interaction results in the creation of a novel surface compound through covalent or coordinate bonds. Chemisorption can occur even when the mineral surface and the polar group of the collector share the same electrical charge, despite the presence of electrical repulsion (Cheng et al., 1993).

Carboxylate collectors can adsorb to surfaces through both physisorption and chemisorption mechanisms (Rao, 2013). Physisorption of carboxylate collectors on mineral surfaces has been observed in various studies. (Eileen Ross L. Espiritu et al., 2018; Moudgil and Chanchani, 1985; Pavez et al., 1996; Predali, 1969). Infrared spectral analysis is usually employed to detect physisorption, revealing the C=O spectra on mineral surfaces treated with carboxylate collector at a pH lower than their point of zero charge (PZC) (Espiritu et al., 2018). When the pH is greater than the PZC, carboxylate collector primarily adsorbs through chemisorption. Several studies showed that the chemisorption of oleate occurs between the lattice cation on mineral surface and anionic carboxylic functional group (Fan et al., 2009; Moon and Fuerstenau, 2003; Yu et al., 2015). The solubility product has been employed to

elucidate the adsorption of collectors on mineral surfaces (Taggart and Hassialis, 1946). When there's a low solubility product between the collector and cations on the mineral surface, it suggests that the collector is firmly and stably adsorbed onto the mineral surface (Liu et al., 2019).

The adsorption of oleate ions on the monazite surface have been widely researched. Most studies concur that, in the alkaline pH range, the adsorption mechanism of oleate ions occurs through chemisorption, given that the monazite surface holds a negative charge (Abeidu, 1972; Cheng et al., 1993; Dixit and Biswas, 1969; Pavez and Peres, 1993). This consensus is rooted in the observation that the flotation recovery of monazite typically was maximum within an alkaline pH range. The ionization of carboxylic acids is contingent upon the solution pH, as described in Eq. 2-1 to 2-4, with the solution equilibria of oleic acid illustrated in Figure 2−6. When the pH exceeds 7.6, oleate ions dissociate into various forms including oleate monomer ions, dimers, and acid soap. Cheng et al. (1993) demonstrated that the optimal flotation recovery of monazite occurs at pH 9. This aligns with the concentration of $CeOH^{2+}$ and $LaOH^{2+}$ in the solution, major components of the monazite surface. This alignment implies that the adsorption of the oleate collector on the monazite surface arises from the chemisorption of dissociated oleate ions to lattice cations such as Ce^{3+} and La^{3+} (Cheng et al., 1993).

$$\mathrm{HOL}_{(l)} = \mathrm{HOL}_{(aq)}, \mathrm{pK}_{sp} = 7.6 \quad (2\text{-}1)$$

$$\mathrm{HOL}_{(aq)} = H^+ + OL^-, \mathrm{pK}_{sp} = 4.95 \quad (2\text{-}2)$$

$$2OL^- = (OL)_2^{2-}, \mathrm{pK}_{sp} = -4 \quad (2\text{-}3)$$

$$\mathrm{HOL}_{(aq)} + OL^- = (OL)_2H^-, \mathrm{pK}_{sp} = -4.7 \quad (2\text{-}4)$$

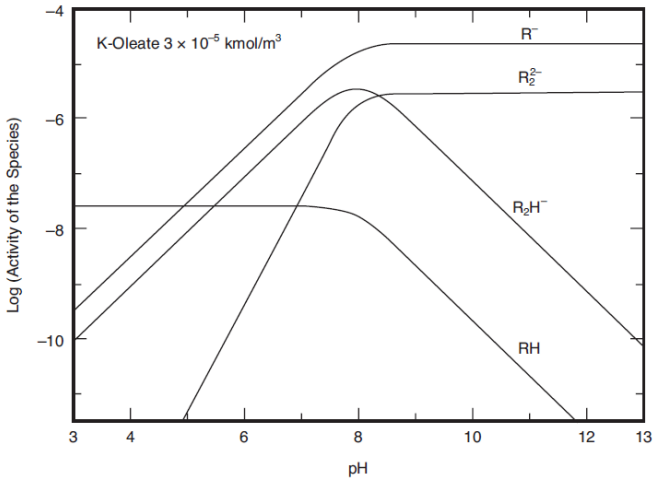

Figure 2−6. The logC−pH diagram for oleate species (Ananthapadmanabhan and Somasundaran, 1988).

2.3.2.2 Frothers

Frother plays a critical role in controlling bubble size and ensuring froth stability (Farrokhpay, 2011; Wills, 1988). At a molecular level, frother is generally heteropolar, surface−active organic compounds, possessing both hydrophilic and hydrophobic parts (Rao, 2013). When introduced to the flotation slurry, the polar parts of frother have an affinity for water, whereas non−polar hydrocarbon parts favor the air phase at the liquid/air interface. Such preferential adsorption causes non−polar groups to stabilize air bubbles, while the polar groups reduce the surface tension of the solution (Bulatovic, 2010)

The consequence of the reduced surface tension is the reduced probability of bubble coalescence; a phenomenon where multiple bubbles merge to form a larger one, ultimately leading to the reduced bubble size. Smaller bubbles tend to rise to the surface more slowly because of reduced buoyancy (Rao, 2013), which improves the probability of bubble−particle collision (Verrelli and Albijanic, 2015; Yoon and Luttrell, 1989).

Froth stability, characterised by the ability of bubbles to resist coalescence and bursting, is important factor to determine the recovery of minerals (Farrokhpay, 2011). Generally, the froth stability can be assessed by measuring the froth volume and lifespan in experiments, considering factors such as reagent dosage, agitation intensity, and the amount of aeration (Wang, 2016). There are various theories to explain the

froth stability using the viscosity of the adsorbed surface film (Oldroyd, 1955; Plateau, 1873), surface tension (Marangoni, 1871), surface elasticity of liquid lamella (Gibbs, 1878), disjoining pressure (Derjaguin, 1955). Despite significant focus over the past century on bubble characteristics, the thin layers separating these bubbles in foams and froths, and the lifespan of froths, there's still no consensus on the factors that determine froth stability (Rao, 2013).

Frother is often categorized into natural compounds, such as pine oil and cresylic acid, and artificial agents such as methyl isobutyl carbinol (MIBC) and polyglycol ethers. The ideal frother should mainly exhibit foaming properties and minimal collecting capabilities, allowing each process to be managed independently (Gupta and Yan, 2016).

2.3.2.3 Modifiers

Modifiers, also known as regulators, play a crucial role in flotation by altering the action of the collector on the mineral surface. Their main function is to either enhance or mitigate the hydrophobic effects applied by collectors on certain mineral surfaces, thereby making the collector action more selective towards specific minerals (Wills, 1988). The function of modifiers can be categorized depending on their purpose of use such as pH modifiers, depressants, Activators (Rao, 2013).

The pH regulators, including Lime (CaO), soda ash (Na_2CO_3), and sulfuric acid, are introduced in the flotation process to adjust the pH of the pulp to optimal conditions for specific reagent−mineral ore interactions (Gupta and Yan, 2016). The pH of the pulp significantly influences the flotation outcomes, determining which minerals rise in the froth and which stay within the pulp. On the other hand, Depressants are chemicals that hinder the attachment of collectors to mineral particles, thereby preventing them from floating (Gupta and Yan, 2016). For example, sodium silicate is widely used to increase selectivity between monazite and gangue minerals by selectively depressing silicate or oxide gangue minerals such as barite, dolomite, goethite, hematite, calcite, quartz and etc (Houot et al., 1991; Pavez and Peres, 1993). In contrast, activators aim to enhance the adsorption of collectors on certain minerals. Abeidu (1972) showed that the activation of monazite was achieved using Na_2S, leading to improved selectivity between monazite and zircon. Sørensen and Lundgaard

(1966) also demonstrated that the addition of $La(NO_3)_3$ enhanced the adsorption of oleic acid collector by enriching the monazite surface with lanthanide ions.

2.3.3 Flotation equipment

Flotation equipment, no matter its scale, can be divided into two primary categories: mechanical and pneumatic cells, with the former being the most commonly used in the industry (Mesa and Brito-Parada, 2019).

2.3.3.1 Mechanical flotation equipment

Mechanical flotation machines are predominantly used, distinguished by a mechanically driven impeller that stirs the slurry and breaks down the incoming air into small bubbles to create a highly turbulent region (Wills, 1988). This turbulence assists in maintaining particles in suspension, producing, and dispersing bubbles, and encouraging bubble−particle interaction (Deglon, 2005). Mechanical cells can be further categorized based on their air injection system into induced−air and forced−air cells (Shen, 2021). Induced−air cells utilize the negative pressure generated by the vortex created through agitation to draw air into the pulp. On the other hand, forced air or supercharged cells receive air from an external and controlled source.

2.3.3.2 Pneumatic flotation equipment

In a pneumatic flotation cell, bubbles are generated by injecting air into the cell at high pressure or velocity (Wills, 1988). The pulp can be introduced separately from the air, as in a flotation column, or injected alongside the air at high pressure, which enhances the contact between bubbles and particles, as seen in the Jameson cell (Mesa and Brito-Parada, 2019). In a flotation column, air is typically injected at the bottom through a sparging system, while pulp is introduced near the top of the column as seen in Figure 2−7. The probability of collisions between bubbles and particles is affected by the distance between the feeding point and the air injection point (Finch, 1995). Therefore, geometry of flotation cell such as the height of the column and the ratio of height to diameter are important factors to affect flotation performance (Yianatos et al., 1988).

The Jameson cell, developed by Mount Isa Mines Ltd and the University of Newcastle in Australia, introduces air by propelling a jet of slurry through a downcomer. This high−pressure jet pulls in air from the atmosphere, and when it impacts with the liquid, it shears the air into fine bubbles. A significant advantage of this cell is its capability to produce clean concentrates in a single stage of operation (Wills, 1988).

A notable distinction of pneumatic flotation cells from mechanical flotation cells is the absence of an impeller in the agitation system, resulting in lower energy and maintenance expenses (Shen, 2021). Furthermore, an essential feature of a flotation column is its incorporation of wash water, which effectively reduces the entrained gangue minerals, yielding high−quality concentrates (Finch and Dobby, 1990).

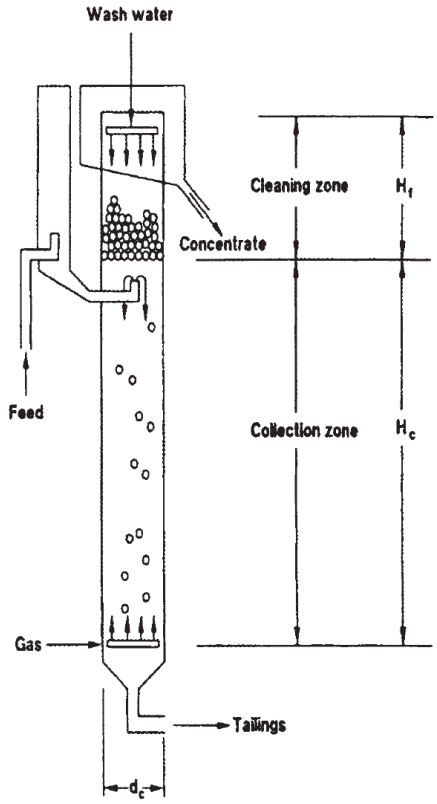

Figure 2−7. Schematic image of flotation column (Rao, 2013).

2.3.3.3 Laboratory scale flotation equipment

· Microflotation cell

The history of small−scale flotation experiments can be traced back to 1944 with the introduction of the Hallimond cell (Hallimond, 1944). This original design featured bubbles of a singular size, limiting the variety in bubble diameters as seen in Figure 2−8(a). Consequently, the absence of varying bubble diameters implies that only certain particles have a chance of colliding and maintaining hydrodynamic stability on the bubble (Drzymala, 1994). To address this shortcoming, a modified version of the Hallimond tube was developed (Rao, 2013). This updated design included distinct features such as a fritted glass disc at the bottom to generate micro sized air bubbles, making it apt for laboratory−scale flotation experiments. Later, in 1971, Partridge and Smith unveiled a small−scale flotation cell as seen in Figure 2−8(b) (Partridge and Smith, 1971). This design, bearing similarities to the Hallimond cell in its foundational principles, allowed for the mixing of flotation slurry using either a mechanical or magnetic stirrer. Utilizing small−scale flotation cells allows for the testing of single mineral or binary mineral systems with minimal amounts (typically 0.5 – 2.0 g). A notable advantage of this approach is that when a single mineral is tested, there's no need for an assay, streamlining the process and saving time (Wills, 1988).

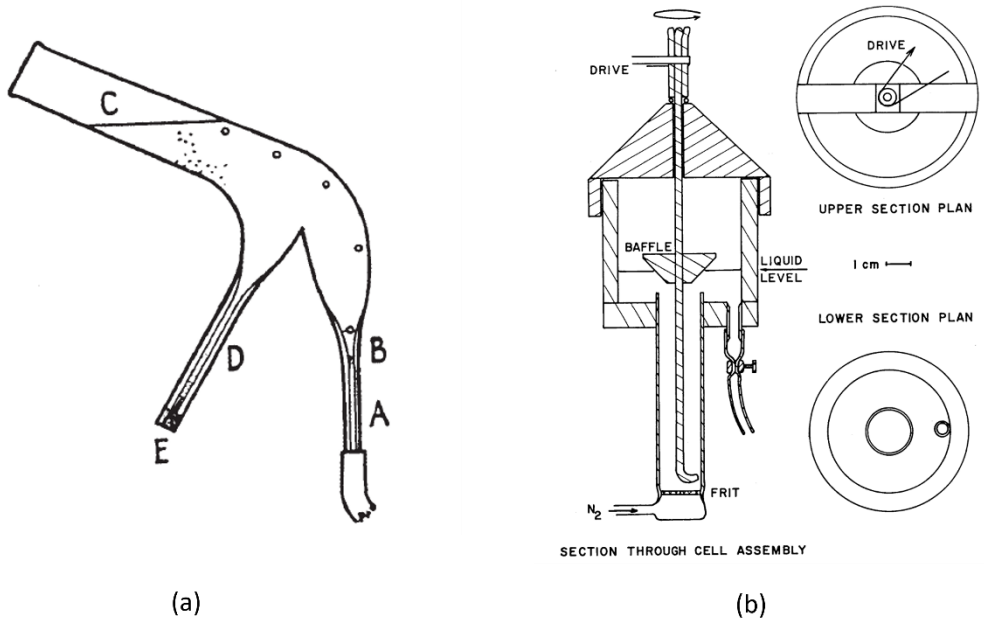

Figure 2−8. Schematic image of (a) Hallimond tube, and (b) Partridge−smith cell.

· Bench scale mechanical flotation cell

The bulk laboratory flotation experiments are performed using bench scale mechanical flotation cells with ore samples of 500 g, 1 kg, or 2 kg (Wills, 1988). These cells operate using mechanical stirring methods, with adjustable rotation rates, closely replicating the design features of their commercial counterparts. The Denver Sub−A type cell is the most widely utilized bench scale mechanical cell. In this cell, air is directed through a hollow tube surrounding a stirring mechanism, which helps move air downward. The air flow and stirrer speed can be adjusted to disperse air into tiny bubbles that float upward through the liquid.

In laboratory flotation machines, the primary goals are to achieve consistent results and to mimic the performance of commercial operations, though these objectives aren't always met (Wills, 1988). Ensuring consistent results in lab tests requires precise control over factors such as impeller speed and air flow rate.

2.4 Influence of water quality on flotation

Securing fresh water for mineral processing plants is becoming increasingly challenging as new mining explorations move to more remote areas due to the depletion of high−grade ore mines. Consequently, water supply costs rise because of the need for long−distance transportation and the development of infrastructure. Furthermore, the mineral processing sector is actively striving to reduce its freshwater consumption in response to challenges such as limited freshwater availability, competition for water resources among various users, community apprehensions, and corporate sustainability initiatives (Liu et al., 2013; Rao and Finch, 1989). Enhancing water efficiency in mineral processing, especially in flotation, primarily focuses on two key approaches: increasing water reuse and utilizing alternative sources to freshwater such as bore water and sea water (Liu et al., 2013).

The quality of water used in flotation can lead to the expected outcomes. Both recycled process water and alternative impure water sources invariably contain various organic or inorganic species which either accumulate during the process or are naturally present in the water source (Muzinda and Schreithofer, 2018). Table 2−4 shows the water quality of impure water derived from different origins. Determining the precise

impacts of impure water, including both recycled and alternative water sources, on flotation quality remains challenging due to a lack of consensus regarding its influence on the process (Ikumapayi and Rao, 2015). Several studies indicate that these impurities can lead to reduced flotation recovery and grade (Broman, 1980; Rao and Finch, 1989), whereas other research observe positive effects from these contaminants (Basilio et al., 1996; Chen et al., 2009; Liu et al., 1993).

An important example of employing impure water in mineral beneficiation is the flotation of sulfide minerals with seawater. The history of the use of sea water in mineral beneficiation dates back to 1930s, where Tocopilla mine in Chile applied the sea water flotation on chalcopyrite (Jeldres et al., 2016). Rey and Raffinot (1966) later noted the successful use of seawater flotation technology in various mills. Pilot tests on Chile's Andacollo deposit, which contains Cu−Mo−Au−Ag ore, showed promising results with sea water using thiocarbamate collector and pine oil frother (Morales, 1975). Recently, various mining operations have incorporated saline waters, including both desalinated and untreated seawater, into their processes as illustrated in Table 2−5 (Philippe et al., 2010). Even though some sulfide ore can be successfully floated using hype saline water containing 60,000 to 80,000 ppm of salts (Quinn et al., 2007; Senior and Thomas, 2005), the use of saline water on the flotation of RE minerals are highly detrimental (Jung et al., 2022).

Table 2−4. Elemental composition of impure water from the different origins (Philippe et al., 2010[1)], Jeldres et al., 2016[2)], Levay et al., 2001[3)], Manono et al., 2019[4)], Senior and Thomas, 2005[5)], Liu and Peng, 2014[6)])

	Composition (mg/L)							
Water type	Mg	Ca	Na	K	HCO_3	S04	Cl	TDS
Raw seawater [1)]	462	1240	11380	228	157	2591	20175	36254
Sea water [2)]	1280	410	10780	390	104	2710	19350	
Desalinated Seawater [1)]	0.6	1.7	75	1.9	1.7	3.8	119	204
Process water [3)]	1820	120	4350	145	176	14418	2087	9,900
Process water [4)]	70	80	153			240	287	1023
Bore water [5)]	3000		20000		75	10000	35000	70000
Bore water [6)]	5100	400	20000	940		23000	32000	

A few studies have investigated the influence of water quality on the flotation of RE minerals such as bastnasite and monazite (Espiritu et al., 2019; Jung et al., 2022; Wang et al., 2020a, 2020b; Zhang et al., 2017; Zhang and Honaker, 2018). The findings reveal that certain ions including Ba^{2+}, F^{-}, Ca^{2+}, and Mg^{2+}, which originate from gangue minerals such as fluorite, barite, calcite, and dolomite, can be detrimental on the flotation recovery of RE minerals. This negative impact arises primarily from the adsorption of hydroxide species of metallic cations such as $Ca(OH)^{+}$, $Ca(OH)_2$, $Mg(OH)^{+}$, and $Mg(OH)_2$ onto RE mineral surfaces, rendering these surfaces more hydrophilic. Additionally, the formation of metallic oleate or metallic hydroxamate precipitates can deplete the concentration of dissolved oleate or hydroxamate species, limiting their availability for mineral surface adsorption. As a result, the flotation of RE minerals is particularly sensitive to the presence of ions such as Ca^{2+} and Mg^{2+}, which are necessarily present in saline water sources. In addition to the aforementioned influence of water quality on RE mineral flotation, there are other potential factors that might induce adverse effects. These include alterations in the charge of the mineral surface, adsorption of dissolved ions on the mineral surfaces, slime coating, and so on (Liu et al., 2013).

Table 2−5. Mining projects using direct saline water and desalinated seawater.

Project	Owner	Country	Water source
Mt Keith	BHP−Billiton	Australia	Saline well
KCGM	Norther Star Resources	Australia	Saline well
Batu Hijau	Newmont	Indonesia	Sea/fresh
Texada	Closed	Canada	Sea
Las Luces	Minera Las Cenizas	Chile	Sea
Michilla	Antofagasta	Chile	Sea
Tocopilla	Closed	Chile	Sea
Escondida	BHP−Billiton	Chile	Reverse Osmosis
Ravensthorpe	BHP−Billiton	Australia	Multiple effect distillation
Mandalong	Centennial Coal	Australia	Reverse Osmosis
Koniambo	Xstrata	New−Caledonia	Reverse Osmosis

2.4.1 Solution properties

2.4.1.1 Reaction with flotation reagents

Dissolved ions in impure water can interact with flotation reagents by leading to the bulk precipitation within the flotation pulp. The occurrence of bulk precipitation can yield unexpected outcomes during flotation operations due to the consumption of flotation reagents such as collectors and modifiers. The primary issue often reported is the consumption of collectors, which leads to a decrease in flotation recovery. Specifically, the ions Ca^{2+} and Mg^{2+} are frequently cited for creating insoluble precipitates with various collectors. Collectors such as fatty acids readily react with these ions to form insoluble precipitates such as Ca−oleate or Mg−oleate, owing to the extremely low solubility product of Ca−oleate or Mg−oleate (Jung et al., 2022; Somasundaran et al., 1991). Several studies have reported a decrease in the recovery of RE minerals in the presence of calcium and magnesium ions, which was due to the depletion of collector concentration (Espiritu et al., 2019; Wang et al., 2020a).

The formation of calcium oleate sometime have positive impact on the flotation recovery of minerals. Wang et al. (2019) found that the flotation recovery of powellite improved when both Ca^{2+} and oleate collector were present, compared to when only the oleate collector was used. This improvement was attributed to enhanced collector adsorption, driven by the hydrophobic interaction between the oleate hydrocarbon chain and the calcium dioleate compound.

Hydroxamate collectors can also form precipitate depending on the solution pH with various metallic cation, which may dissolve from the ore during the processing (Agrawal, 1980). Lenormand et al. (1979) showed that the recovery of malachite was lower at pH 6 due to the precipitate of hydroxamate collector with Cu^{2+} dissolved from malachite. Marion et al. (2017) explained that the decrease in malachite recovery at higher temperatures was due to an increase in copper dissolution. This elevated dissolution led to greater consumption of the collector as more Cu−hydroxamate precipitate was formed. Zhang et al. (2017) reported that when the dosages of Ca^{2+} and hydroxamic acid were increased, bulk precipitation of hydroxamic acid occurred. Similarly, sulfide xanthate collectors can also react with a variety of metal ions, leading to the formation of metal xanthate precipitates such as cupric xanthate or lead xanthate (Poling and Leja, 1963; Rao, 2013; Wang, 2016).

Not only do collectors react with dissolved ions present in impure water, but modifiers also interact with them, potentially affecting the flotation process. Tannin is frequently employed as a depressant in flotation. It also forms colored precipitates when interacting with ions such as calcium, iron, and lead (Somasundaran and Wang, 2006).

2.4.1.2 Water structure

Water is a highly organized liquid because of its intricate network of hydrogen bonds (Frank and Wen, 1957). When electrolytes are dissolved in water, they dissociate into ions, which are then surrounded by water molecules due to the dipolar nature of water molecule (Marcus, 2009). This rearrangement of water molecules disturbs water structure surrounding the ions, differing from the bulk water structure. Frank and Wen (1957) introduced a simplified model of water structure modified by ions, comprising three distinct regions as illustrated in Figure 2−9. The innermost region (region A) is characterized by immobilization, where water molecules are tightly bound to the ion. The following region (region B) has a water structure that is less ice−like compared to the normal structure of water. In the outermost region (region C), the water retains its normal structure in a typical manner.

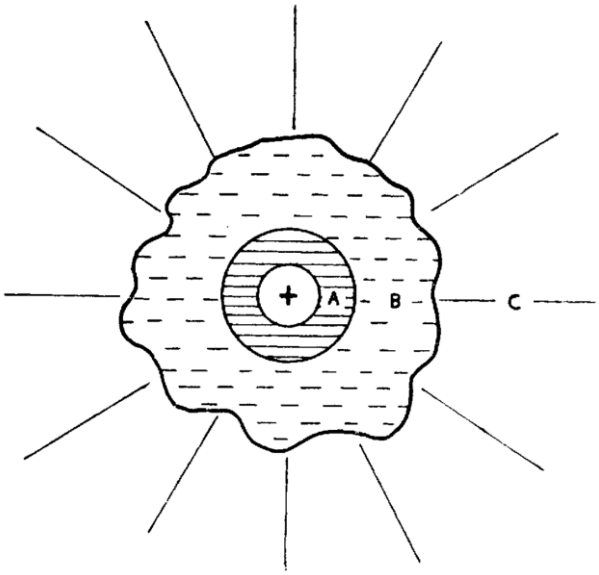

Figure 2−9. A schematic model of water structure modified by an ion. A. immobilization region, B. Structure breaking region, C. Bulk water structure region.

The phenomenon of structure−breaking is believed to arise from an approximate balance in a particular region (region B) where two opposing forces are exerted on each water molecule (Gurney, 1953). One of these forces is the typical structural alignment caused by neighboring water molecules, promoting a regular arrangement. The other force is caused by the ionic field surrounding the ions, which aims to re−orient the water molecules in a different manner. In this region (region B), these two forces are in competition, and as a result, the typical orderly arrangement of water molecules is disrupted, leading to what's termed as structure breaking.

The concept of structure making and structure breaking by ions in relation to their effects on water structure are widely recognized and utilized to explain various behaviors observed in electrolyte solutions (Marcus, 2009). The extensive discussion, development, and review on this topic have been conducted by (Ben-Naim, 1974; Frank and Evans, 1945; Franks, 1979; Wilhelm et al., 1977). Generally, it is understood that certain ions enhance the fluidity of water and are typically categorized as structure breaking ions. These are large inorganic ions, such as Cs^+ and I^-. On the other hand, small inorganic ions such as Li^+, Mg^{2+}, F^-, and Cl^- lead to an increase in the solution viscosity, and these ions are referred to as structure making ions (Hancer et al., 2001). Marcus (2009) suggested a classification of water structure making, breaking ions, and borderline ions as seen in Table 2−6. This classification was based on the calculation of a geometrical factor (ΔG_{HB}), which describes the degree of hydrogen bonding of water structure. It is important to note that the impact of water structure alteration, either making or breaking, is contingent upon the pairing of ions between cations and anions. For example, according to Table 2−6, Cl^- is categorized as a structure-breaking ion. Nevertheless, in the presence of Na^+ ions, Cl^- functions as a structure maker, whereas it acts as a structure breaker in conjunction with K^+ ions (Hancer et al., 2001).

The alteration in water structure can influence the interaction of collectors at the interface surrounding the mineral particles in froth flotation as illustrated in Figure 2−10. Hancer et al. (2001) suggested that when a collector adsorbs at the salt interface, it either displaces interfacial water or penetrates through the water structure. If the water structure is tightly hydrogen bonded due to the presence of structure making anions and cations, it will be challenging for collector molecules to reach the surface and be adsorbed. Conversely, if those ions tend to disrupt the water structure, creating

a favorable condition for collector molecule adsorption, the flotation of soluble salt minerals will become feasible.

Table 2−6. Classification of ions affecting the structure of water (Marcus, 2009).

Ions	ΔG_{HB}
Structure breaking ions	
I^-, I_3^-, ClO_4^-, BrO_4^-, IO_4^-, MnO_4^-, TcO_4^-, ReO_4^-, $AuCl_4^-$, $Ag(CN)_2^-$, $Au(CN)_2^-$, $S_2O_8^{2-}$, $S_4O_6^{2-}$, $Cr_2O_7^{2-}$, $PdCl_6^{2-}$, $PtCl_6^{2-}$, $Fe(CN)_6^{3-}$, $Co(CN)_6^{3-}$, $Fe(CN)_6^{4-}$	≤−1.1
Br^-, Br_3^-, SCN^-, BF_4^-, SiF_6^{2-}	−1.1 to −0.9
K^+, Rb^+, Cs^+, Tl^+, Cl^-, SH^-, CN^-, N_3^-, OCN^-, NO_2^-, NO_3^-, ClO_3^-, $Al(OH)_4^-$, S^{2-}, Se^{2-}, $S_2O_6^{2-}$	−0.9 to −0.7
$CH_3NH_3^+$, $(CH_3)_4N^+$, Ra^{2+}, SH^-, HF_2^-, ClO_2^-, BrO_3^-, HCO_2^-, HSO_3^-, HSO_4^-, SeO_4^{2-}, CrO_4^{2-}, $S_2O_3^{2-}$, $S_2O_4^{2-}$, $P_2O_7^{4-}$	−0.7 to −0.4
NH_4^+, $B(OH)_4^-$, SO_4^{2-}, MoO_4^{2-}, WO_4^{2-}, $C_2O_4^{2-}$	−0.4 to −0.1
Borderline ions	
Na^+, Ag^+, $(C_2H5)_4N^+$, Ba^{2+}, Pb^{2+}, F^-, IO_3^-, HCO_3^-, $H_2PO_4^-$	−0.1 to 0.1
Structure making ions	
Li^+, Cu^+, Au^+, $(C_6H_5)_4As^+$, Sr^{2+}, Sn^{2+}, Al^{3+}, Cr^{3+}, Bi^{3+}, OH^-, $CH_3CO_2^-$, $B(C_6H5)_4^-$, CO_3^{2-}, SO_3^{2-}	0.1−0.4
Ca^{2+}, Eu^{2+}, Hg_2^{2+}, Sc^{3+}, Co^{3+}, Tl^{3+}, Pu^{4+}, HPO_4^{2-}	0.4−0.7
$(C_3H_7)_4N^+$, V^{2+}, Cr^{2+}, Mn^{2+}, Cu^{2+}, Cd^{2+}, Sm^{2+}, Yb^{2+}, Gd^{3+}, V^{3+}, Fe^{3+}, Ga^{3+}, Rh^{3+}, U^{3+}, Pu^{3+}, AsO^{43-}	0.7−0.9
Mg^{2+}, Co^{2+}, Ni^{2+}, Zn^{2+}, Y^{3+}, La^{3+} to Eu^{3+}, Tb^{3+} to Lu^{3+}, Th^{4+}, U^{4+}, PO_4^{3-}	0.9−1.1
$(C_4H_9)_4N^+$, Fe^{2+}, UO_2^{2+}	≥1.1

The initial examination of the influence of ions on hydration was carried out through coal flotation studies in 1963 (Klassen and Mokrousov, 1963). The adsorption of ions

on coal particle surfaces results in a lowered electrochemical potential, which in turn diminishes the stability of the adjacent hydration layers, leading to their disruption. Such destabilization of the hydration layers around coal particles enhanced their surface hydrophobicity. In 1970, Laskowski and Iskra (1970) carried out experiments using methylated quartz, discovering that efficient flotation was only achieved when the surface was highly hydrophobic. They also observed a significant increase in the flotation rate with a higher concentration of KCl. This was attributed to a quicker thinning and rupturing of the film between the particle and bubble as the electrolyte levels increased. Blake and Kitchener (1972) also demonstrated that an increase in KCl concentration led to a growing instability in films surrounding hydrophilic silicate and methylated hydrophobic silica surfaces. However, it was noted that films with smaller diameters retained more stability as opposed to those with larger diameters. This finding suggests that a higher ionic strength corresponds to a decrease in film stability. Arnold and Aplan (1986) discovered that coal flotation performed better in tap water compared to distilled water. They proposed that the existence of ions such as Ca^{2+}, Mg^{2+}, Na^{+}, Cl^{-}, and SO_4^{2-}, contributed to the destabilization and significant reduction in thickness of the hydration layer on the surface of the coal particles. Hancer et al. (2001) observed that flotation of soluble minerals could be achieved with either DAH or SDS using salts recognized as structure breakers. On the contrary, for salts acting as structure makers, flotation was not attainable with these collectors. The importance of this observation was further highlighted through measurements of contact angle and surface tension, which provided insights into interfacial water behaviors. Ma and McCall (2012) found that the presence of potassium cations enhanced the recovery rate of kaolinite compared to sodium ions. This was linked to the superior water−structure−breaking capability of potassium cations, which effectively reduced the zeta potential of kaolinite more than sodium, leading to the aggregation of particles.

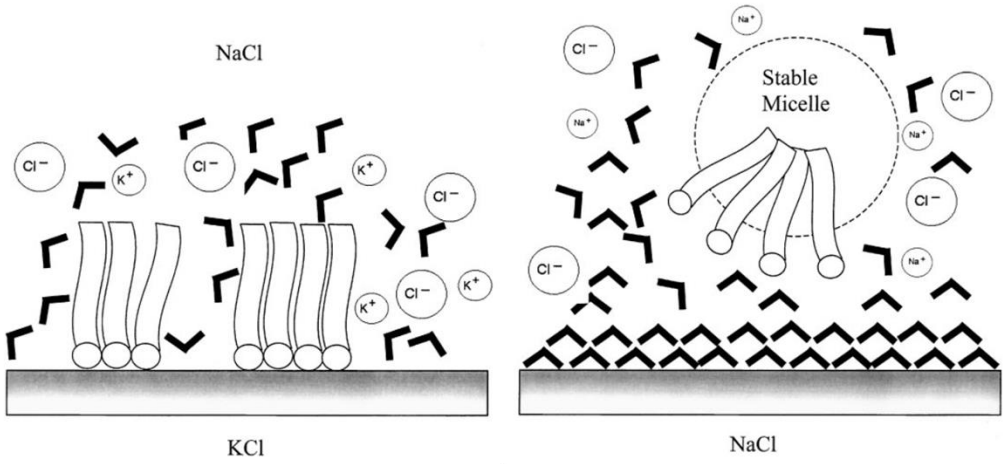

Figure 2−10. Collection adsorption on the salt surface in the presence of structure making (NaCl) and breaking ions (KCl) (Hancer et al., 2001).

2.4.2 Surface properties

2.4.2.1 Electric double layer

The electric double layer (EDL) is a foundational concept in the field of surface chemistry, especially when investigating colloidal systems and interfaces. When a mineral is submerged in an aqueous solution, it leads to the formation of an area with electrical discrepancies at the interface between the solid surface and the bulk solution. In this interface, a surplus charge (positive or negative) appearing to be fixed on the solid surface is accurately offset by a dispersed region of ions carrying equal yet opposite charges, known as counterions. This occurrence is recognized as the electrical double layer.

The EDL consists of two primary layers as seen in Figure 2−11, which is simplified model suggested by (Stern, 1924). The innermost layer, known as the Stern layer, is characterized by ions that are directly adsorbed onto the surface. These ions are relatively immobile. Beyond the Stern layer lies the diffuse layer, a region where ions are more loosely associated, gradually diminishing in concentration as one moves further from the surface. These two layers function collectively, neutralizing the inherent charge of the particle or surface, thereby maintaining electrical neutrality. The zeta potential (ζ) refers to the potential observed just beyond the Stern plane.

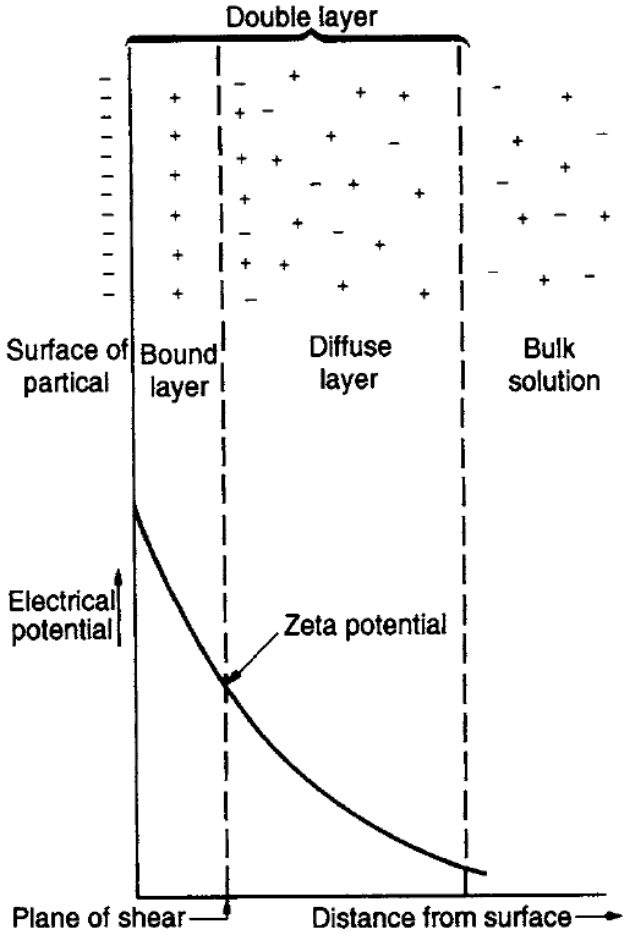

Figure 2−11. Schematic diagram of electrical double layer.

The nature of the zeta potential is not static; it's influenced by factors such as ionic strength and the valency of ions in the solution as seen in Figure 2−12. An increase in ionic strength, for instance, generally compresses the diffuse layer, reducing the repulsive potential between particles. Multivalent ions can have a more pronounced effect on the zeta potential compared to monovalent ions, due to their higher charge density. The depression of the electrical double layer can enhance flotation efficiency for several reasons, one of which is the reduction in repulsion forces between mineral particles and bubbles (Dai et al., 1999; Kurniawan et al., 2011). This decrease in repulsion forces can promote better attachment between particles and bubbles, which is crucial for effective flotation.

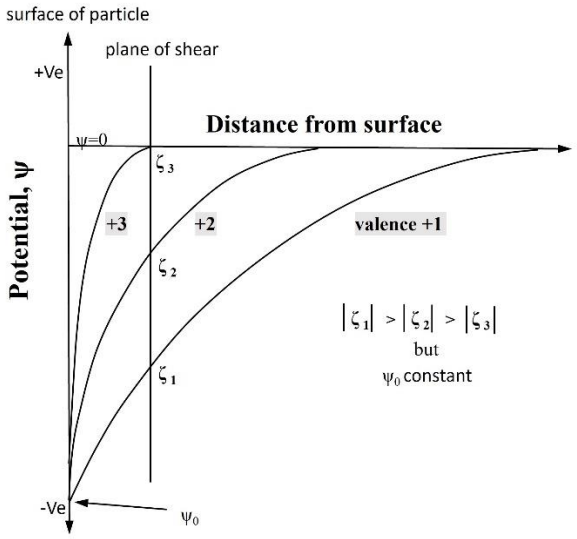

Figure 2−12. Compression of electrical double layer by ions with different valence (Rao, 2013).

The electrical double layer at interfaces significantly influences not only flotation but also various mineral processing operations. The alteration in zeta potential can lead to modifications in the rheology of the flotation pulp, as it affects the interparticle interactions, which are primarily governed by the attraction and repulsion forces between mineral particles. For instance, when the zeta potential of mineral particles decreases, it leads to decreased repulsive interactions between particles (Laskowski, 1970; Laskowski et al., 1991). This weakened repulsion, in turn, promotes the aggregation of particles. As a result, there's a consequent increase in the viscosity of the pulp (Ancey and Jorrot, 2001; Chen et al., 2019; G. Li et al., 2017).

The sign and magnitude of zeta potential significantly influence the adsorption of flotation agents on mineral surfaces. Iwasaki et al., (1960) showed that the adsorption of anionic collectors in goethite recovery was highest within an acidic pH range where the mineral surface had a positive charge, whereas the efficacy of cationic collectors was highest within an alkaline pH range where the goethite particle had a negative charge. Espinosa-Gomez et al. (1987) reported that the zeta potential of pyrochlore decreased due to the adsorption of metallic cationic species, which in turn reduced the flotation recovery. This reduction in recovery was attributed to the decreased adsorption of cationic collector on the mineral surface. In addition, a high surface

charge can hinder the chemisorption of collectors due to the strong electrostatic repulsion between collectors and mineral surface (Shi et al., 2012).

Slime coatings are managed by electrical double layer forces between oppositely charged of mineral particles, a phenomenon known as heterocoagulation (Jeldres et al., 2016; Xu et al., 2003). Zhao and Peng (2014) showed that the decreased electrostatic attraction between kaolinite and chalcopyrite reduced the slime coating of kaolinite on chalcopyrite surface, thus the recovery of chalcopyrite increased.

Flotation kinetics are also directly related to the effect of double layers between bubble and particle (Fuerstenau and Pradip, 2005). Li et al. (2018) demonstrated that in the presence of sodium (Na^+) and potassium (K^+), the zeta potential of molybdenite was reduced due to surface oxidation/leaching. This reduction led to an increase in the electrostatic repulsion forces between the negatively charged bubbles and the molybdenite surface, ultimately resulting in a decline in flotation recovery.

2.4.2.2 Adsorption of ions on mineral surface

The presence of dissolved ions in water can lead to their adsorption onto the mineral surface, potentially impacting the flotation performance. In alkaline pH solutions, metal ions undergo hydrolysis and may precipitate as hydrophilic metal hydroxides, sulfates, or carbonates when their concentrations surpass their respective solubility limits (Fuerstenau et al., 1985; Levay et al., 2001). The adsorption of these metallic hydroxides on mineral surfaces by electrostatic adsorption can create a hydrophilic surface layer, which, in turn, can influence the functionality of collectors (Fornasiero and Ralston, 2006; Rao, 2013).

Calcium and magnesium ions frequently present in impure water sources either due to natural dissolution from their original environment or from the addition of lime (CaO) during processing operations. The flotation recovery of RE minerals can be adversely impacted by the adsorption of Ca or Mg hydroxide. Espiritu et al. (2018b) explained that the decrease in flotation recovery of monazite and bastnaesite was attributed to the adsorption of $Ca(OH)_2$ and $Mg(OH)_2$ through strong covalent bonds, which consequently hindered the adsorption of the hydroxamate collector. Similar outcomes were noted in a study on bastnasite flotation using the oleate collector in the presence of Ca^{2+}, where the adsorption of calcium carbonate and hydroxide compounds

emerged as the primary reason for the reduced flotation recovery of bastnasite (Wang et al., 2020a). Zhang et al. (2017) demonstrated that $CaOH^+$ species adsorbed to the monazite surface via hydrogen bonding and electrostatic attraction, which impact on the collector adsorption. At lower concentrations of Ca^{2+} in the solution, the competitive adsorption between $CaOH^+$ and hydroxamate collector resulted in reduced collector adsorption. However, at higher concentrations of Ca^{2+}, the physically adsorbed $CaOH^+$ provided additional active sites for the collector adsorption, thereby increasing the collector adsorption.

The RE ions dissolved from the surface of RE mineral have been reported to exhibit a strong correlation with flotation performance of RE minerals. Cheng et al. (1993) demonstrated that the distribution of hydroxyl species $Y(OH)^{2+}$ closely matched the adsorption and flotation response of xenotime when using oleate collector. Geneyton et al. (2021) also reported that an increased concentration of La^{3+} resulted in higher adsorption of sodium oleate collector on the synthesized monazite surface. This is because the adsorbed La^{3+} ions act as a bridge between the lattice oxygen ions and oleate collector ions.

The detrimental effects of calcium and magnesium extend to other minerals too. The recovery of sphalerite was observed to decrease in the presence of these ions, resulting from the adsorption of $Ca(OH)_2$ or $Mg(OH)_2$ precipitates via the heterocoagulation process (Lascelles et al., 2003). The reduction in sphalerite recovery was more pronounced with Mg^{2+} as compared to Ca^{2+}, given that the formation of $Mg(OH)_2$ takes place at around pH 9, whereas $Ca(OH)_2$ forms at around pH 12. Ikumapayi et al. (2012) showed that the recovery of galena was reduced when the calcium concentration increased in the process water. This was due to the reduction of negative surface charges by the adsorption of calcium carbonate or sulfate species, consequently inhibiting the adsorption of xanthate on the mineral surfaces. Investigations on the impact of multivalent ions on coal flotation reveal that these electrolytes hinder coal flotation in the pH region where metal hydroxide precipitation occurs (Celik and Somasundaran, 1986; Rao and Finch, 1989).

Other dissolved ions also contribute to the decrease in flotation recovery of minerals. The reduction in sphalerite recovery was observed with the presence of Zn^{2+} in recycled process water, which also slightly inhibits chalcopyrite and pyrite recovery,

yet benefits the recovery of galena (Coetzer et al., 2003). Boulton et al. (2005) also reported that excessive amount of Cu led to the decrease in sphalerite flotation due to the $Cu(OH)_2$ adsorption on the surface.

The adsorption of dissolved ions doesn't invariably lead to adverse effects on flotation recovery. Some dissolved metallic ions, possibly released from the ore during processing, can actually facilitate the adsorption of collectors. The impact of Ca^{2+} on spodumene flotation was examined using a mixture of sodium oleate (NaOL) and dodecyl amine as a collector, resulting in the enhanced recovery of spodumene (Wang and Yu, 2007). Mg^{2+} was found to effectively improve the flotation of spodumene when NaOL was used as a collector (Liu et al., 2015). The activation of quartz when anion collector is used in the presence of Ca^{2+} and Mg^{2+} has been reported by many studies (Filippov et al., 2019; Free and Miller, 1996; Mielczarski et al., 2000; Ren et al., 2018). The activation mechanisms through Ca^{2+} and Mg^{2+} adsorption have been proposed for two possible reasons. Firstly, the adsorbed Ca^{2+} or Mg^{2+} provide additional active sites for collector adsorption (Liu et al., 2015; Ren et al., 2018). Secondly, the surface precipitation of Ca oleate or Mg oleate enhances collector adsorption, consequently leading to improved flotation recovery (Filippov et al., 2019; Free and Miller, 1996; Mielczarski et al., 2000).

2.4.3 Rheological properties

2.4.3.1 Pulp rheology

Rheology is the science studying how fluids deform and flow when subjected to stress (Farrokhpay, 2012). The flow characteristics of a fluid are represented by plotting the shear stress in relation to the applied shear rate to the fluid, which is referred to as rheogram. Figure 2−13 shows the typical fluid types exhibiting Newtonian or non−Newtonian behaviour, with the latter including dilatant, plastic, pseudo−plastic, and Bingham behaviours (Mewis and Wagner, 2012). As illustrated in Figure 2−13, the viscosity remains unchanged across the entire range of shear rates for a Newtonian fluid; on the other hand, for non−Newtonian fluids, the viscosity varies with changes in the shear rate. Two key terms commonly referred to in rheology studies are: yield stress, defined as the point of interception of the flow curve with the shear stress axis

at a zero−shear rate; and viscosity, represented by the slope of the line linking a particular point on the flow curve to the origin (Farrokhpay, 2012).

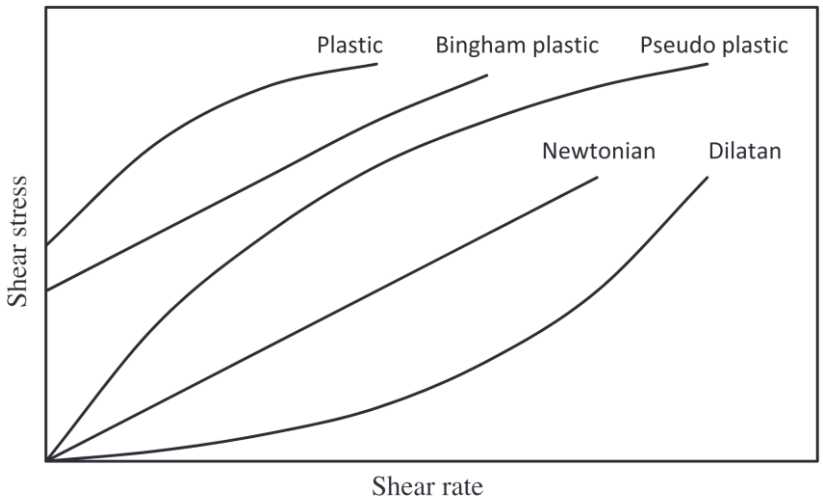

Figure 2−13. Rheogram of different types of fluids.

The rheology of flotation pulp is affected by various factors such as solid particle volume faction, particle size, particle shape, charge of particles, chemistry of suspension medium (Farrokhpay, 2012; Wang and Li, 2020). The apparent pulp viscosity generally increases with the increase in the solid concentration, largely due to the energy dissipation from friction among particles (Behkish et al., 2007; Tadros, 2011). Farrokhpay et al. (2013) reported that the reduction in particle size of gold ore led to a rise in pulp viscosity, especially when the solid concentration was more than 25%. The decrease in particle size could give rise to more intricate rheological characteristics such as shear thickening and aggregation of network structures (Boger, 2009; Chen et al., 2019; Farrokhpay et al., 2013). At the same solid concentration, the level of friction among irregular particles is higher compared to that among spherical particles, thereby exhibiting higher viscosity (Mueller et al., 2010).

The presence of dissolved ions can also alter the rheological properties of flotation pulp. Farrokhpay and Zanin (2012) showed that the viscosity of zinc sulfide ore flotation pulp increased with the presence of dissolved ions such as NaCl, $CaCl_2$, and $AlCl_3$. Similarly, it was observed that the presence of NaCl increased the viscosity of coal flotation pulp, resulting in improved coal flotation (G. Li et al., 2017). Conversely, higher concentrations of NaCl or $BaCl_2$ led to a decrease in viscosity in bentonite clay

mineral slurry (Abu-Jdayil, 2011). Basnayaka et al. (2017) also reported a decrease in the viscosity of bentonite slurry in the presence of Ca^{2+}.

The increase in pulp viscosity in the presence of ions can be attributed to the alteration of electrical double layer surrounding mineral particles, thereby affecting the electrostatic interaction forces between particles. For example, the reduced zeta potential of mineral particles results in a reduction of repulsion forces between particles (Laskowski and Iskra, 1970; Laskowski et al., 1991; G. Li et al., 2017). As a consequence, the decrease in repulsion forces can lead to the increase in particle aggregation via the operation of van der Waals attraction forces, ultimately an elevation in pulp viscosity (Ancey and Jorrot, 2001; Chen et al., 2019; G. Li et al., 2017). Ong et al. (2008) showed that the maximum yield stress of aluminium oxide dispersion was achieved at near PZC where the van der Waals attraction forces are present only while electrostatic repulsion is absent. Friend and Hunter (1971) proposed that a correlation exists between the yield stress and the zeta potential of the particles in suspensions, which are influenced solely by electrostatic and van der Waals forces, as depicted by Eq. 2-5.

$$\tau_B = \tau_{B\,max} - k\zeta^2 \tag{2-5}$$

where τ_B is the yield stress, $\tau_{B\,max}$ is the maximum yield stress achieved at a zeta potential (ζ) of zero, k is a constant for mono disperse spherical particles.

The rheology of flotation pulp exhibits strong relationship with the flotation recovery (Fu et al., 2018; Liu et al., 2018; Patra et al., 2012; Shabalala et al., 2011; Y. Wang et al., 2015). Kirjavainen (1992) showed that the presence of mica particles changes the fluid type of the pulp to Bingham plastic fluid, resulting in the increased entrainment of gangue minerals due to the yield stress. Shabalala et al. (2011) examined the effects of pulp viscosity on gas dispersion in a flotation cell, demonstrating that an increase in pulp viscosity resulted in the formation of smaller bubbles within the impeller zone. Nonetheless, the dispersion of these bubbles was poor, leading to a lower gas holdup. Wang et al. (2015) suggested that a decrease in Cu mineral recovery was noted in the highly viscous flotation pulp due to a reduction in the frequency of bubble–particle collisions and the mobility of bubble–particle aggregates.

2.4.3.2 Entrainment

Entrainment in flotation refers to the mechanical transport of particles by froth without being attached to air bubbles (Rao, 2013). Unlike in true flotation where the attachment of particles to bubbles is due to their hydrophobic properties, entrained particles just fill the spaces between bubbles in the froth column, leading to the recovery of both valuable and undesired minerals through entrainment. Therefore, entrainment is typically considered detrimental to the grade because it leads to the recovery of the more prevalent gangue mineral, thereby reducing the quality of the concentrate (Smith and Warren, 1989).

The entrainments are affected by various factors such as water recovery, solid percentage, particle size, air flow rate, rheological properties of pulp and froth (Wang et al., 2015). Johnson (1972) demonstrated that the recovery of siliceous gangue mineral through entrainment was directly correlated with the recovery of water in the concentrate in pilot and plant scale tests. The size of particles significantly influences the process of entrainment. The probability of particle recovery by entrainment also tends to increase as the particle size decreases. Smith and Warren (1989) explored particle entrainment in flotation and discovered that the recovery through entrainment becomes notable for particles smaller than 30 μm. The reason is probably that fine particles in the pulp phase can be readily suspended in the water or the water film around the bubbles, unlike the coarse particles, giving them a better opportunity to rise through the froth into the concentrate (Wang et al., 2015). The rate of air flow is another factor influencing entrainment. Yianatos et al. (1998) demonstrated that the overall recovery of Cu mineral in column flotation mainly improved due to substantial entrainment beyond the critical superficial air rate.

As discussed in 2.4.3.1, the water quality can alter the rheological properties of flotation pulp due to the dissolved ions leading to the change of zeta potential. The viscosity also contributes to the increased entrainment of hydrophilic gangue mineral particles, making the control of viscosity in flotation pulp of paramount importance (Moudgil, 1993). Fu et al. (2018) highlighted that higher pulp viscosity led to enhanced froth stability, thereby causing significant chlorite entrainment due to slower foam drainage. Similarly, Chen et al. (2017) observed that increased viscosity resulted in reduced copper mineral recovery due to increased entrainment of gangue minerals.

Furthermore, Kirjavainen (1992) demonstrated that elevated yield stress in flotation pulp transformed the pulp into a Bingham plastic fluid, leading to increased gangue mineral entrainment.

2.4.4 Bubble/froth properties

2.4.4.1 Inhibition of bubble coalescence

When two air bubbles move toward one another, they generate a thin liquid film between them under the influence of the capillary pressure, and the thickness of the film gradually decreases due to the liquid drainage (Ata, 2008). As the thickness of thin films decreases, the drainage process decelerates, and the disjoining pressure between the film surfaces starts to impact the drainage of the film (Stubenrauch and Klitzing, 2003; Yaminsky et al., 2010). The stability of the liquid film is governed by the equilibrium between capillary pressure and disjoining pressures. When the time required for the drainage exceeds the contact time of the bubbles, the liquid film is considered stable, preventing coalescence. Conversely, if the drainage occurs more rapidly, the liquid film ruptures at a certain thickness referred to critical thickness. This critical thickness is affected by factors such as the concentration of chemicals, surface contaminants, the speed of approaching bubbles, and gas solubility (Firouzi et al., 2015; Horn et al., 2011; Oolman and Blanch, 1986).

The coalescence of bubbles is highly dependent on the electrolytes in the solution because it can affect the intermolecular forces and rheology around liquid film between bubbles (Firouzi et al., 2015). Marrucci and Nicodemo (1967) conducted measurements of the average bubble size within a bubble column, in the presence of various electrolytes such as KCl, KOH, KNO, KI, K_2SO_4, $CuSO_4$, K_3PO_4, $AlCl_3$, and $Co(NO_3)_2$, across different superficial gas velocities. The results indicated that smaller bubbles were produced as the salt concentration increased, due to the increased electrical repulsive forces on the bubble surface, which in turn inhibited the coalescence between bubbles. The impact of various salts and their concentrations on the coalescence of bubble pairs was investigated (Lessard and Zieminski, 1971). A notable reduction in the coalescence percentage was observed at a specific concentration for each salt, termed as the transition concentration. This transition concentration was discovered to be unique for each salt. Craig et al. (1993) evaluated

how electrolytes influenced the inhibition of bubble coalescence by applying a combining rule based on the characteristics of the cationic/anionic pair. Each anion and cation were assigned a property, either α or β. It was found that the combination of αα or ββ salts inhibits bubble coalescence, while the combinations of αβ or βα salts has no effect on bubble coalescence. This combining rule allows for predictions regarding whether an electrolyte would inhibit the coalescence of gas bubbles in the presence of ions in solution.

Table 2−7. A combining rule of electrolyte on bubble coalescence (Craig et al., 1993).

		β	α	α	α	α	α	α	β	α
	ions	H^+	Mg^{2+}	Na^+	Ca^{2+}	K^+	NH_4^+	Cs^+	Me_4N^+	Li^+
α	OH^-	X	I.S.		I.S.	✓				
α	Cl^-	X	✓	✓	✓	✓	✓		X	✓
α	Br^-	X		✓		✓		✓	U.	
α	NO_3^-	X		✓	✓	✓	✓			✓
β	ClO_3^-	U.	U.	X	U.	I.S.	U.	I.S.	U.	U.
α	SO_4^{2-}	X	✓	✓	I.S.		✓			✓
β	ClO_4^-	✓	X	X	U.	I.S.	X	I.S.	U.	
β	CH_3COO^-	✓	X	X		X	X	X	✓	
α	$Oxalate^{2-}$	X	I.S.	I.S.	I.S.	✓	I.S.	U.	U.	

Combining rules: αα or ββ gives ✓, αβ or βα gives X, I.S. = insufficiently soluble, U. = salt unavailable, addition of salt: prevents coalescence ✓, Has no effect on coalescence X

2.4.4.2 Froth stability

Froth stability refers to the capability of bubbles within the froth to withstand coalescence and bursting (Triffett and Cilliers, 2004). A more stable froth experiences fewer coalescence and bursting events. These factors influence the structure and volume of the froth that is carried over the cell weir into the concentrate launder, and consequently, affect the recovery of both valuable and gangue minerals (Farrokhpay, 2011). Handling an overly stable froth is challenging, whereas an unstable froth is

typically not desirable (Subrahmanyam and Forssberg, 1988). A more stable froth captures a higher quantity of valuable particles attached to the bubbles, but it also tends to recover more gangue minerals, usually due to entrainment (Triffett and Cilliers, 2004). Therefore, achieving the appropriate froth stability is essential.

Froth stability is mainly influenced by the type and concentration of the frother, along with the amount and characteristics of the suspended particles, particularly their hydrophobicity and size (Johansson and Pugh, 1992; Schwarz and Grano, 2005). It was reported that it can be also affected by a various parameter such as pH of pulp, airflow rate, collector conditioning time, specific surface area of particles and solid content (Aktas et al., 2008; Farrokhpay, 2011; Laskowski et al., 2013; Ramos et al., 2013)

Numerous studies have shown that dissolved ions significantly contribute to enhancing froth stability above a certain concentration, termed as the transition concentration. (Farrokhpay and Zanin, 2012; Kurniawan et al., 2011; Peng et al., 2020; Quinn et al., 2007). Quinn et al. (2007) reported that the presence of NaCl and Na_2SO_4 in the flotation pulp increased the gas hold up, leading to the higher froth stability as the gas bubbles provide structural support to the froth. Kurniawan et al. (2011) investigated the effect of $MgCl_2$, NaCl, and $NaClO_3$ on the froth stability in coal flotation. The study showed that the froth stability was enhanced the most in the presence of $MgCl_2$, whereas $NaClO_3$ had the least impact on the froth stability. Corin et al. (2011) carried out a study to examine the impact of ionic strength on the flotation of platinum−bearing ore. It was discovered that a higher ionic strength in the plant water improved froth stability, which in turn led to increased mass pull and water recovery. Farrokhpay and Zanin (2012) evaluated the froth height with the presence of cations such as Al^{3+}, Ca^{2+}, and Na^{+} using zinc sulfide ore. The findings indicated that the maximum froth stability was observed with Al^{3+}, while Na^{+} had the least impact, suggesting a direct correlation between the valence of the cation and froth stability. Peng et al. (2020) demonstrated that the use of seawater resulted in stronger froth ability and stability in molybdenite flotation pulp compared to the use of fresh water. However, no significant difference was observed when only Ca^{2+} or Mg^{2+} was present in the solution, suggesting a negligible role of these ions on the froth stability of seawater.

Several studies have assessed froth stability using seawater and found a decrease in froth stability. Castro et al. (2012) evaluated froth height using a laboratory flotation cell with Cu−Mo ore and discovered that frothability was generally lower in seawater compared to fresh water. Similarly, Ramos et al. (2013) observed that a more stable froth was achieved in fresh water than in seawater, particularly at higher solid percentages exceeding 30%. In a related study, Laskowski et al. (2013) found that the height of the froth layer was reduced in the presence of seawater components such as NaCl, Mg^{2+}, Ca^{2+} and SO_4^{2-} compared to fresh water during Cu−Mo sulfide ore flotation. This was attributed to the surface precipitation of hydroxide particles and the coagulation of particles.

2.5 Chapter summary

In this chapter, the significance of water quality in flotation processes was underscored through a comprehensive literature review. It was pointed out that changes in water quality might produce unexpected outcomes in flotation processes due to alterations in solution, surface, and rheological characteristics of the flotation system. With the growing challenges of freshwater availability and the rising costs associated with water transport, there has been a marked push in mineral processing operations to optimize water use. This has led to the consideration of alternative water sources, including seawater, bore water, and recycled process water, with a particular focus on flotation processes. While the utilization of these alternative water sources has proven effective for sulfide mineral flotation without affecting the grade and recovery, their use in RE mineral flotation has posed difficulties. Several studies have studied the impact of dissolved ions in flotation water on RE mineral flotation, mostly focusing on single or binary mineral systems. Yet, there was an obvious gap in understanding the effects of water quality on the flotation of RE phosphate minerals, which involve a complex mineral system. In this research, the role of water quality in the flotation of RE phosphate minerals was scrutinized. The influence of dissolved ions on both the main valuable mineral and the associated gangue mineral in RE ore was assessed. Building on the findings from individual mineral studies, the flotation of RE ore was analyzed in-depth to demonstrate the effects of water quality on its flotation and to identify the mechanisms by which ions could adversely affect flotation efficacy.

Chapter 3. Materials and methodologies

3.1 Material

3.1.1 Pure minerals

Pure minerals of monazite and goethite were handpicked from a mine in Western Australia for single mineral studies. The XRD analysis showed that the purity of monazite and goethite was 67% and 82%, respectively, as seen in Figure 3−1. It is noted that the composition of the remaining portions of both minerals was identified as an amorphous phase. The chemical compositions of each mineral, analysed using XRF, are shown in Table 3−1. Chemical composition of monazite and goethite. Each sample was ground with a mortar and pestle and then screened to collect −75 +38 μm size fraction for the microflotation, adsorption test and XPS analysis.

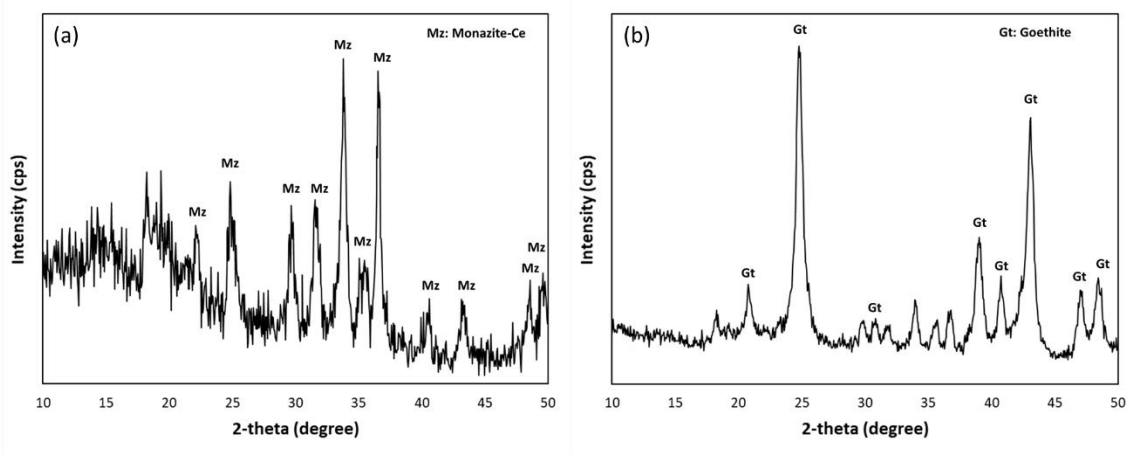

Figure 3−1. XRD spectrum of (a) monazite and (b) goethite sample.

Table 3−1. Chemical composition of monazite and goethite.

Elements (%)	Goethite	Monazite
L.O.I.	14.38	6.20
La_2O_3	1.13	13.20
CeO_2	1.89	25.86
Pr_6O_{11}	0.23	2.81
Nd_2O_3	0.92	10.91
Sm_2O_3	0.14	1.28
Gd_2O_3	0.05	0.47
Y_2O_3	0.06	0.37
Fe_2O_3	56.89	1.27
CaO	0.75	3.04
MgO	0.74	0.04
P_2O_5	4.73	24.84
Al_2O_3	6.24	4.59
MnO	4.65	0.21
SO_3	0.37	1.38
SiO_2	4.75	0.60
SrO	0.31	0.77
ThO_2	0.02	0.24
Nb_2O_5	0.15	0.29
TiO_2	1.04	1.09
ZrO_2	0.11	0.05
ZnO	0.15	0.07
BaO	0.31	0.43
Total	100	100

3.1.2 Ore sample

The RE ore was provided by Lynas Rare earth Ltd in Western Australia. The provided ore was crushed using a cone crusher with a closed side setting of 3 mm (W300−3, Wescone, Australia); the top particle size of the received ore was −5 cm. Table 3−2 shows the elemental composition of the ore characterized by X−ray fluorescence (XRF, Epsilon 3 XLE, Malvern Panalytical, UK). The total REO grade was determined from the XRF results by summing the percentage of CeO_2, La_2O_3, Pr_6O_{11}, Nd_2O_3, Sm_2O_3, Y_2O_3, and Gd_2O_3 (see Table 3−2). Mineralogical composition of feed ore was determined by quantitative evaluation of minerals by scanning electron microscopy (QEMSCAN) as shown in Table 3−3. The most dominant RE minerals in the sample were monazite group mineral, and the most important gangue minerals were iron oxide minerals such as goethite and limonite. The distribution of mineral liberation classes of monazite group mineral after grinding (D80 −38μm) and their images are provided in Figure 3−2. As shown in Figure 3−2(a), the liberation data show varying degrees of liberation for the monazite group minerals. Approximately 75 % of the monazite is classified as either well liberated or high−grade middlings. For composite particles, monazite is mostly associated with Fe−oxides/oxyhydroxides group as shown in Figure 3−2(b) considering that these Fe minerals are major gangue minerals in the ore.

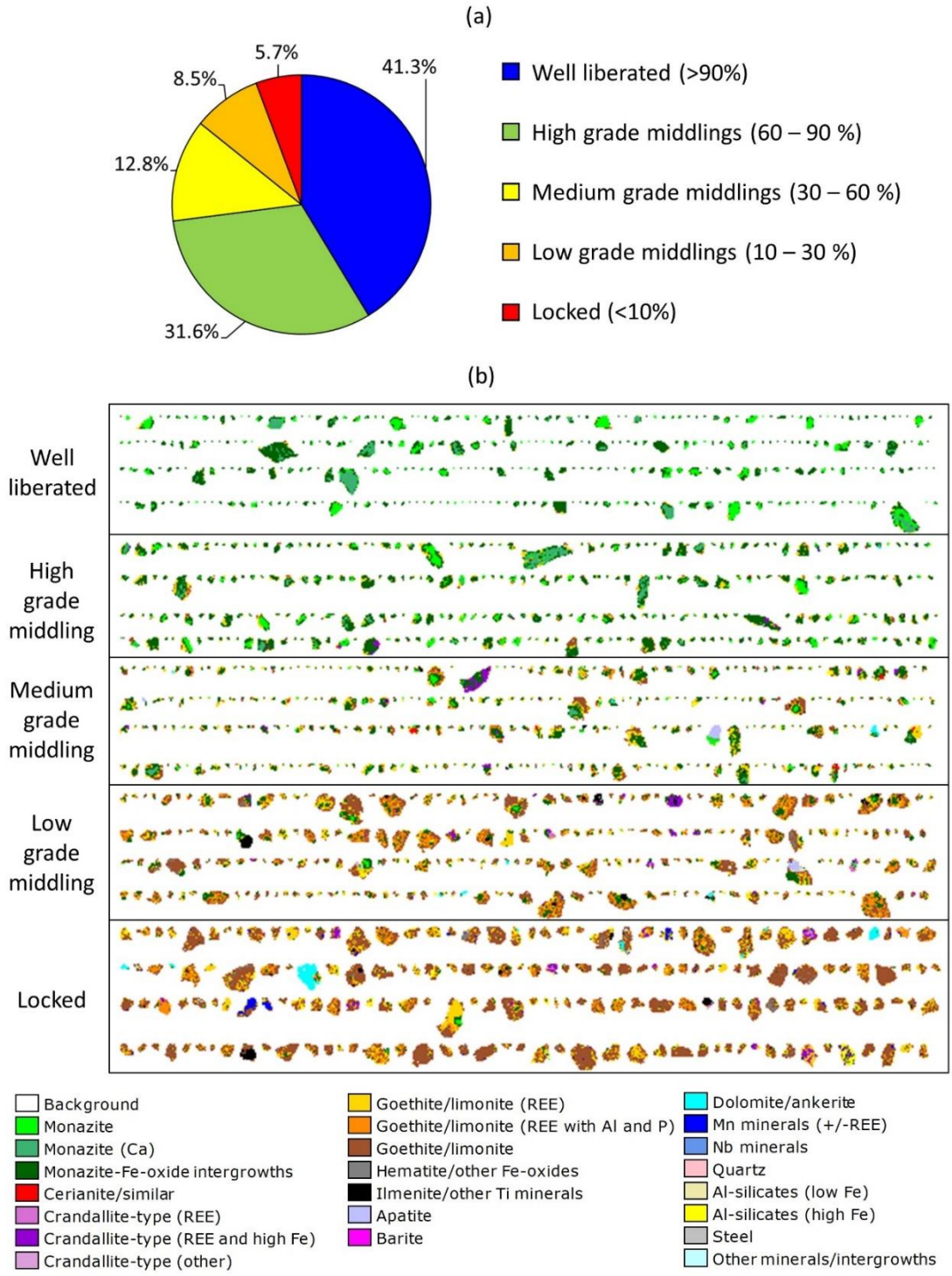

Figure 3–2. Mineral liberation of monazite group minerals analysed by QEMSCAN; (a) the distribution of liberation classes and (b) image grid showing mineral liberation of monazite group minerals.

Table 3−2. Chemical composition of RE ore by XRF.

Elements	Fe_2O_3	SiO_2	Al_2O_3	P_2O_5	MnO	CaO	TiO_2	MgO
Contents (%)	52.73	6.63	5.57	5.18	1.59	1.47	1.23	1.22
Elements	CeO_2	La_2O_3	Nd_2O_3	Pr_6O_{11}	Nb_2O_5	Sm_2O_3	Y_2O_3	Gd_2O_3
Contents (%)	4.38	2.35	2.06	0.49	0.32	0.26	0.13	0.10

Table 3−3. The feed mineralogy analysed using QEMSCAN.

Mineral	Mass %
Monazite	2.8
Monazite (Ca)	2.4
Monazite−Fe−oxide intergrowths	10.2
Cerianite/similar	0.5
Crandallite−type (REE)	0.5
Crandallite−type (REE and high Fe)	1.2
Crandallite−type (other)	0.1
Goethite/limonite (REE)	9.4
Goethite/limonite (REE with Al and P)	4.2
Goethite/limonite	51.6
Hematite/other Fe−oxides	3.7
Ilmenite/other Ti minerals	3.4
Apatite	0.9
Barite	0.1
Dolomite/ankerite	2.2
Mn minerals (+/−REE)	2.0
Nb minerals	0.2
Quartz	0.9
Al−silicates	2.9
Other minerals/intergrowths	0.6
TOTAL	100.0

3.1.3 Chemicals

Na_2SiO_3 (44% in solution, Bisely Pty Ltd, Australia) and NaOH (99%, Chem−supply Pty Ltd., Australia) were used as a depressant and pH, respectively, during the grinding. Additionally, Sylfat FA2 collector (Kraton Corporation, USA), diesel (>95%, Puma Energy, Australia), HCl (99% purity, Chem−Supply Pty Ltd, Australia), NaOH (99%, TCI America Inc., America), $CaCl_2$ (AR grade, Chem−supply Pty Ltd, Australia), and $MgCl_26H_2O$ (AR grade, Chem−supply Pty Ltd, Australia), and Na_2SiO_3 depressant (44% in solution, Bisely Pty Ltd) were used for the flotation experiments. The chemical composition of Sylfat FA2 collector is given in Table 3−4. It should be noted that diesel was used in this study to enhance the solubility of fatty acid collectors (Kou et al., 2010; Snow et al., 2004).

Table 3−4. Chemical composition of the FA2 Sylfat collector.

Species	Oleic acid	Linoleic acid	Palmitic acid	Stearic acid	Others	FA2 Sylfat
wt. %	54.31	30.64	5.28	7.65	2.12	100

Copper nitrate (95% purity, Univar solutions), triethylenetetramine (60% purity, Sigma−Aldrich, America), ethanolamine (98% purity, Sigma Aldrich, America), isobutanol (99% purity, Sigma Aldrich, America), cyclohexane (95% purity, Univar solutions, America) and diethylammonium diethyldithiocarbamate (97% purity, Sigma Aldrich, America) were used for the adsorption experiments.

3.2 Methodologies

3.2.1 Microflotation experiments

Flotation tests were conducted to investigate the influence of the water quality on the flotation performance of monazite or goethite. Before the flotation experiments, the ground mineral sample was mixed with water to obtain 1% solid ratio. The synthetic water with various concentrations of $CaCl_2$, $MgCl_2$, NaCl and KCl were prepared in this study. The mineral samples were conditioned for 5 min using 2×10^{-4} mol/L of sodium oleate collector (99% purity, TCI America), different concentrations of sodium silicate depressant (98% purity, Redox Pty Ltd) and 30 ppm MIBC frother (98% purity,

Orica Limited). It should be noted that sodium silicate was added considering that this reagent was typically used to depress gangue minerals during RE mineral flotation. The pH of the solutions was modified using NaOH and HCl. The conditioned pulps were transferred to a 90 ml modified Partridge−Smith flotation column (25 mm in diameter and 180 mm in length) as seen in Figure 3−3 (Partridge and Smith, 1971). Magnetic stirring was used at the bottom of the flotation column to provide the mixing of particles in the cell; the speed of the magnetic bar was 400 rpm. The air was introduced at the bottom of the column through fritted glass disc at air flow rate of 50 ml/min. All the concentrates were collected after 3 min of flotation time. Each experiment was repeated three times with the standard deviation of less than 5%. These experiments were conducted at 22±1°°C.

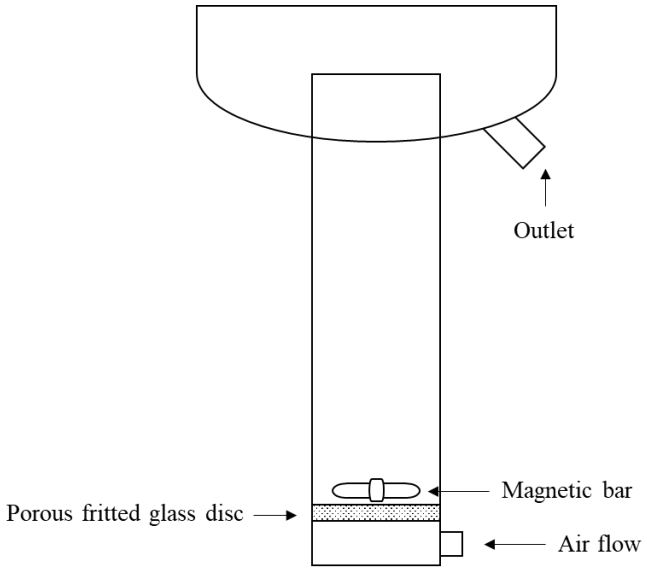

Figure 3−3. Microflotation column cell.

3.2.2 Bench scale flotation experiments

One kilogram of the ore was wet−ground in a rod mill (Labtech Essa Pty Ltd., Australia) using 22 rods at 22 % charge volume for 20 min; the particle size for D_{10}, D_{50}, and D_{90} after the grinding were 1.5, 11.5, and 39 µm, respectively (see Figure 3−4). The total mass of the rods used for the grinding was 16.5 kg (750 g of each) and the dimension of a rod was 20 mm in diameter and 250 mm in length. During the grinding, 1,000 ml of the tap water (Kalgoorlie, Australia) was used with 3,800 g/t of

Na_2SiO_3 depressant and 1,800 g/t of NaOH to achieve pH 10. It should be noted that the tap water, analysed by inductively coupled plasma optical emission spectroscopy (ICP−OES, 5100, Agilent, USA), contained 26.19 mg/L of Ca^{2+} and 11.33 mg/L of Mg^{2+}.

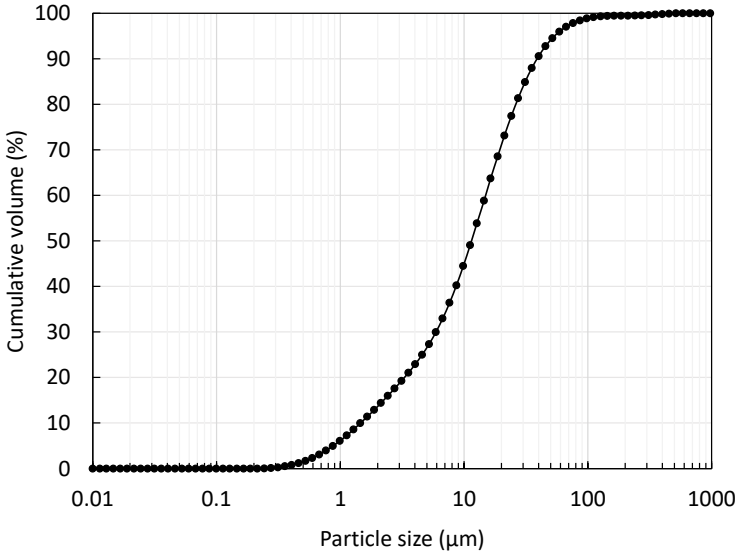

Figure 3−4. Particle size distribution of ore sample after grinding.

Figure 3−5 shows the experimental procedure for each flotation stage. As seen in Figure 3−5, after the grinding process, one−stage roughing and three−stage scavenging flotation process was conducted. The flotation concentrate was collected from the roughing and all the scavenging stages and then two cleaning stages were performed to collect the final flotation products.

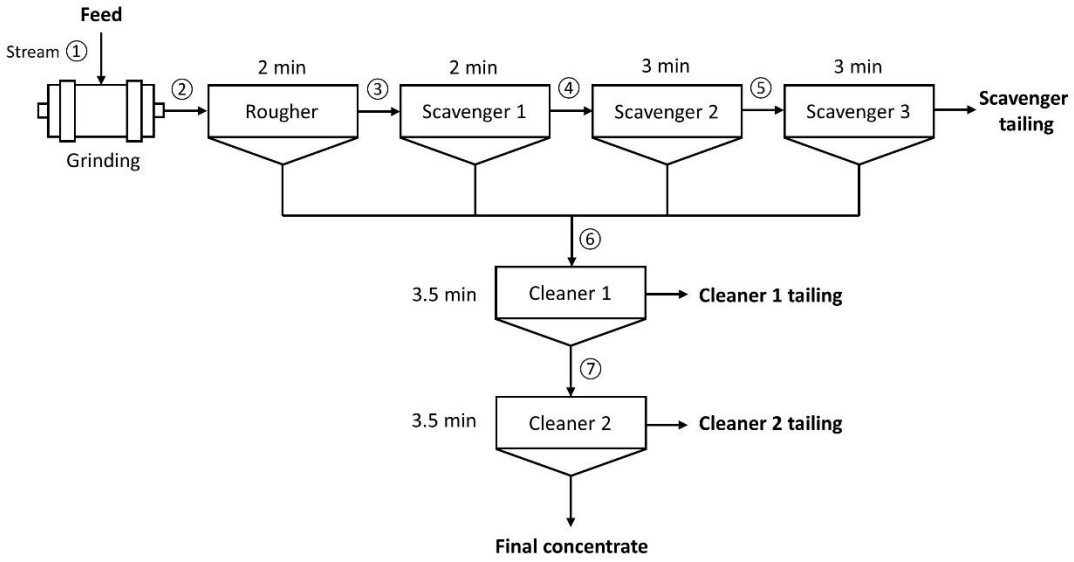

Figure 3−5. The procedure of bench flotation experiments.

The roughing and scavenging stages were conducted using a 5 L flotation cell (ESSA® FTM101, FLSmidth) at 900 rpm while the cleaning stages were performed using a 3 L flotation cell (ESSA® FTM101, FLSmidth) at 700 rpm. The air flow rate was kept as 2.5 L/min during the experiments. During the cleaning stage, the solid percentage was lower than during the roughing and scavenging stages if a 5 L cell was used; thus, the RE minerals recovery reduced in the cleaning stage probably due to the reduced solid percentage and a lower probability of bubble−particle collisions. It means, in the cleaning stage, it is very important to maintain a higher solid percentage, which is possible to achieve in a smaller cell (i.e., 3 L cell), and thus increase flotation recovery of RE minerals; the solid percentage in the first cleaning stage was around 20% while that in the second cleaning stage was around 10%.

Table 3−5 presents the chemicals used in the grinding stage and each flotation stage. All experiments were performed using the synthetic water obtained by mixing tap water and different concentrations of salts such as $CaCl_2$, $MgCl_2$, NaCl, Na_2SO_4, $NaHCO_3$, KCl, K_2SO_4 and $KHCO_3$, and the pulp pH was maintained at pH 10 in each flotation stage. Each flotation stage was conditioned for 4 min and then the flotation concentrates were collected for 2 min in the roughing stage and the first scavenging stage, 3 min for the second and third scavenging stage, and 3.5 min for the cleaning stages (see Figure 3−5). All concentrates and tailings were filtered, weighed, and assayed using XRF.

Table 3−5. Reagent scheme of bench flotation experiments.

Stream	Na_2SiO_3 (g/t)	NaOH (g/t)	Diesel (g/t)	Sylfat FA2 (g/t)
1	3,800	1,800	−	−
2	−	−	1,100	2,200
3	−	−	350	700
4	300	400	200	400
5	−	−	−	−
6	600	200	350	700
7	300	100	−	−

3.2.3 Zeta potential measurement experiments

Zeta potential experiments were carried out using Malvern NanoZ zeta sizer (Malvern, UK). Mineral samples were ground using a mortar and pestle and screened through 10 µm sieve to collect the undersize fraction. Before zeta potential experiments, the samples were conditioned for 15 min at 0.1% solid ratio in the presence of 1×10^{-4} mol/L NaCl as a background electrolyte. The conditioning procedure was similar to the flotation experiments. The pH of the solution was adjusted with HCl and NaOH solution. After conditioning, large particles were allowed to settle down from the suspension. Then, the supernatant was collected and transferred to a zeta potential measurement cell. All the tests were conducted in triplicates, and the mean value of measurement was used for further analysis.

3.2.4 UV−Vis spectroscopy analysis

The adsorption experiments were carried out by the solution depletion method (Gregory, 1966). The solution was centrifuged at 4000 rpm to separate solution from solid particles and the clear supernatants were used for experiments. This method is based on the mixing oleate solutions, copper – triethylenetretramine mixture (copper nitrate, 95% purity, Univar solutions; triethylenetetramine, 60% purity, Sigma Aldrich; ethanolamine, 98% purity, Sigma Aldrich), and 20% isobutanol (99% purity, Sigma Aldrich) and 80% cyclohexane solvent (95% purity, Univar solutions). The solution mixture was allowed to stand for 10 minutes to have two separate liquid phases. Finally,

the organic phase was transferred to a test tube and 2 drops of diethylammonium diethyldithiocarbamate dye (97% purity, Sigma Aldrich) were added to colour the organic phase. In other words, the oleate ions in the solution form copper oleate complex with the addition of copper nitrate reagent at first, then the copper oleate can be extracted into an organic phase by mixing with the extractant (the mixture of cyclohexane and isobutanol). After that, the copper ions in the copper oleate complex can form copper dithiocarbamate complex by adding dithiocarbamate dye into the organic phase; it means by measuring copper dithiocarbamate concentration, it is possible to determine the concentration of oleate ions (i.e., 2 mols of oleate ions are equal as 1 mol of copper ions). The formed copper dithiocarbamate complex has the maximum UV−Vis absorption at 435 nm wavelength as reported in the literature (Hogarth and Onwudiwe, 2021; Magee, and Hill, 1985). The UV−vis spectrophotometer (Lambda35, PerkinElmer, USA) was used in this measurement and the absorption of the final organic solution was determined at 435 nm wavelength. Based on the maximum absorbance values, the calibration curve was determined as seen in Figure 3−6. The adsorption kinetics using the monazite−oleate system showed that the adsorption equilibrium was achieved after 2 min as seen in Figure 3−7. Thus, the duration of all the adsorption experiments using monazite was 2 min. The specific surface area for monazite and goethite were 0.1028 and 0.3387 m^2/g, respectively.

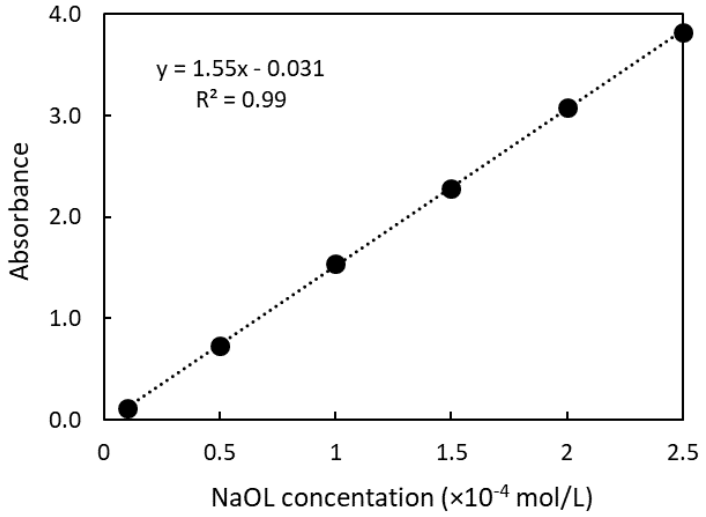

Figure 3−6. Standard curve fitting using the absorbance at 435 nm wavelength of different concentration of oleate solutions.

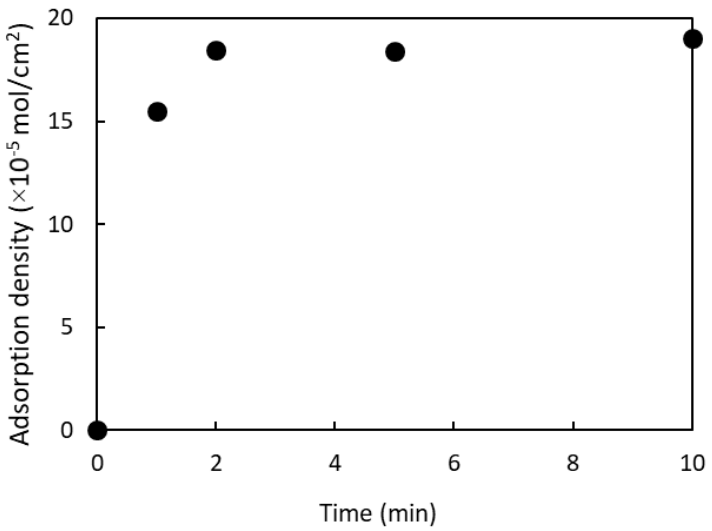

Figure 3−7. Adsorption kinetics tests of monazite using 2×10^{-4} mol/L sodium oleate.

3.2.5 X−ray diffraction (XRD) analysis

The XRD analysis was conducted using an Olympus diffractometer with Co−Kα radiation, scanning a range between 5 and 55° (2θ). Figure 3−1 shows the XRD spectrum of the single minerals as determined by this XRD analysis. Diffractograms were analysed using the X−Powder software package.

3.2.6 X−ray photoelectron spectroscopy (XPS) analysis

XPS analysis was carried out to investigate the effects of $CaCl_2$ and $MgCl_2$ on surface changes of monazite. The mineral sample was conditioned in a similar procedure to the flotation tests. After conditioning, samples were filtered and washed using deionized water followed by drying a desiccator under the vacuum at room temperature for 24 h. The XPS analysis was carried out with Kratos Axis Supra instrument (Kratos Analytical, UK) using monochromatic Al Kα radiation (1486.7 eV) at 225W. The spectral data were processed using CasaXPS software and the C 1s binding energy of 284.8 eV was used to calibrate the spectrum.

3.2.7 Ore mineralogy

The mineralogical properties of feed ore were examined using QEMSCAN (Quantitative Evaluation of Minerals by Scanning Electron Microscopy) analysis to determine the liberation of RE mineral particles after the grinding and the mineralogy of the ore sample. For this analysis, polished blocks were made by mixing the sample with high−purity graphite to ensure particle separation and reduce density segregation. The sample−graphite mixtures were subsequently embedded in molds using epoxy resin. After curing the resin, the epoxy block was cut and polished to expose a fresh surface, and the surface was coated with carbon for enhancing conductivity of the polished section. The sample was measured using the particle mineralogical analysis (PMA) measurement mode on QEMSCAN with 1.5 µm pixel. The QEMSCAN data was processed using Bruker Esprit software to provide compositions of particles.

3.2.8 Rheological measurement experiments

The rheological properties of flotation pulp were measured using DV1 MLV digital viscometer (Brookfield, USA). The flotation pulp, collected in the roughing stage, was used for the rheological measurements. For each measurement, 16 ml of the conditioned pulp was introduced into the UL adapter, which is ideal for low viscosity materials, using the LV4 spindle. A rheogram was produced using the shear rate ranging between 0.612 s^{-1} and 122.3 s^{-1}. All rheological measurements were performed at room temperature (25 ± 2 °C).

3.2.9 Entrainment experiments

The flotation experiments were conducted without using a collector to determine the non−selective recovery of particles. It should be noted that the ore primarily contains goethite as the major gangue mineral (65.2% of the mass composition), along with minor oxide minerals such as ilmenite (3.4%), dolomite (2.2%), and silicate minerals (3.8%) as seen in Table 3−3. Due to their hydrophilic nature, these minerals are not naturally floatable (Gence, 2006; Iveson et al., 2000; Nuri et al., 2014; Yoon and Yordan, 1991). Therefore, any recovery of these minerals without using a collector is considered to occur through entrainment. The same method was used to prepare the

flotation pulp as in the bench scale flotation experiment. The ground slurry was placed into a 2 L mechanical flotation cell and tap water was added to create a solid percentage of 22%. The pulp was agitated at 600 rpm for 5 min with different anions using the same reagents as those used in the flotation experiments. Then, 30 mg/L of MIBC was added to create the froth phase. The air flow rate was 10 L/min and synthetic water was added during the experiments to maintain the slurry level. The froth phase was collected at intervals of 1, 2, 5, 10 and 15 min by scrapping every 10 s, and the mass of the slurry and dried samples were measured to calculate the water recovery and mass recovery. All experiments were carried out three times and the mean values were used.

3.2.10 Settling experiments

The settling behavior of a flotation feed slurry was investigated in the presence and absence of anions used in the flotation experiments. The feed slurry was prepared after wet grinding (50 % solid percentage); 500 ml of the slurry was collected and conditioned with different types of anions for a period of 10 min. The conditioned feed slurry was then introduced into the 500 mL graduated cylinders. The slurry was left undisturbed for 144 h to allow settling of particles, and the photographs were taken for analysis.

3.3 Thermodynamic calculations

The calculation of the standard Gibbs free energy formation (ΔG^{θ}) for the reaction between oleate ions and cations such as Ca^{2+} and Mg^{2+} was performed as follows:

$$\Delta G^{\theta}_{M^{n+}} = RTln(K_{sp}\alpha_{(M^{n+})}\alpha^{n}_{(OL^{-})}) \quad (3\text{-}1)$$

$$M^{n+} + OL^{-} = M(OL)_{n}, \quad K_{sp} = [M^{n+}][OL^{-}]^{n} \quad (3\text{-}2)$$

where R is the universal gas constant (8.314 J/(molK)), T is the temperature in K and K_{sp} is the solubility product of metallic oleate.

The reaction coefficients ($\alpha_{(OL^-)}$ and $\alpha_{(M^{n+})}$) were calculated as follows:

$$H^+ + OL^- = HOL, \quad K^H = \frac{[HOL]}{[H^+][OL^-]} \tag{3-3}$$

$$\alpha_{(OL^-)} = 1 + K^H[H^+] \tag{3-4}$$

$$\alpha_{(M^{n+})} = 1 + \beta_1[OH^-] + \beta_2[OH^-]^2 + \cdots + \beta_n[OH^-]^n \tag{3-5}$$

where K^H is the dissociation constant of oleic acid, $\alpha_{(OL^-)}$ is the protonation constant, $\alpha_{(M^{n+})}$ is the hydrolysis coefficient of metallic ions, and β_n is the cumulative stability constant. The thermodynamic constants are presented in Table 3−6.

The standard Gibbs free energy for Ca^{2+} and Mg^{2+} with SiO_3^{2-} were calculated as follows:

$$\Delta G^{\theta}_{M^{2+}} = RT\ln(K_{sp(M-Si)}\alpha_{(M)}\alpha_{(Si)}) \tag{3-6}$$

where R is the ideal gas constant (8.314 J/molK), T is the temperature in K, $K_{sp(M-Si)}$ is the solubility product of metallic silicate, $\alpha_{(M)}$ is the hydrolysis constant of Ca^{2+} and Mg^{2+} and $\alpha_{(Si)}$ is the protonation constant of SiO_3^{2-}.

The hydrolysis constant of Ca^{2+} and Mg^{2+}, and the protonation constant of SiO_3^{2-} were calculated as follows:

$$\alpha_{Ca} = 1 + \beta_{1(Ca)}[OH^-] + \beta_{2(Ca)}[OH^-]^2 \tag{3-7}$$

$$\alpha_{Mg} = 1 + \beta_{1(Mg)}[OH^-] + \beta_{2(Mg)}[OH^-]^2 \tag{3-8}$$

$$\alpha_{Si} = 1 + K_1^H[H^+] + K_1^H K_2^H[H^+]^2 \tag{3-9}$$

The solubility product and reaction coefficients used in the calculation are listed in Table 3−6.

Table 3−6. Species and reaction coefficient.

Species	Chemical reactions	Thermodynamic constants	References
Ca^{2+}	$Ca^{2+} + OH^- = Ca(OH)^+$ $Ca(OH)^+ + OH^- = Ca(OH)_2$	$\beta_{1(Ca)} = 10^{1.4}$ $\beta_{2(Ca)} = 10^{2.77}$	(Jung et al., 2022)
Mg^{2+}	$Mg^{2+} + OH^- = Mg(OH)^+$ $Mg(OH)^+ + OH^- = Mg(OH)_2$	$\beta_{1(Mg)} = 10^{2.58}$ $\beta_{2(Mg)} = 10^{1}$	(Jung et al., 2022)
SiO_3^{2-}	$H^+ + SiO_3^{2-} = HSiO_3^-$ $H^+ + HSiO_3^- = H_2SiO_3$	$K_1^H = 10^{12.56}$ $K_2^H = 10^{9.43}$	(Somasundaran and Wang, 2006)
$CaOL_2$	$Ca^{2+} + 2OL^- = CaOL_2$	$K_{sp(CaOL_2)} = 10^{-15.4}$	(Fang et al., 2020)
$MgOL_2$	$Mg^{2+} + 2OL^- = MgOL_2$	$K_{sp(MgOL_2)} = 10^{-13.8}$	(Fang et al., 2020)
$CaSiO_3$	$Ca^{2+} + SiO_3^{2-} = CaSiO_{3(s)}$	$K_{sp(CaSiO_3)} = 10^{-11.08}$	(Yuehua et al., 2003)
$Mg_3Si_4O_{10}(OH)_{2(s)}$	$3Mg^{2+} + 4SiO_3^{2-} + 2H^+ = Mg_3Si_4O_{10}(OH)_{2(s)}$	$K_{sp(Mg_3Si_4O_{10}(OH)_2} = 10^{-54.50}$	(Nied et al., 2016)

3.4 DLVO (Derja−guin−Landau−Verwey−Overbeek) theory calculations

The interaction energy between fine particles was calculated based on the DLVO theory, which is a widely used model that explains the stability and interaction between colloidal particles in various electrolytes. The total interaction energy (E_{tot}) was given as the sum of the van der Waals forces (E_{vdw}) and the electrostatic forces (E_{edl}) between two particles as presented in Eq. 3-10.

$$\mathrm{E_{tot}} = \mathrm{E_{vdw}} + \mathrm{E_{edl}} \tag{3-10}$$

The van der Waals interaction energy E_{vdw} between two particles is determined by Eq. 3-11.

$$\mathrm{E_{vdw}} = -\frac{\mathrm{A}}{6\mathrm{H}}\left(\frac{\mathrm{R_1R_2}}{\mathrm{R_1+R_2}}\right) \tag{3-11}$$

where, R_1 and R_2 are the particle size and H (m) is the distance between two particles. A is the effective Hamaker constant between particles in aqueous medium, which can be calculated using Eq. 3-12.

$$\mathrm{A} = (\sqrt{\mathrm{A_m}} - \sqrt{\mathrm{A_w}})^2 \tag{3-12}$$

where A_m is the Hamaker constant of mineral particles as follows: 1.37×10^{-19} J for goethite (Golikova et al., 2002; Peppersack et al., 2022) or 2.0×10^{-19} J for monazite (Azizi et al., 2017; Otsuki et al., 2007) and A_w is the Hamaker constant of water (3.7×10^{-20} J) in vacuum(Azizi et al., 2017).

The electrostatic interaction force was determined by using Eq. 3-13.

$$\mathrm{E_{edl}} = \pi\varepsilon_0\varepsilon_\mathrm{r}\left(\frac{\mathrm{R_1R_2}}{\mathrm{R_1+R_2}}\right)(\zeta_1^2+\zeta_2^2)\left\{\frac{2\zeta_1\zeta_2}{\zeta_1^2+\zeta_2^2}\ln\left[\frac{1+\exp(-\kappa\mathrm{H})}{1-\exp(-\kappa\mathrm{H})}\right]+\ln[1-\exp(-2\kappa\mathrm{H})]\right\} \tag{3-13}$$

where ε_0 is the dielectric constant in vacuum (8.854×10^{-12} C^2/Jm), ε_r is the dielectric constant of medium (78.5 C^2/Jm), ζ_i is the zeta potential of mineral for i (i=1, 2), κ is the thickness of electric double layer, which was calculated using Eq. 3-14.

$$\kappa^{-1} = \sqrt{\frac{\varepsilon_0 \varepsilon_r k_B T}{e^2 \sum_i n_i z_i^2}} \quad (3\text{-}14)$$

where k_B is the Boltzman constant (1.38×10^{-23} J/K), T is the absolute temperature (298 K), e is the elementary electric charge (1.602×10^{-19} C), Z_i is the valence of the ion i, n_i is the number of ions of type i per unit volume in the bulk solution, which was calculated by using Eq. 3-15.

$$n_i = C_i \times N_A \times 1000 \quad (3\text{-}15)$$

where C is the molar concentration of ion i (mol/L), N_A is the Avogadro constant (6.023×10^{23} /mol).

Chapter 4. Influence of monovalent and divalent cations on monazite flotation*

4.1 Introduction

A few studies have been carried out to investigate the effect of dissolved ions using saline water on flotation of RE bearing minerals. For example, Wang et al. (2020a; 2020b) studied the flotation of bastnasite using sodium oleate to investigate the effects of dissolved ions from gangue minerals such as barite and fluorite. It was suggested that Ca^{2+}, F^{-} and Ba^{2+} dissolved from the gangue minerals reduced the recovery of bastnaesite probably due to the formation of insoluble oleate products with metallic ions. Flotation performance of monazite was investigated using a hydroxamic acid collector in the presence of different ions dissolved from calcite (Zhang et al., 2017; Zhang and Honaker, 2018). It was found that the Ca^{2+} in the solutions was detrimental to the monazite recovery due to the preferential adsorption of calcium hydroxide on monazite surfaces, leading to a lower flotation recovery. Espiritu et al. (2019) also investigated the effects of dissolved ions from dolomite on monazite flotation using the DFT simulation and found that Ca^{2+} and Mg^{2+} reduced the floatability of monazite due to the adsorption of calcium or magnesium carbonate/hydroxide on monazite and the precipitation of calcium or magnesium oleate. However, there is no research experimentally investigating the flotation performance of monazite with sodium oleate (a common collector for RE minerals) in the presence of different cations found in plant water. Therefore, the main focus of this chapter is to understand the flotation mechanisms of monazite with sodium oleate in the presence of different cations (Ca^{2+}, Mg^{2+}, Na^{+} and K^{+}) by integrating microflotation experiments with colloid and surface characterizations using zeta potential, XPS and UV adsorption.

---

* This chapter includes results from the following peer-reviewed publication: Jung, M., Tadesse, B., Dick, C., Logan, A., Dyer, L., Albijanic, B., 2022. Influence of monovalent and divalent cations on monazite flotation. *Colloids and Surfaces A: Physicochemical and Engineering Aspects.* 653, 129975.

4.2 Results and discussion

4.2.1 Flotation experiments of monazite

4.2.1.1 Effect of pH and sodium silicate

Figure 4−1 shows the influence of pH on monazite recovery in distilled water. As seen in Figure 4−1(a), the maximum monazite recovery was achieved at pH 8 probably due to the highest concentration of oleate ions at this pH; thus, all the experiments were conducted at pH 8. This agrees well with the results obtained by some authors (Abeidu, 1972; Cheng et al., 1993; Espiritu and Waters, 2018; Pavez and Peres, 1993). Sodium silicate is added typically during RE flotation to depress oxide minerals and thus this chemical was also used in this work to simulate the chemical conditions during flotation of monazite from its ore (Abaka-Wood et al., 2019, 2018b; Anderson et al., 2016; Chelgani et al., 2015b; Pavez and Peres, 1993). As illustrated in Figure 4−1(b), the depression of monazite recovery was not significant in the presence of sodium silicate less than 6×10^{-3} mol/L, however, monazite was depressed noticeably above 6×10^{-3} mol/L. Therefore, the concentration of sodium silicate was 6×10^{-3} mol/L for all the experiments.

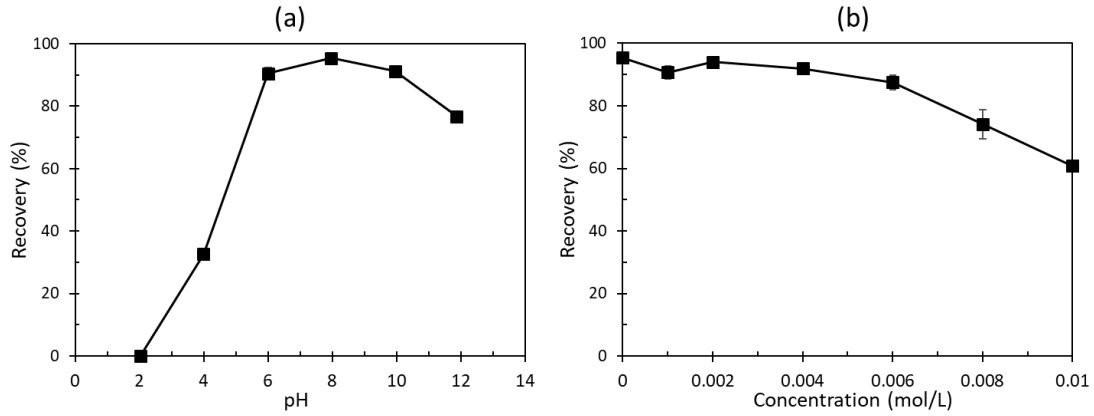

Figure 4−1. Effect of (a) pH and (b) sodium silicate at pH 8 on the recovery of monazite in the presence of 2×10^{-4} mol/L sodium oleate.

4.2.1.2 Effect of Ca^{2+}, Mg^{2+}, Na^{+} and K^{+} on flotation

Figure 4−2(a) showed that the increase in Ca^{2+} resulted in a low flotation recovery of monazite probably due to the formation of calcium oleate precipitate, reducing the concentration of oleate ions in a solution. As a result, less amounts of oleate ions were

adsorbed on monazite surfaces (see Figure 4−11(a) and Figure 4−12(a)), reducing the flotation recovery of monazite. Similar observations were also found in the presence of Mg^{2+} as shown in Figure 4−2(b). However, Mg^{2+} was less detrimental for monazite flotation than Ca^{2+}. It should be noted that sodium silicate that was used as the depressant may interact with divalent ions affecting the flotation results. However, according to the species distribution diagram (Arantes and Lima, 2013; Sjoeberg and Oehman, 1986), the predominant species of sodium silicate is monosilicate acid such as $Si(OH)_4$ at pH lower than 9, and monosilicate and polysilicate ions become predominant at pH higher than 9. Thus, the interaction of silicate ions with divalent ions was neglected because the flotation experiments were carried out at pH 8 where the uncharged monosilicate acid was predominant.

The presence of Na^+ and K^+ slightly reduced monazite flotation recovery as seen in Figure 4−2(c) and Figure 4−2(d). The reason is that the oleate concentration in the solution did not change significantly with increasing in Na^+ and K^+ concentration (see Figure 4−3).

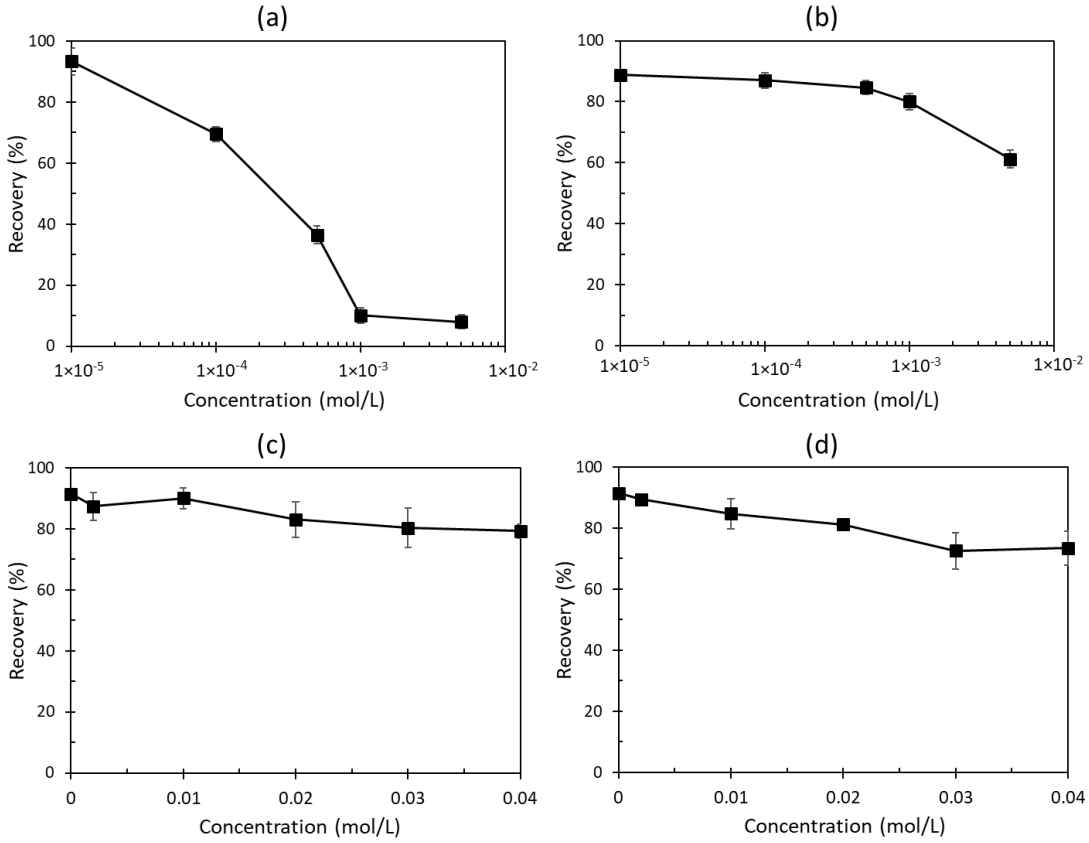

Figure 4−2. Effect of (a) Ca^{2+}, (b) Mg^{2+}, (c) Na^{+} and (d) K^{+} ions on the recovery of monazite in the presence of 6×10^{-3} mol/L sodium silicate and 2×10^{-4} mol/L sodium oleate at pH 8.

4.2.1.3 Flotation solution chemistry of oleate in the presence of Ca^{2+}, Mg^{2+}, Na^{+} and K^{+}

Flotation performance of monazite in the presence of different ions is affected by solution chemistry. For this reason, it is important to determine the concentration of oleate ions in the solution in the presence of Ca^{2+}, Mg^{2+}, Na^{+}, and K^{+}. Figure 4−3 shows the concentration of residual oleate ions in the solution in the presence of different concentrations of monovalent and divalent cations without adding monazite powder in the solution. As seen in Figure 4−3, the concentration of oleate was significantly reduced from the initial concentration of 2×10^{-4} mol/L in the presence of Ca^{2+} due to the formation of insoluble calcium oleate; the solubility product of calcium oleate is very low (Ksp = $10^{-15.4}$). A similar effect was also observed in the presence of Mg^{2+}, however, the concentration of oleate in the presence of Mg^{2+} was higher than that in the presence of Ca^{2+}. The reason is that the solubility product of magnesium

oleate (Ksp = $10^{-13.8}$) was 40 times higher than that of calcium oleate. The presence of Na^+ and K^+ did not reduce the concentration of oleate ions in the solutions considering that sodium oleate and potassium oleate have a very high solubility product (Ksp = $10^{-5.92}$).

The difference between the solubility of monovalent and divalent oleate salts may be explained by considering the attractive forces between different cations and oleate ions. The electrolytes dissolved in the water dissociate into hydrated ions, and their degree of hydration is closely related to the degree of binding strength between the hydrated ion and other ions (Kang et al., 2020; Vlachy et al., 2009). It was found that the binding strength of cations toward carboxylate increased in an order of $Na^+ > K^+$ using electromotive force measurements (Feinstein and Rosano, 1967) and $Ca^{2+} > Mg^{2+}$ using the computational simulation based on the density functional theory (Agulhon et al., 2012). The degree of hydration of different cations can be found in Hofmeister series which presents an order of tendency of salts to the stabilization of protein from aqueous solution: $NH_4^+ > K^+ > Na^+ > Cs^+ > Li^+ > Mg^{2+} > Ca^{2+} > Ba^{2+}$ (Kang et al., 2020). In this series, the strength of hydration forces tends to increase from left to right. It means that the binding strength between divalent cations and oleate ions is stronger than that between monovalent ions and oleate ions. Thus, the formation of metallic oleate salts is likely to be more favourable in the order of $Ca^{2+} > Mg^{2+} > Na^+ > K^+$, and this series is well correlated to the flotation recovery results in Figure 4−2.

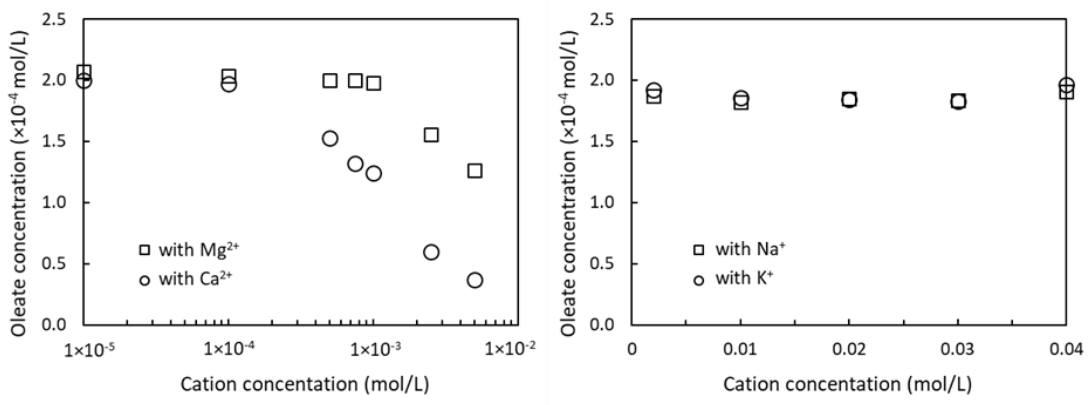

Figure 4−3. Oleate concentration in the presence of Ca^{2+}, Mg^{2+}, Na^+ or K^+ and 6×10^{-3} mol/L sodium silicate.

Figure 4−4 shows the changes in the free energy formation of calcium oleate, magnesium oleate, potassium oleate and sodium oleate as a function of pH. As seen in Figure 4−4, the free energy formations of calcium oleate and magnesium oleate was much lower than the free energy formations of potassium oleate and sodium oleate, demonstrating that the formation of calcium oleate and magnesium oleate were much more favourable than the formation of sodium and magnesium oleate.

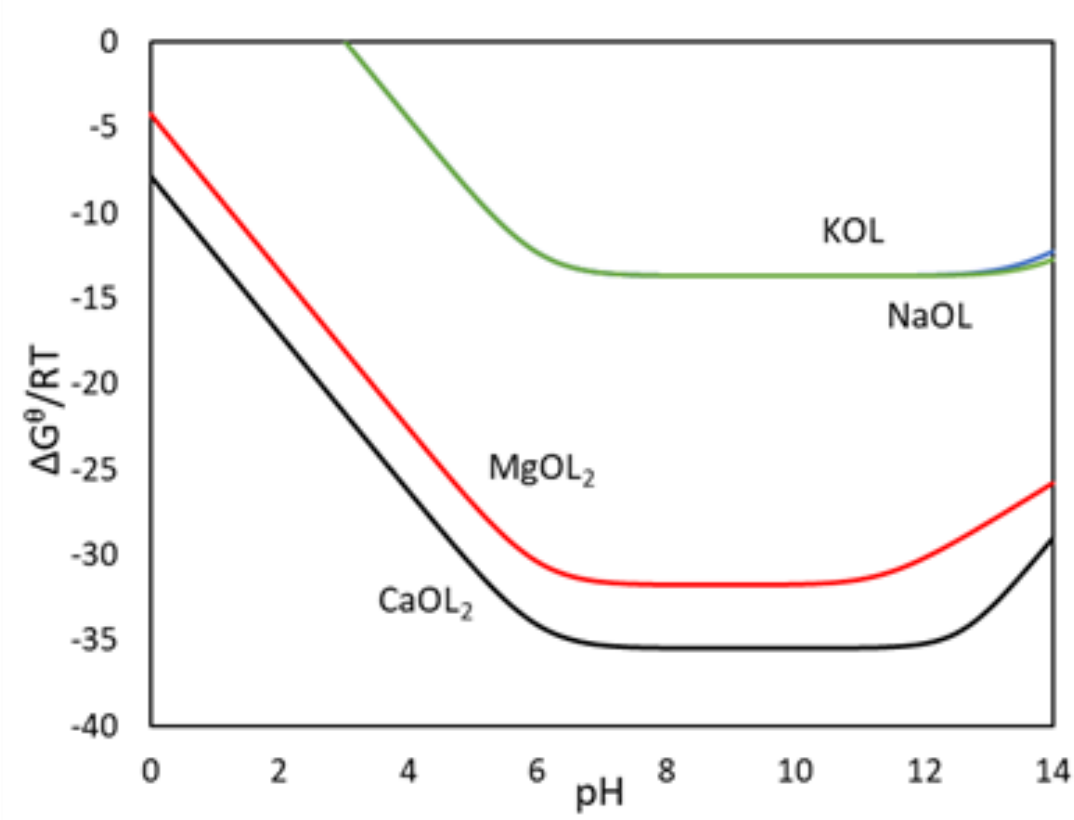

Figure 4−4. The free energy of the reaction between ions and oleate ions by pH.

4.2.2 Zeta potential of monazite

4.2.2.1 Zeta potential of monazite in distilled water

Figure 4−5 shows the zeta potential of monazite in the absence and presence of sodium silicate and sodium oleate. As shown in Figure 4−5, the PZC of monazite in distilled water was at pH 7.2, which agrees with the literature (Cheng, 2000; Espiritu et al., 2018b; Zhang et al., 2017). The PZC of monazite in the presence of 6×10^{-3} mol/L sodium silicate and 2×10^{-4} mol/L sodium oleate were shifted to pH 5.5 and pH 3.5, respectively, indicating the adsorption of silicate ions and oleate ions on the monazite

surface. However, there is no significant difference in the zeta potential of monazite in the presence of oleate and silicate ions than that in the presence of oleate ions only. It means that the adsorption of oleate ions on monazite was more significant than the adsorption of silicate ions on the same mineral, and that silicate ions do not appear to interfere with oleate adsorption on monazite.

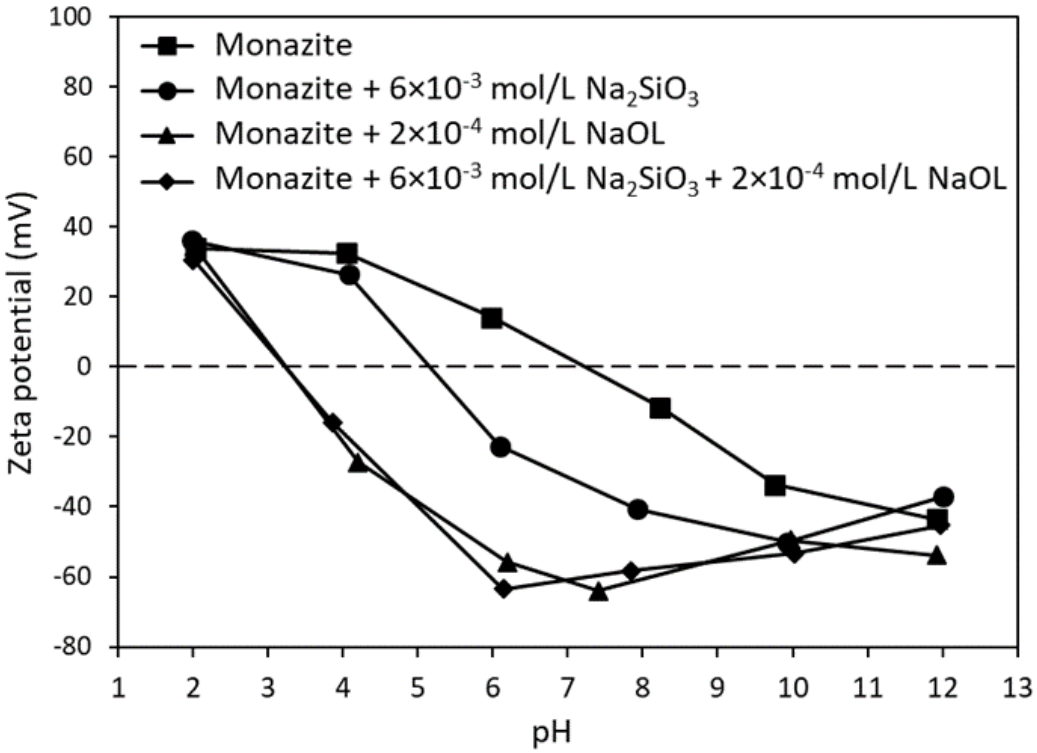

Figure 4−5. Zeta potential of monazite as a function of pH before and after conditioning in 2×10^{-4} mol/L NaOL and 6×10^{-3} mol/L Na_2SiO_3, respectively.

4.2.2.2 Effect of Ca^{2+}, Mg^{2+}, Na^{+} and K^{+}

The influences of different cations on the zeta potential of monazite particle are shown in Figure 4−6 to Figure 4−9. As seen in Figure 4−6 to Figure 4−9, the increase in concentrations of all cations made the zeta potential of monazite less negative due to the adsorption of monovalent or divalent ions on monazite surfaces; however, the presence of cations did not change the PZC. In the case of divalent cations, different metal ion species are formed in the solutions (Ca^{2+} and $CaOH^{+}$; Mg^{2+} and $MgOH^{+}$ (see Figure 4−10)) while in the case of monovalent ions, one type of metal ions are formed in the solutions (Na^{+} and K^{+}). It means that the ionic strength of solutions in the

presence of divalent ions is higher than that of monovalent ions (e.g., when the solution concentration of monovalent or divalent ions is 0.005 mol/L, the ionic strength of solutions containing divalent ions is 0.015 mol/L and that of solutions containing monovalent ions is 0.005 mol/L); the ionic strength is calculated using the well−known equation:

$$Ionic\ strength = \frac{1}{2}\sum_{i=1}^{n} c_i z_i^2 \quad (4\text{-}1)$$

where ci is the concentration of ion (mol/L), zi is the ion charge.

Considering that solutions with divalent metal ions have higher ionic strength than solutions with monovalent metal ions, the same shift in zeta potential was achieved with a larger shift of monovalent metal ion concentrations and a lower shift of divalent ion concentrations. For example, the change of zeta potential from −60 mV to −40 mV of monazite at pH 8 was achieved when the concentration of NaCl or KCl changed from 0 to 2×10^{-2} mol/L; the same change in zeta potential was accomplished when the concentration of $CaCl_2$ or $MgCl_2$ changed from 0 to 5×10^{-4} mol/L at pH 8. This agrees with the results obtained by (Gulgonul, 2019), who found that divalent ions compressed more electrical double layers of Teflon particles than monovalent ions.

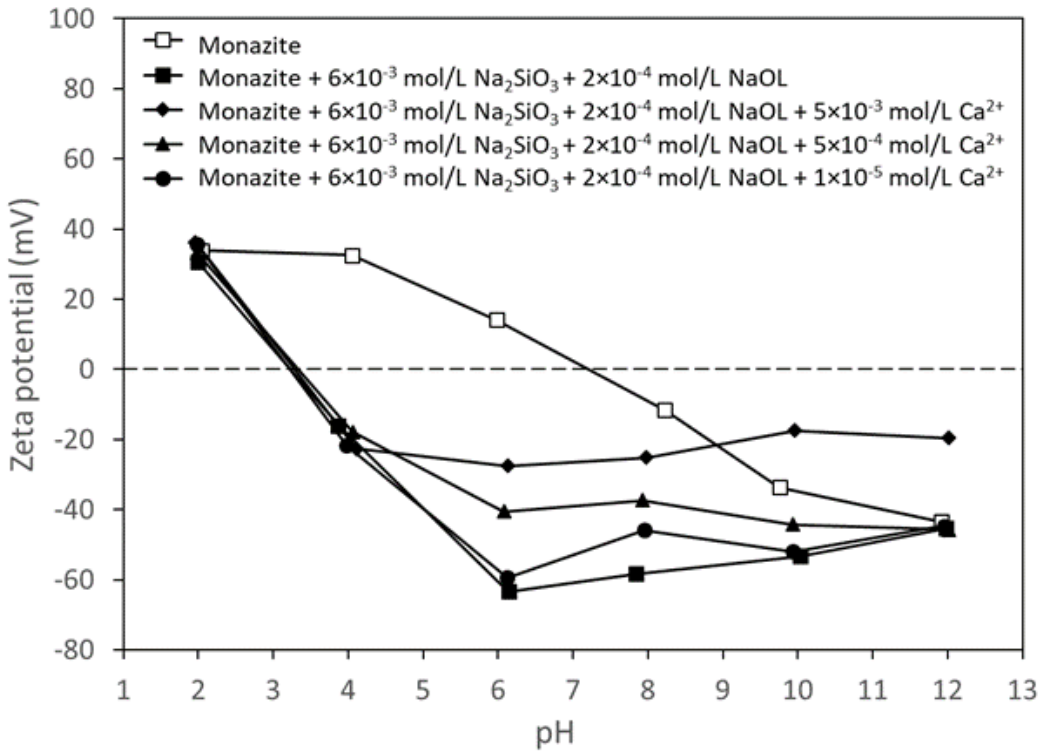

Figure 4−6. Zeta potential of monazite particles in the difference concentration of Ca^{2+} ions.

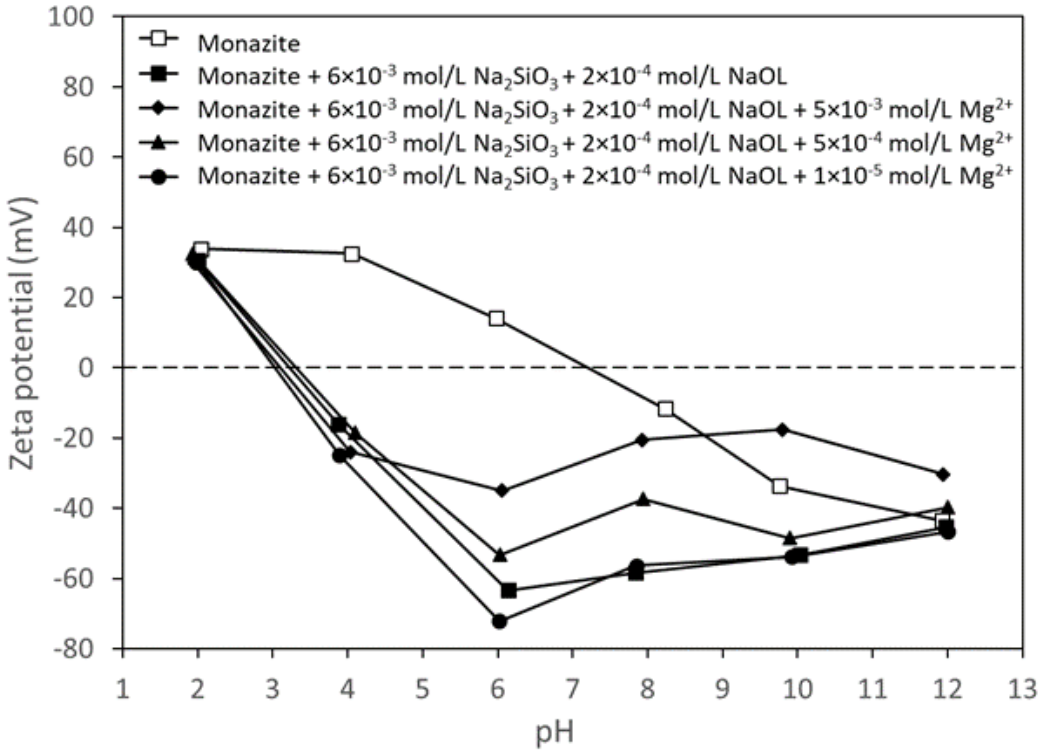

Figure 4−7. Zeta potential of monazite particles in the difference concentration of Mg^{2+} ions.

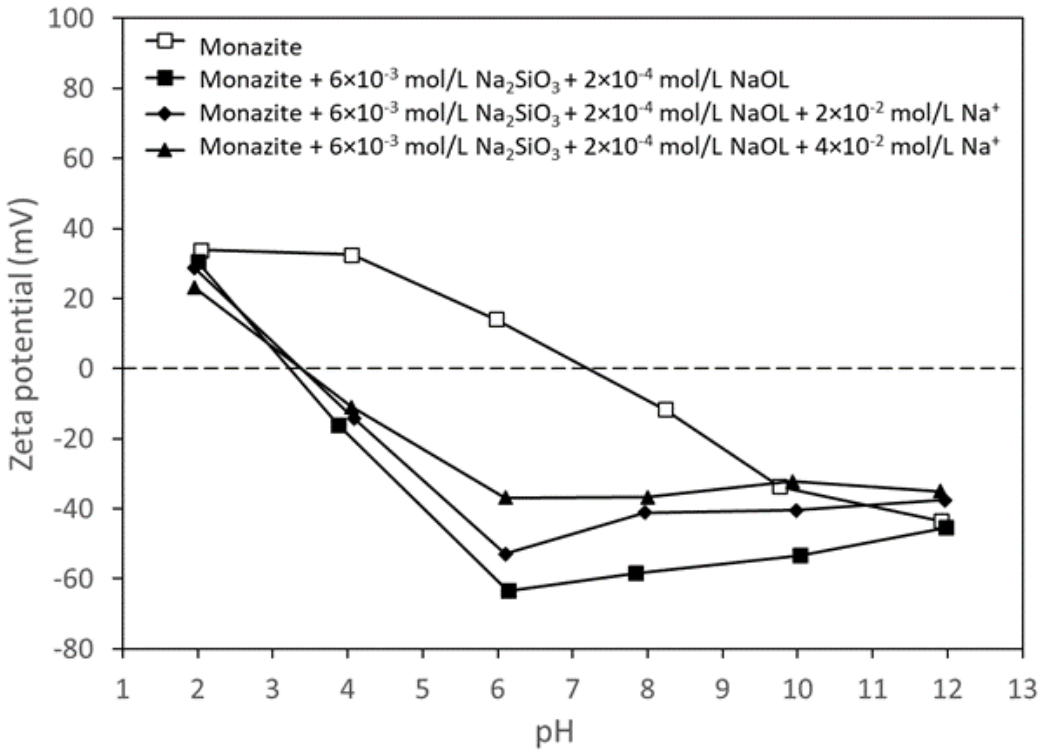

Figure 4−8. Zeta potential of monazite particles in the difference concentration of Na^+ ions.

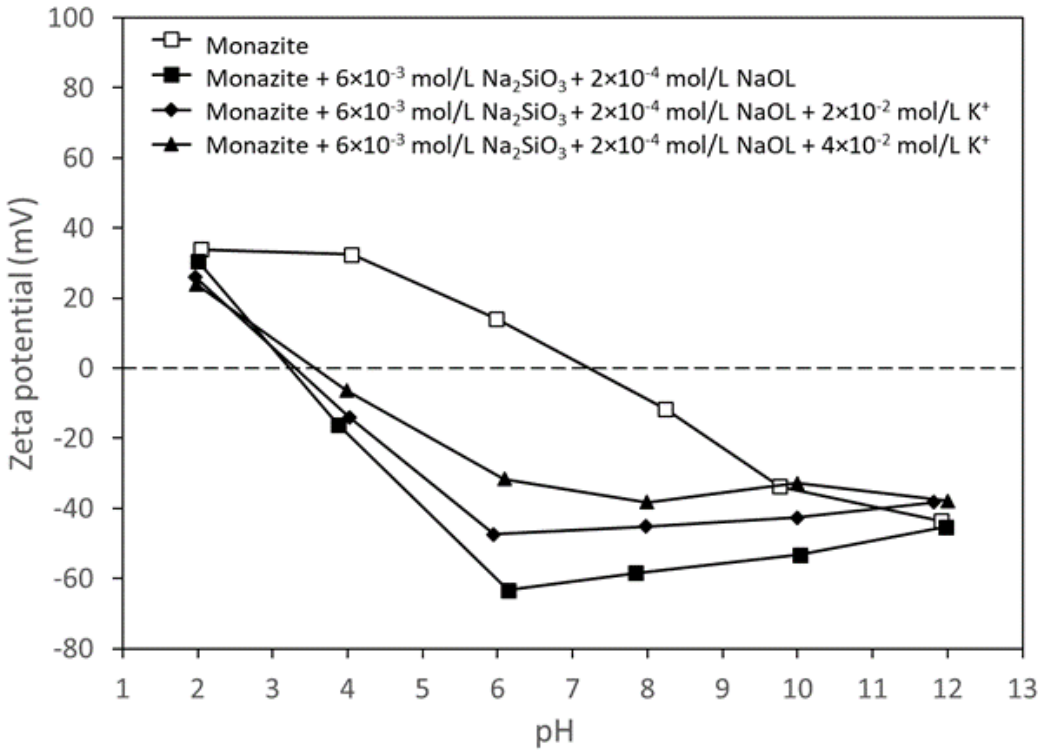

Figure 4−9. Zeta potential of monazite particles in the difference concentration of K^+ ions.

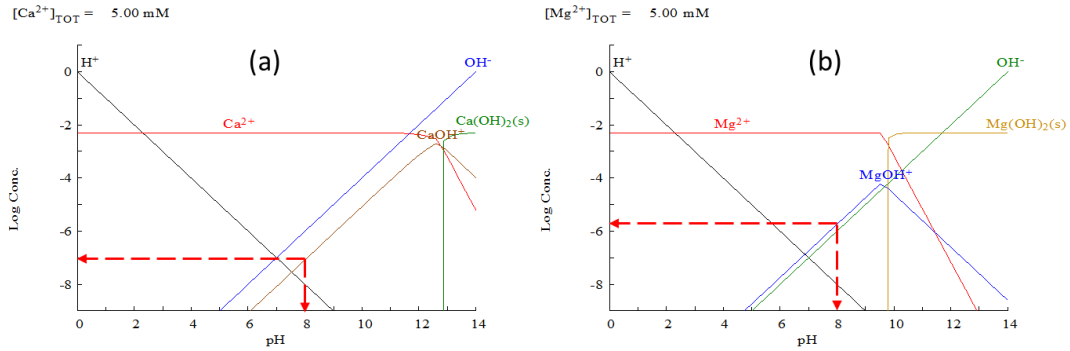

Figure 4−10. LogC−pH diagram of (a) calcium and (b) magnesium species; the calculations were performed using Medusa open−source software.

4.2.3 Adsorption of oleate on monazite

Figure 4−11 shows the influence of both monovalent and divalent ions on the adsorption of oleate on monazite surfaces. As seen in Figure 4−11, the increase in Ca^{2+} concentrations resulted in reduced adsorption of oleate due to the formation of insoluble calcium oleate (Figure 4−11(a)). The same trend was also observed in the presence of Mg^{2+} (Figure 4−11(b)); however, the adsorption of oleate in the presence of Ca^{2+} was significantly lower than that in the presence of Mg^{2+}. The increase in Na^{+} or K^{+} concentrations did not affect oleate adsorption considering that these monovalent ions did not react with oleate ions (Figure 4−11(c) and Figure 4−11(d)).

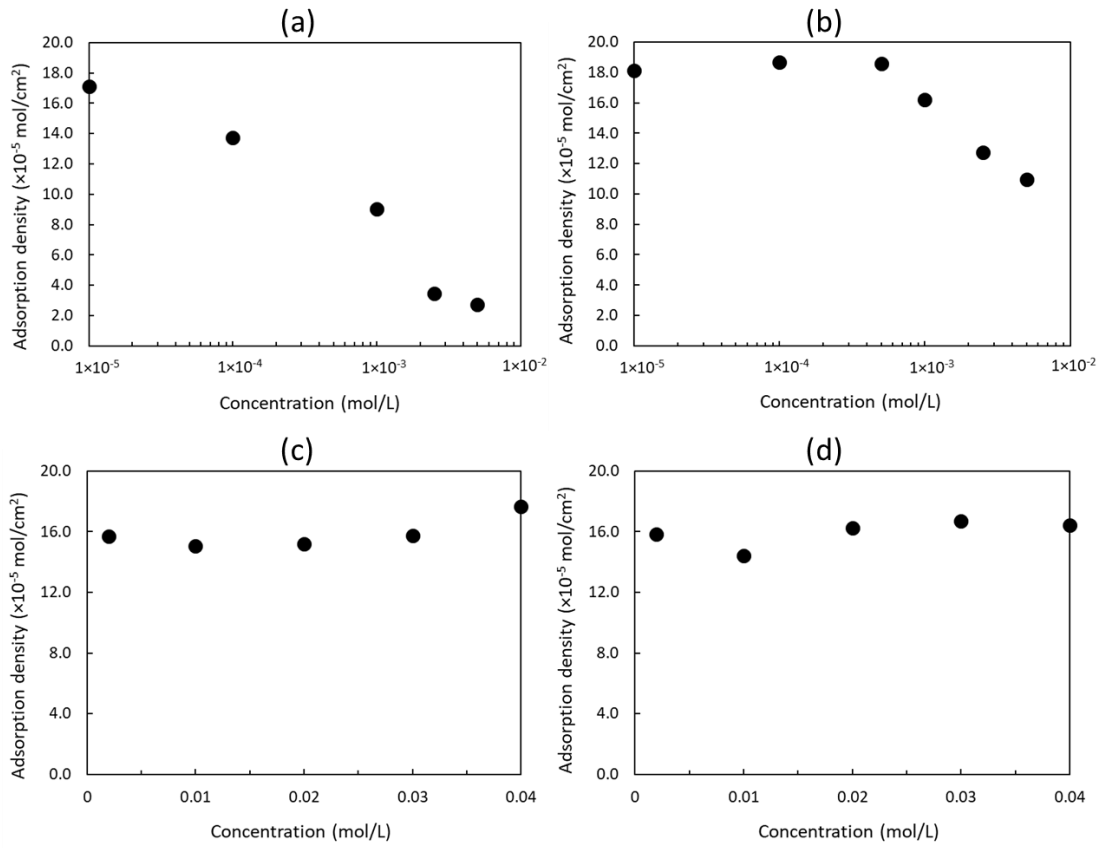

Figure 4−11. Effects of (a) $CaCl_2$, (b) $MgCl_2$, (c) NaCl, and (d) KCl on the adsorption density of oleate on monazite in the presence of 2×10^{-4} mol/L sodium oleate and 6×10^{-3} mol/L sodium silicate.

4.2.4 XPS analysis of monazite surface

Table 4−1 and Figure 4−12 show the elemental composition on monazite surfaces. As seen in Table 4−1 and Figure 4−12, when monazite particles were conditioned in the presence of sodium oleate in distilled water, the percentage of carbon (C 1s) on monazite surfaces was the highest probably due to high adsorption of oleate, which agrees well with the adsorption results obtained in this work (Figure 4−1). The percentage of carbon on monazite surfaces was lower in the oleate solutions in the presence of Ca^{2+} or Mg^{2+} probably due to the lower adsorption of oleate. This observation agrees well with our adsorption data (see Figure 4−11).

Table 4−1 also shows that the presence of Ca^{2+} led to slight adsorption of Ca^{2+} or calcium oleate. A similar trend was also observed in the presence of Mg^{2+} due to the adsorption of Mg^{2+} or magnesium oleate. It is noted that the monazite surface contains

Ca^{2+} as an impurity (see Table 3−1); therefore, the XPS spectrum of monazite + NaOL shows Ca^{2+} 2p peaks in Figure 4−12(c).

Table 4−1. Elemental composition on the surface of monazite before and after conditioning.

	Monazite + NaOL	Monazite + Na_2SiO_3 + NaOL + $CaCl_2$	Monazite + Na_2SiO_3 + NaOL + $MgCl_2$
C 1s	17.0%	10.8%	9.9%
O 1s	58.1%	66.6%	65.3%
Ca 2p	1.9%	2.2%	1.9%
Mg 1s	1.5%	1.5%	2.0%
Al 2p	2.8%	2.2%	2.5%
Ce 3d	5.7%	5.0%	5.7%
La 3d	3.1%	2.7%	3.1%
P 2p	9.1%	8.4%	9.0%

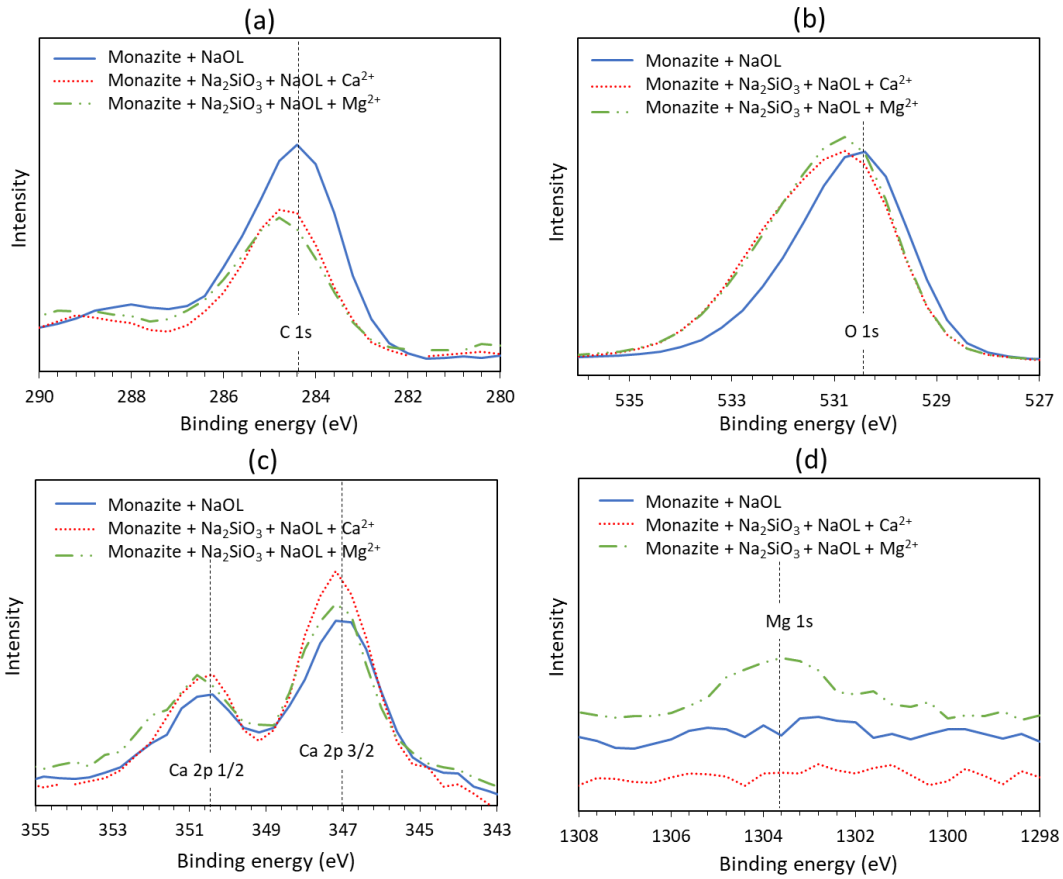

Figure 4−12. XPS spectra of monazite conditioned in 2×10^{-4} mol/L sodium oleate, 6×10^{-3} mol/L sodium silicate, 5×10^{-3} mol/L calcium chloride, or 5×10^{-3} mol/L magnesium chloride; (a) C 1s, (b) O 1s, (c) Ca 2p, and (d) Mg 1s.

4.3 Chapter summary

This paper investigated the monazite flotation mechanism with an oleate collector in the presence of different ions (Ca^{2+}, Mg^{2+}, Na^{+}, and K^{+}) by integrated microflotation and surface characterization analysis using zeta potential, XPS and UV adsorption. It was found that the presence of Mg^{2+} or Ca^{2+} were highly unfavourable to monazite flotation due to the formation of insoluble products with divalent metal ions, leading to less adsorption of oleate ions on monazite surfaces and hence reduced flotation recovery of monazite. The presence of Na^{+} or K^{+} influenced the flotation recovery of monazite slightly considering that these ions do not react with oleate ions. All these results were confirmed using adsorption experiments, XPS analysis and zeta potential measurements. A significant amount of further work is required to investigate the effect of various ions on flotation performance of different RE minerals such as bastnaesite and xenotime.

Chapter 5. Influence of cations on the rare earth phosphate mineral flotation*

5.1 Introduction

Previous studies have often examined the effect of dissolved ions from gangue minerals on the flotation recovery of pure single minerals using the microflotation experiments (Jung et al., 2022). However, there is limited information about investigating the effects of Ca^{2+} and Mg^{2+} on the flotation of ore bearing RE minerals. Moreover, further studies are needed to understand the possible interactions between Ca^{2+} and Mg^{2+} and Na_2SiO_3 to quantify the effect of divalent cations on the flotation operation of RE minerals. Thus, this chapter was aimed at investigating the effects of divalent cations such as Ca^{2+} and Mg^{2+} on the flotation of RE minerals by simulating the flotation circuit. The effects of divalent cations were investigated using the bench scale flotation experiments in the presence of different concentrations of Ca^{2+} and Mg^{2+} using the fatty acid collector and Na_2SiO_3 depressant. Adsorption experiments, rheology measurement, and solution chemistry studies were carried out to better understand the possible mechanisms.

5.2 Results and discussion

5.2.1 Effect of divalent cations on the flotation performance

Figure 5−1 shows the effect of divalent cations (Ca^{2+} or Mg^{2+}) on the flotation recovery of RE minerals (Figure 5−1(a)) and FeO minerals (Figure 5−1(c)), and the grade of these minerals (Figure 5−1(b) and Figure 5−1(d)) in the presence of fatty acid and sodium silicate at pH 10. As seen in Figure 5−1(a), the recovery of RE minerals did not change significantly in the presence of divalent cations when the concentrations of $CaCl_2$ or $MgCl_2$ were less than 100 mg/L. However, the flotation recovery greatly

* The results in this chapter will be included in the following manuscript: Jung, M., Tadesse, B., Dick, C., Logan, A., Dyer, L., Albijanic, B., 2024. Understanding the role of water quality in separation of rare earth minerals from iron oxide minerals in a flotation circuit. *Minerals Engineering,* 205, 108461.

reduced when the concentrations of $CaCl_2$ or $MgCl_2$ were higher than 100 mg/L, particularly during the cleaning stage of flotation considering that in this stage, the grade of RE minerals is the highest (see Figure 5−1(b)). Figure 5−1 also shows that the increase in the concentration of divalent cations resulted in a higher FeO recovery, especially in the roughing and scavenging stages because in this stage, the grade of FeO minerals is the highest (see Figure 5−1(d)). The results also indicated that the flotation performance deteriorated more in the presence of Mg^{2+} than Ca^{2+}. Section 3.2. provides the explanations of the flotation mechanisms.

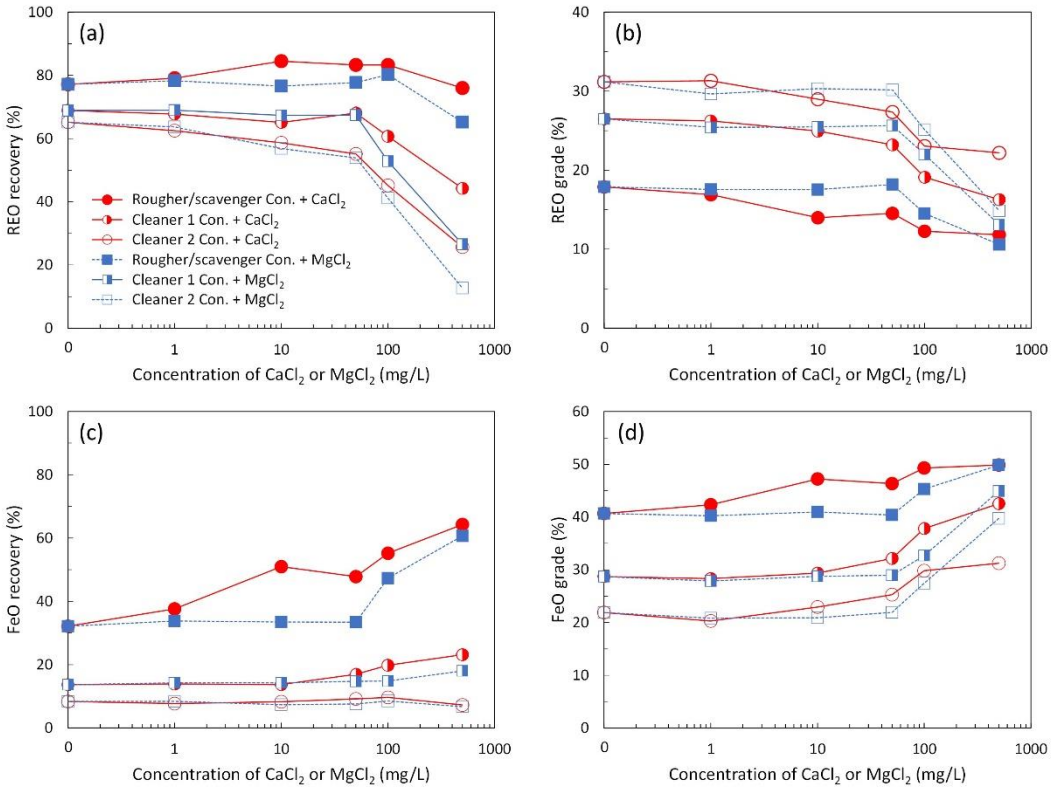

Figure 5−1. The effect of $CaCl_2$ and $MgCl_2$ on the (a) REO recovery (b) REO grade, (c) FeO recovery and (d) FeO grade.

5.2.2 Proposed flotation mechanism

Figure 5−2 shows the proposed adsorption mechanism on RE minerals after the grinding and before flotation in the presence and absence of divalent cations. It is worth mentioning that the predominant silicate species at pH 10 is monomeric silica ($SiO(OH)^{3-}$) (Hao et al., 2021). Therefore, it is hypothesized that the adsorption of

sodium silicate take place in the form of a silicate monomer. As seen in Figure 5−2(a) and Figure 5−2(c), after the grinding, SiO_3^{2-} rarely adsorbed on monazite surfaces while the opposite was true in the case of fatty acid based on the results obtained in our previous work using pure monazite in distilled water (Jung et al., 2022). Figure 5−2(b) shows that SiO_3^{2-} adsorbed on FeO surfaces during the grinding which agrees well with the literature (Davis et al., 2002; Dietzel, 2011; Hansen et al., 1994; Jordan et al., 2007; Swedlund and Webster, 1999; Yang et al., 2008), and thus oleate ions cannot be adsorbed on FeO surfaces as shown in Figure 5−2(d). A similar finding was reported by (Qi et al., 1993), where the presence of adsorbed SiO_3^{2-} on hematite surface hindered the adsorption of oleate.

When the divalent cations are added to the flotation pulp during the conditioning process (Figure 5−2(e)), in the case of monazite, divalent cations react with the fatty acid collector, leading to the formation of insoluble products (e.g., $Ca(RCOO)_2$ or $Mg(RCOO)_2$) thus reducing the amount of available fatty acid collector ions in the pulp (Araújo and Lima, 2017). This is also supported in our previous works using pure monazite (Jung et al., 2022). Therefore, the increase in the concentration of divalent cations reduced the REO recovery (see Figure 5−1(a)). In the case of FeO minerals, the added divalent cations react with the adsorbed SiO_3^{2-} and act like a bridge between oxygen atoms of adsorbed SiO_3^{2-} and carboxylate ions (Figure 5−2(f)), increasing adsorption of fatty acid collector ions and thus recovery of FeO mineral. This mechanism was observed in the case of magnetite (Dixon, 1985; Potapova et al., 2010) and it is hypothesized that a similar mechanism occurred on FeO minerals. It means that the higher the concentration of divalent cations, the higher the recovery of FeO (see Figure 5−1(c)).

Figure 5−1 also shows that the recovery values of RE minerals and FeO minerals are higher in the presence of Ca^{2+} than that in the presence of Mg^{2+}. It means that both RE minerals and iron minerals are more hydrophobic in the presence of Ca^{2+} than in the presence of Mg^{2+}. The reason is that Ca^{2+} binds stronger to oxygen atoms in fatty acid collector ions than Mg^{2+} (see Figure 5−3) considering that the solubility product of calcium oleate was 40 times lower than that of magnesium oleate (Jung et al., 2022). By contrast, magnesium atoms prefer binding to oxygen atoms in SiO_3^{2-} than calcium atoms (see Figure 5−3) because the solubility product of magnesium silicate

precipitate was significantly lower than that of calcium silicate (Nied et al., 2016; Yuehua et al., 2003).

The affinity of SiO_3^{2-} for divalent cations such as Ca^{2+} and Mg^{2+} on mineral surfaces is often reported in literatures (Chen and Tao, 2005; Marinakis and Shergold, 1985; Rao et al., 1989). Rao et al. (1989) demonstrated the preferential adsorption of polymeric silica onto Ca^{2+} sites on the calcite surface, leading to the reduced flotation recovery of calcite. Marinakis and Shergold (1985) also explained the adsorption of SiO_3^{2-} on calcite surface was due to the chemical interaction between silicic acid ($Si(OH)_4$ or $SiO(OH)_3^-$) and Ca^{2+} cationic surface site. Chen and Tao (2005) showed that the depression effect of Na_2SiO_3 was more pronounced for magnesite than for dolomite, implying a stronger affinity of SiO_3^{2-} for Mg^{2+} compared to Ca^{2+}. These finding suggest that when Ca^{2+} or Mg^{2+} adsorb onto the surface of RE minerals, they can enhance the affinity of SiO_3^{2-} for these mineral surfaces, leading to the reduced flotation recovery. Cao et al. (2022) showed that the flotation recovery of bastnaesite was notably reduced when both Ca^{2+} and SiO_3^{2-} coexisted in the flotation pulp, compared to when either Ca^{2+} or SiO_3^{2-} was introduced individually. This reduction was attributed to the enhanced adsorption of SiO_3^{2-} caused by the formation of the hydrophilic $Ca{-}SiO_3$ complex on the surface of bastnaesite.

It is also true that the adsorption of SiO_3^{2-} can enhance the adsorption of Ca^{2+} and Mg^{2+}, which may lead to the increased flotation recovery of minerals. For instance, it has been widely studied that the adsorption of Ca^{2+} can improve the flotation recovery of various oxide minerals, such as spodumene, calcite, fluorite, and quartz (Filippov et al., 2019; Free and Miller, 1996; Hao et al., 2018; Liu et al., 2015; Ren et al., 2018). However, the underlying mechanism remains a topic of debate. Two possible explanations are: 1) the increase in active sites for collector adsorption due to Ca^{2+} adsorption, and 2) the adsorption of Ca−dioleate precipitates on mineral surfaces. Despite variations in the minerals examined in this study compared to those in the literature, the results validate the suggested mechanism wherein SiO_3^{2-} adhering to Fe mineral surfaces can form binding interactions with Ca^{2+} or Mg^{2+}. As a result, it led to the increased flotation recovery of Fe mineral.

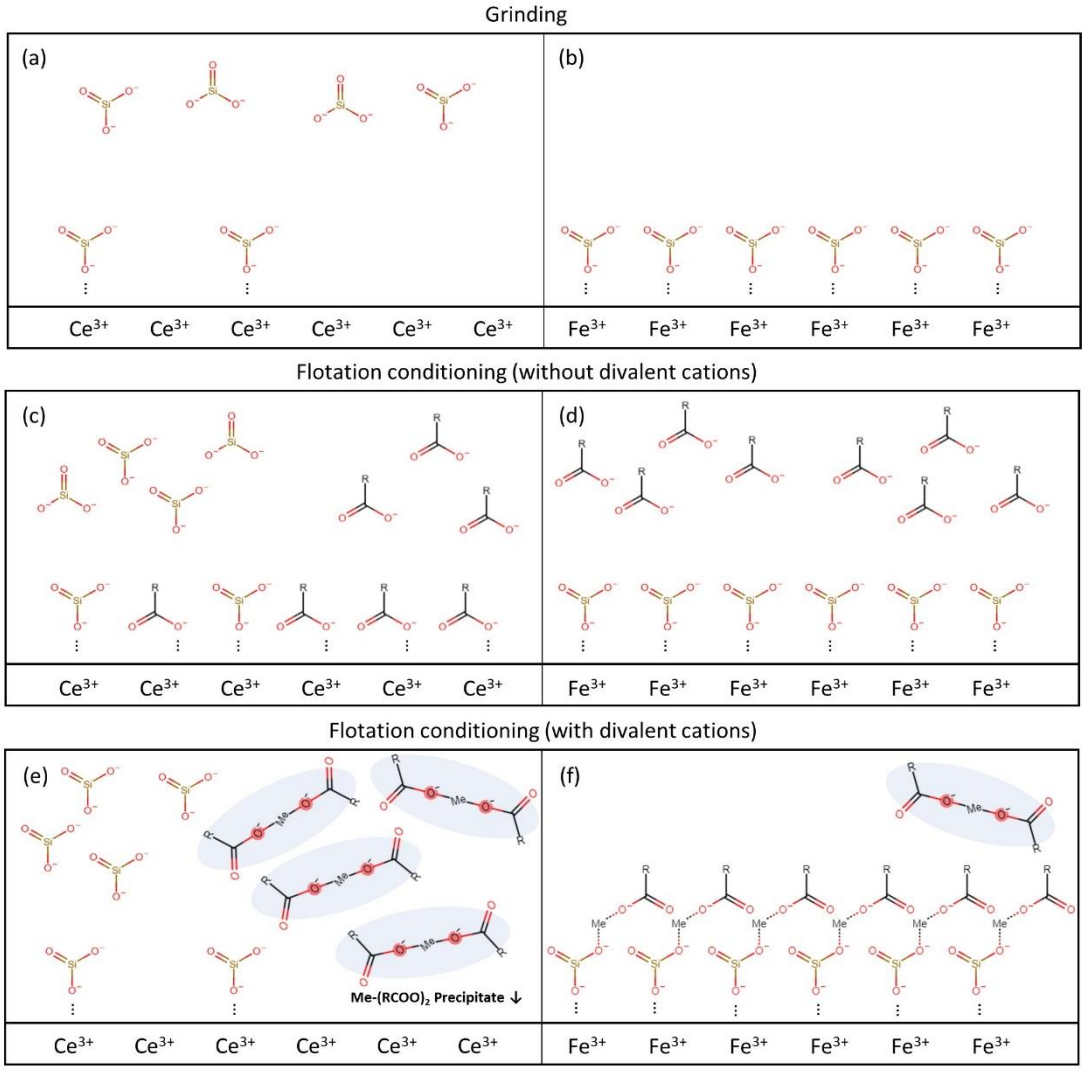

Figure 5−2. The adsorption mechanism of SiO_3^{2-}, divalent cations and carboxylate ion (Me denotes divalent cations such as Ca^{2+} and Mg^{2+}).

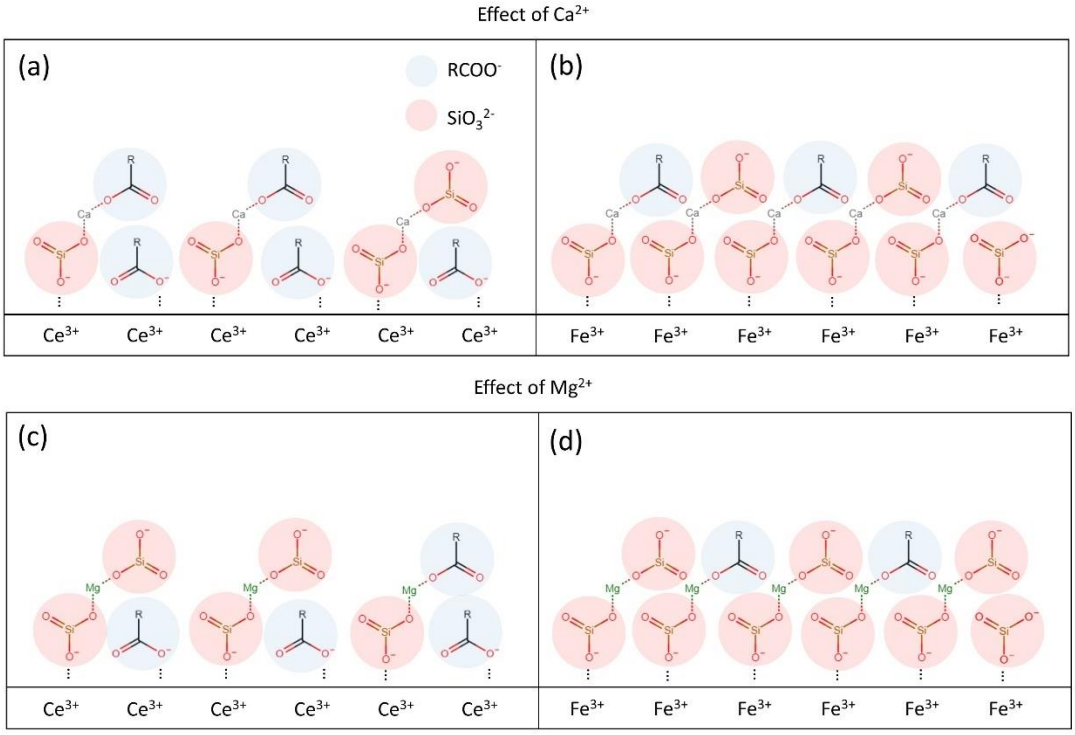

Figure 5−3. The effect of Ca^{2+} or Mg^{2+} on the synergistic adsorption of SiO_3^{2-} and fatty acid ions on RE minerals and iron oxide mineral surfaces; the effect of Ca^{2+} on the (a) RE mineral and (b) iron oxide mineral surface, and the effect of Mg^{2+} on the (c) RE mineral and (d) iron oxide mineral surface.

5.2.3 Effect of divalent cations on fatty acid concentration

Figure 5−4 presents the influence of different concentrations of divalent cations, Ca^{2+} and Mg^{2+}, on the concentration of fatty acid in the flotation pulp at pH 10. The results show that when the concentration of $CaCl_2$ or $MgCl_2$ are less than 100 mg/L, the concentration of dissolved fatty acid collector remains unchanged. However, when the concentration of $CaCl_2$ or $MgCl_2$ increased beyond 100 mg/L, the concentration of dissolved fatty acid collector decreases significantly, leading to a lower flotation recovery of RE minerals (see Figure 5−1). This is probably because at lower concentrations of Ca^{2+} and Mg^{2+}, the added divalent cations are adsorbed onto the mineral surfaces. This was proved by the observation that the concentration of Ca^{2+} or Mg^{2+} did not increase when the less than 100 mg/L of $CaCl_2$ or $MgCl_2$ were added into the flotation pulp as seen in Figure 5−6. At higher concentrations of these cations, the amount of added divalent cations can exceed the maximum adsorption capacity of the

mineral surfaces. As a result, some of the Ca^{2+} or Mg^{2+} may remain dissolved in solution, as shown in Figure 5−6. Therefore, the reduction in fatty acid concentration in the flotation pulp was a result of the creation of insoluble compounds, such as $Ca(RCOO)_2$ or $Mg(RCOO)_2$, with extremely low solubility products, leading to the low Gibbs free energies (see Figure 5−5). It should be noted that the following calculation assumed a reaction between oleate ions and cations; detailed calculations are provided in the supplementary materials.

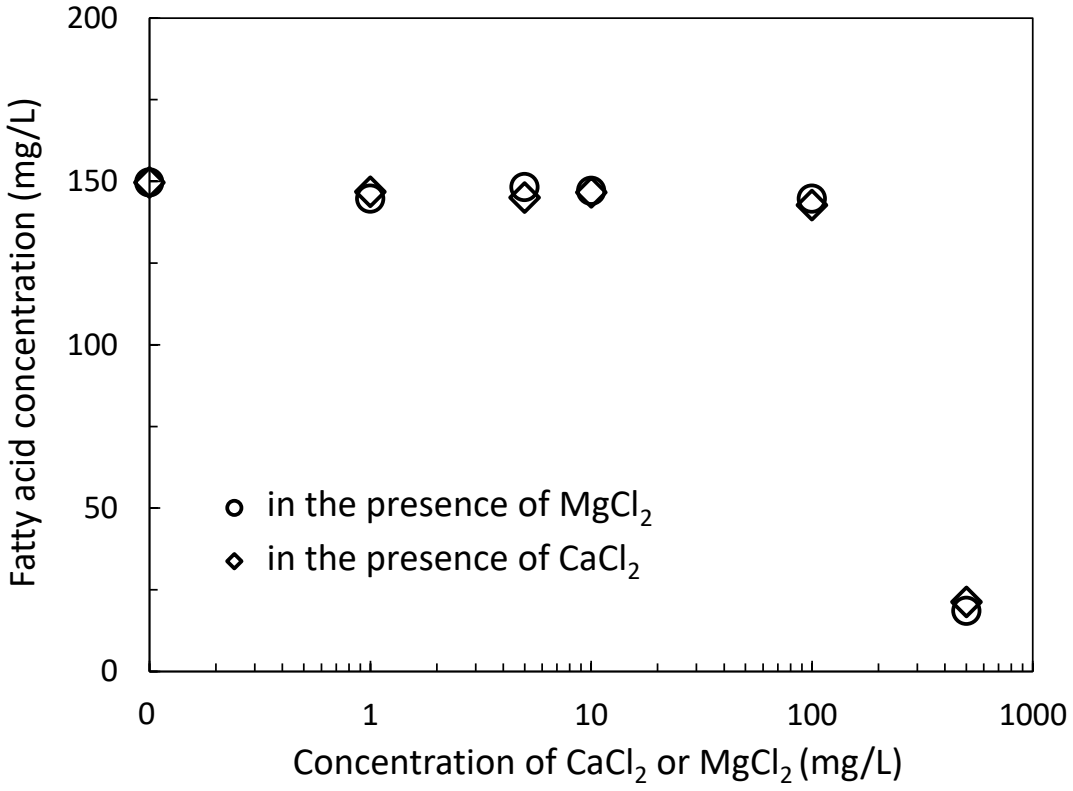

Figure 5−4. Effects of $CaCl_2$ and $MgCl_2$ concentrations on the fatty acid concentration.

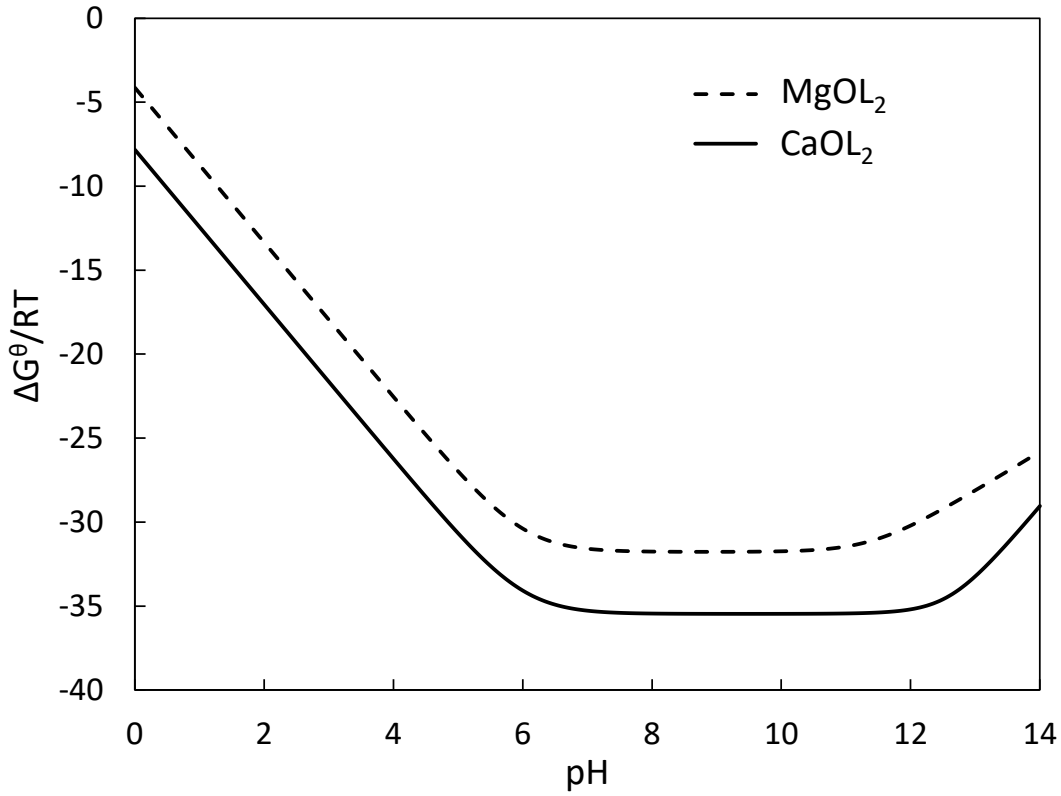

Figure 5−5. The free energy of the reaction between oleate ions and cations such as Ca^{2+} and Mg^{2+} by pH (Jung et al., 2022).

5.2.4 Effect of divalent cations on sodium silicate concentration

Figure 5−6 shows the impact of adding $CaCl_2$ and $MgCl_2$ on the concentrations of divalent cations in the rougher feed for concentrations ranging from 1 mg/L to 500 mg/L. The results demonstrate that when the concentration of $CaCl_2$ or $MgCl_2$ is less than 100 mg/L, an increase in divalent cations in the flotation pulp does not lead to a corresponding increase in the flotation pulp. This suggests that divalent cations are being adsorbed on the mineral surfaces, which may be due to SiO_3^{2-} already being adsorbed during grinding. The added divalent cations could then react with the adsorbed SiO_3^{2-} to form silicate salts ($CaSiO_3$ or $MgSiO_3$) on the mineral surfaces. However, at $CaCl_2$ or $MgCl_2$ concentrations above 100 mg/L, significant amounts of divalent cations can be found in the flotation pulp, and fatty acid ions may react with these cations.

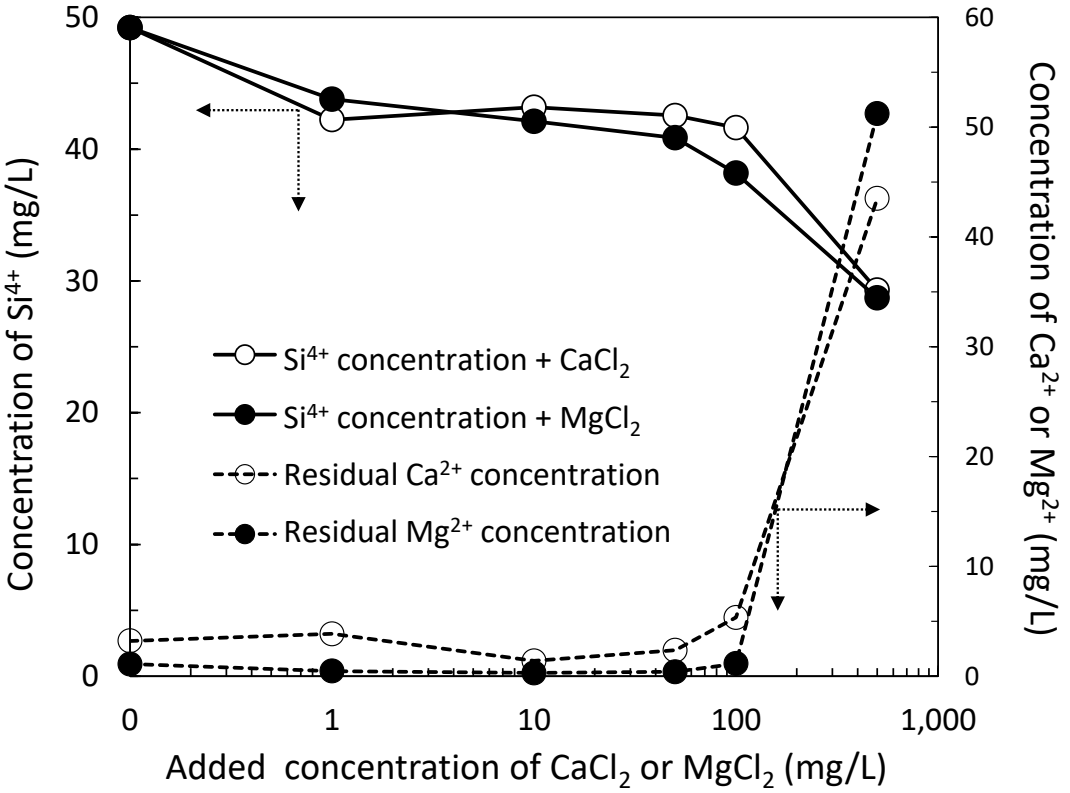

Figure 5−6. The residual concentration of Si^{4+} (primary axis) and divalent cations (secondary axis) in the presence of different concentration of $CaCl_2$ and $MgCl_2$ in the flotation pulp.

Figure 5−7 shows the Si^{4+} concentration measurements obtained in the presence of Ca^{2+} and Mg^{2+} in deionized water at pH 10. As illustrated in Figure 5−7, the concentration of Si^{4+} gradually decreased with the increasing Ca^{2+} and Mg^{2+} concentrations. The experimental results confirm that the concentration of Si^{4+} decreases more significantly in the presence of Mg^{2+} than Ca^{2+}. Moreover, almost all Si^{4+} were depleted from the solution when 500 mg/L Mg^{2+} were present, whereas some Si^{4+} remained in the presence of 500 mg/L Ca^{2+}. This observation is consistent with the species distribution diagrams (i.e., calcium−silicate, and magnesium−silicate system) shown in Figure 5−8, which indicates that $Mg_3Si_4O_{10}(OH)_2$ was more

prevalent than $CaSiO_3$. Thus, the results suggest that the binding of SiO_3^{2-} are more favourable to Mg^{2+} than those to Ca^{2+}.

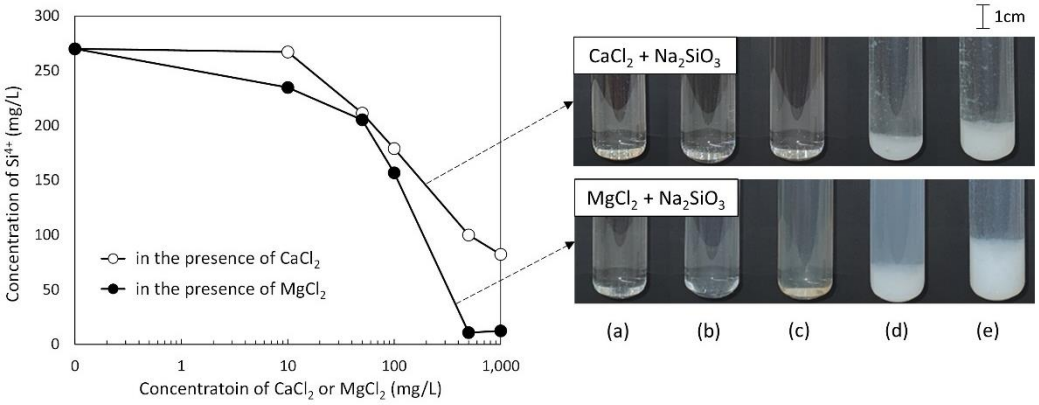

Figure 5−7. Sodium silicate solution behaviour with the initial concentration of 1000 mg/L when the concentration of $MgCl_2$ or $CaCl_2$ is (a) 10 mg/L, (b) 50 mg/L, (C) 100 mg/L, (d) 500 mg/L, and (e) 1000 mg/L.

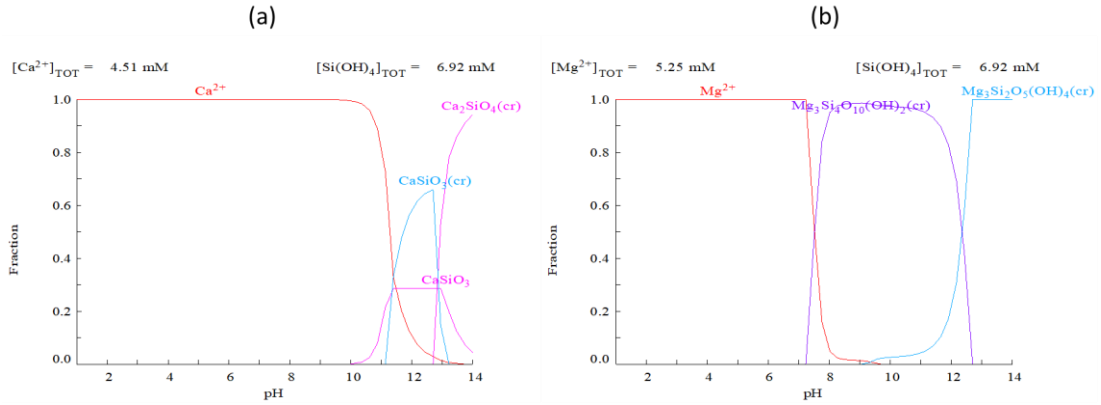

Figure 5−8. The species distribution diagram of calcium−silicate and magnesium−silicate system.

Figure 5−9 illustrates the changes in the free energy formation (ΔG^{θ}) between divalent cations and SiO_3^{2-} as a function of pH. As shown in Figure 5−9, the free energy formation for $Mg_3Si_4O_{10}(OH)_2$ was significantly lower than that for $CaSiO_3$, indicating that the formation of $Mg_3Si_4O_{10}(OH)_2$ was much more favourable than the formation of $CaSiO_3$ at pH 10. These findings are supported by measurements shown in Figure

5−7, which demonstrate that Mg^{2+} tend to consume more Si^{4+} than Ca^{2+}. Detailed calculations are provided in the supplementary materials.

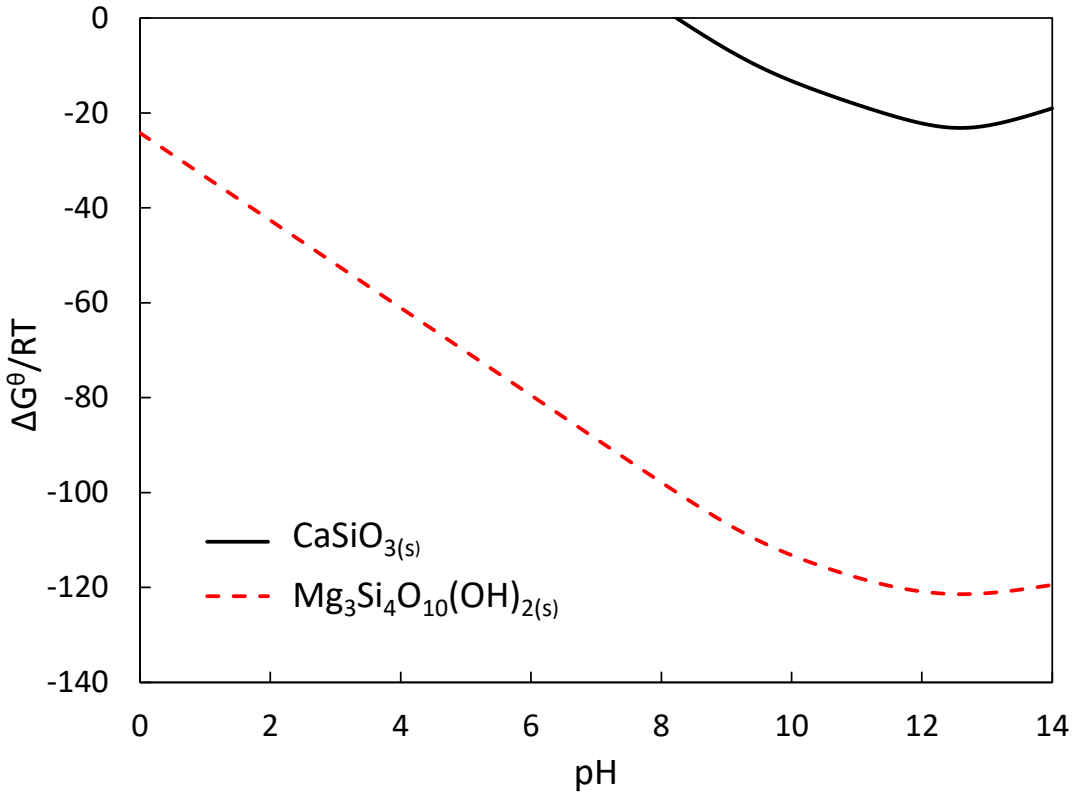

Figure 5−9. The free energy of the reaction between divalent cations and SiO_3^{2-} by pH.

5.2.5 Effect of $CaCl_2$ and $MgCl_2$ on the viscosity of flotation pulp

The rheological properties of flotation pulp are crucial for determining flotation performance. High pulp viscosity can reduce flotation efficiency by decreasing the motion of particles and bubbles and increasing bubble coalescence, and thus reducing the probability of particle and bubble collision (Becker et al., 2013; Sajjad and Otsuki, 2022). Therefore, in this study, the rheological measurements were carried out to investigate the effect of Ca^{2+} and Mg^{2+} on the rheological properties of flotation pulps.

Figure 5−10 presents the impact of $CaCl_2$ and $MgCl_2$ on flotation pulp rheology measurements at pH 10. As seen in Figure 5−10(a), the presence of $CaCl_2$ and $MgCl_2$ less than 100 mg/L does not affect pulp viscosity because there was no change in

interactions between particles in this experimental range. However, the viscosity of the pulp increases significantly in the presence of 500 mg/L $CaCl_2$ or $MgCl_2$, transforming the pulp from a Newtonian fluid to a Bingham plastic fluid (see Figure 5−10(b) and Figure 5−10(c)). This increase in pulp viscosity is likely caused by the reduced repulsion forces between particles resulting from the presence of divalent cations in the solution after 500 mg/L of $CaCl_2$ and $MgCl_2$ as seen in Figure 5−6. The increase in pulp viscosity resulted in a reduced flotation recovery (see Figure 5−1).

Sodium silicate is known for its ability to act as both a depressant and a dispersant. The dispersion of particles is mainly due to the adsorption of negatively charged silicate species on mineral surfaces at alkaline pH conditions, where monosilicate ($SiO(OH)^-$) becomes dominant (Hao et al., 2021). This results in an increase in electronegativity of the particles, leading to an increase in the repulsive forces between particles. On the contrary, the decreased magnitude of zeta potential of mineral particles can reduce the repulsive forces between particles, ultimately leading to the higher aggregation at near PZC where zeta potential becomes zero (Baldassarre et al., 2015). Farrokhpay and Zanin (2012) explained that the neutralisation of negative zeta potential resulted in the increase in the pulp viscosity due to the particle aggregation. Therefore, the observed increase in pulp viscosity was probably due to the compression of electric double layer by the presence of Ca^{2+} and Mg^{2+} in the flotation pulp as seen in Figure 5−6.

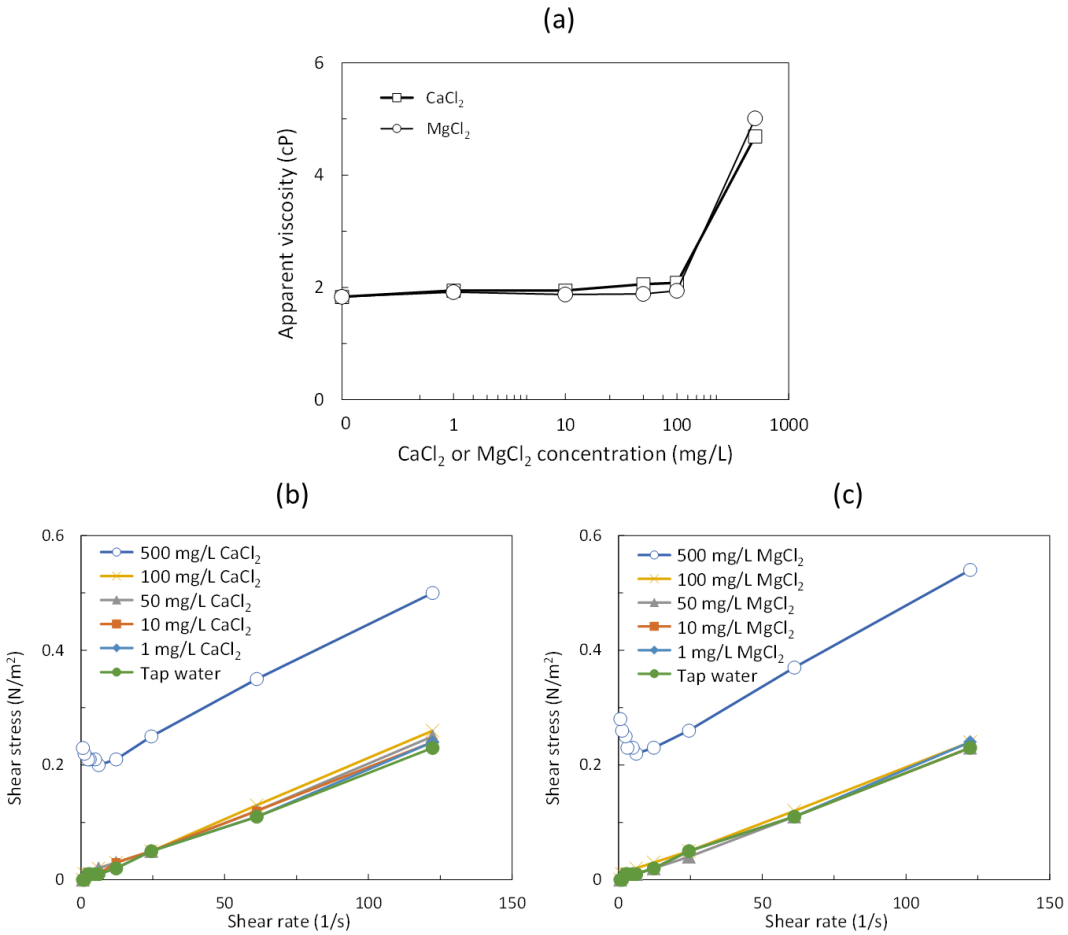

Figure 5−10. The effect of the different concentrations of divalent cations (a) on the apparent viscosity and on the shear stress in the presence of (b) $CaCl_2$ and (c) $MgCl_2$; The apparent viscosities were obtained at 100 s^{-1}, at which the average shear rate in the flotation cell is (Ralston et al., 2007).

5.3 Chapter summary

In this study, the effects of Ca^{2+} and Mg^{2+} on the flotation of RE minerals were investigated through multi−stage batch flotation experiments, adsorption experiments, rheological measurements, and solution chemistry. The results indicated that both Ca^{2+} and Mg^{2+} had a negative impact on the selectivity and recovery of RE minerals due to the chemical reaction between the divalent cations and the collector and depressant. The formation of insoluble calcium and magnesium carboxylate compounds resulted in the depletion of residual collector concentration and a lower RE recovery. Moreover, the divalent cations acted as a bridge between the oxygen atoms of the adsorbed SiO_3^{2-} and carboxylate ions. This resulted in an increased adsorption of fatty

acid collector ions, ultimately leading to a higher recovery of FeO. The negative impacts of Mg^{2+} were more pronounced compared to those of Ca^{2+}, perhaps because magnesium has a greater attraction for SiO_3^{2-} whereas calcium has a stronger preference for oleate. The presence of $CaCl_2$ or $MgCl_2$ increased the flotation pulp viscosity, which may be attributed to the reduced repulsion forces between particles due to the compression of the electrical double layer by the presence of divalent cations. This study highlights the significance of water quality in enhancing RE flotation.

Chapter 6. Influence of anions on the rare earth phosphate mineral flotation*

6.1 Introduction

The influence of dissolved cations on flotation of RE minerals have been examined by various studies(Cao et al., 2022; Espiritu et al., 2019; Jung et al., 2022; Wang et al., 2020b, 2020a; Zhang et al., 2017; Zhang and Honaker, 2018). However, there is no study investigating the influence of various anions on flotation of RE minerals. Therefore, the objective of this chapter was to investigate the effects of specific dissolved ions such as Cl^-, SO_4^{2-}, and HCO_3^- on changes in pulp properties and their subsequent impact on the flotation efficiency of RE minerals. Bench−scale flotation experiments were conducted to evaluate the effects of anions on RE flotation efficiency, closely simulating industrial flotation circuit conditions. Measurements of pulp viscosity, zeta potential, and settling experiments were performed to understand the underlying mechanisms during flotation and establish the relationship between the rheological properties of flotation pulp and the flotation efficiency of RE minerals.

6.2 Results and discussion

6.2.1 Flotation behaviour in the presence of different anions

The bench scale flotation experiments were performed to evaluate the effect of different anions on the flotation of RE ore using fatty acid collector and sodium silicate depressant at pH 10. Figure 6−1 shows the effect of NaCl, Na_2SO_4, and $NaHCO_3$ on the recovery of RE minerals (Figure 6−1(a)) and FeO minerals (Figure 6−1(b)) as well as the grade of these minerals (Figure 6−1(c) and Figure 6−1(d)). The results revealed that higher levels of anion concentrations caused a decrease in the recovery of RE minerals, while simultaneously increasing the recovery of FeO minerals. It is

* This chapter includes results from the following peer-reviewed publication: Jung, M., Tadesse, B., Dick, C., Logan, A., Dyer, L., Albijanic, B., 2023. Rheological properties of rare earth minerals flotation pulp in the presence of anions. *Journal of Rare Earths,* In press, https://doi.org/10.1016/j.jre.2023.10.006

important to note that the decrease in the recovery of RE minerals was more significant in the cleaner 2 stage, which had the highest grade of RE minerals. On the other hand, the increase in the recovery of FeO minerals was more prominent in the rougher/scavenger stages, which had the highest grade of FeO minerals.

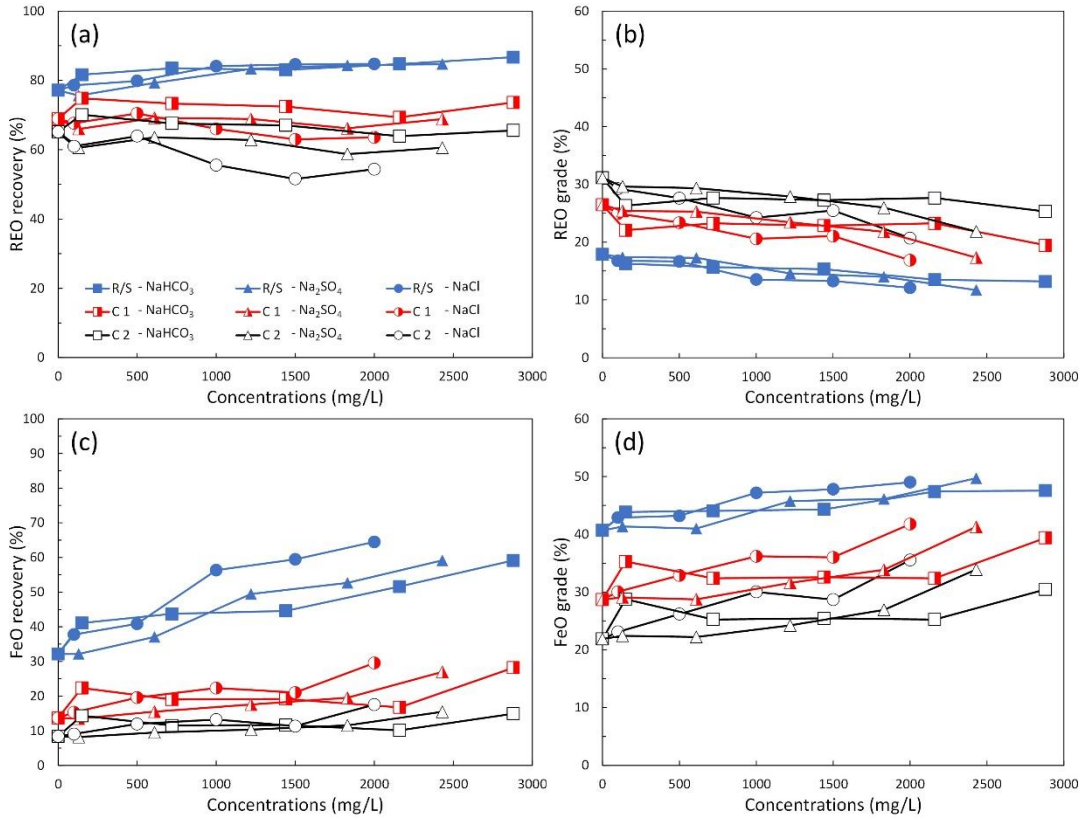

Figure 6−1. Effects of NaCl, Na_2SO_4 and $NaHCO_3$ on (a) REO recovery, (b) REO grade, (c) FeO recovery and (d) FeO grade; R/S, C1 and C2 denote the rougher/scavenger concentrate, cleaner 1 concentrate and cleaner 2 concentrate, respectively.

As shown in Figure 6−1(a), the largest decrease in the recovery of RE minerals in the cleaner 2 stage was observed when NaCl was added to the pulp, followed by Na_2SO_4 and $NaHCO_3$. Conversely, the recovery of FeO minerals in the rougher/scavenger stage increased the greatest in the presence of NaCl, followed by Na_2SO_4 and $NaHCO_3$ as seen in Figure 6−1(c). This results clearly shows that the flotation efficiency was adversely affected in the presence of dissolved anions such as NaCl, Na_2SO_4 and $NaHCO_3$. Thus, the separation efficiency was reduced in the order of NaCl > Na_2SO_4> $NaHCO_3$ as seen in Figure 6−3(a); the separation efficiency was defined as the

difference between the recovery of RE minerals (R_m) and FeO minerals (R_g) as seen in Eq. 6-1, which was proposed by (Schulz, 1970).

$$\text{Separation efficiency (S.E.)} = \mathrm{R_m} - \mathrm{R_g} \tag{6-1}$$

In addition to examining the influence of NaCl, Na_2SO_4, and $NaHCO_3$ on the flotation experiments, the effects of KCl, K_2SO_4, and $KHCO_3$ were also investigated, and the findings are illustrated in Figure 6−2. The results consistently demonstrated that the presence of KCl, K_2SO_4, and $KHCO_3$ had a detrimental effect on the flotation experiments. Moreover, the negative impact followed a significant order of KCl > K_2SO_4 > $KHCO_3$; for example, the decrease of RE mineral recovery and the increase of FeO mineral recovery were significant in this order. Moreover, the separation efficiency decreased the most in the presence of KCl and the least in the presence of $KCHO_3$ as seen in Figure 6−3(b). It aligns with the results obtained from the flotation experiments conducted with NaCl, Na_2SO_4, and $NaHCO_3$.

It was hypothesized that the reduced flotation efficiency was the result of the changes in the rheology of the flotation pulp. Therefore, additional investigations were conducted in order to comprehensively examine the impact of these ions on the viscosity of the flotation pulp.

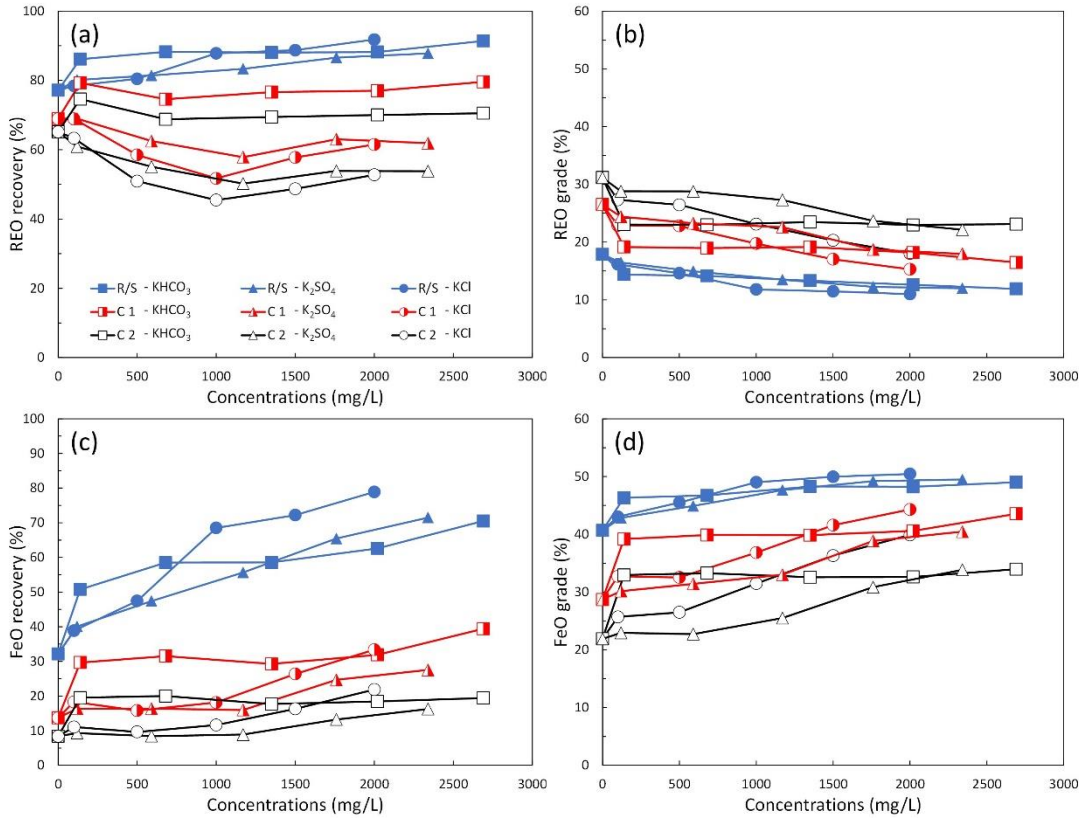

Figure 6−2. Effects of KCl, K_2SO_4 and $KHCO_3$ on (a) REO recovery, (b) REO grade, (c) FeO recovery and (d) FeO grade; R/S, C1 and C2 denote the rougher/scavenger concentrate, cleaner 1 concentrate and cleaner 2 concentrate, respectively.

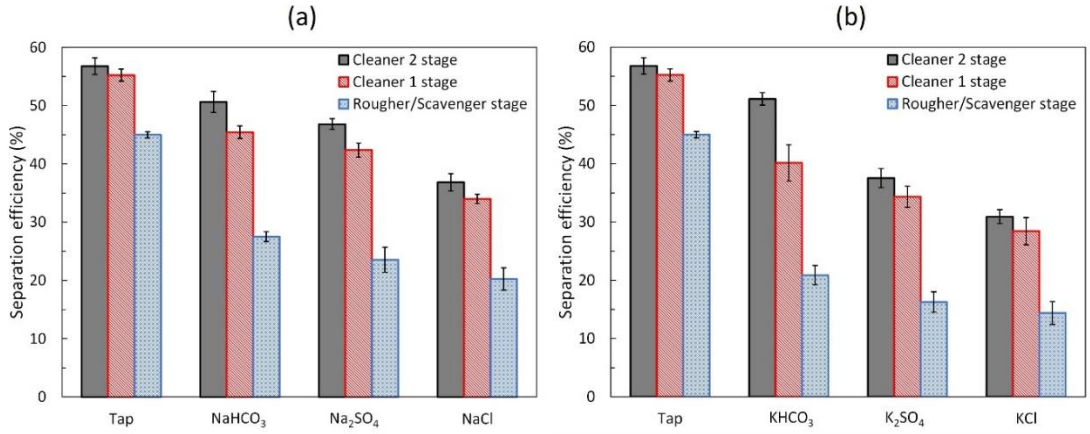

Figure 6−3. The separation efficiency in the presence of (a) NaCl, Na_2SO_4 and $NaHCO_3$ and (b) KCl, K_2SO_4 and $KHCO_3$.

6.2.2 Effect of anions on the viscosity of flotation pulp

Figure 6−4 illustrates the relationship between shear rate and apparent pulp viscosity in the presence of different concentrations of anions in the flotation pulp. As seen in Figure 6−4(a), a substantial increase in apparent viscosity was observed as the concentration of NaCl increased, followed by Na_2SO_4. However, the effect of $NaHCO_3$ concentration on the apparent viscosity was insignificant, which agrees well with literature (Özcan et al., 2003; Ozdemir et al., 2007). Similarly, Figure 6−4(b) showed that the increase in the pulp viscosity was the highest when KCl was introduced and the lowest when $KHCO_3$ was presented in the flotation pulp. These findings align with the flotation results shown in Figure 6−1 and Figure 6−2, demonstrating that the elevated pulp viscosity leads to a decrease in the flotation separation efficiency between RE minerals and FeO minerals.

It is postulated that the increase in pulp viscosity in the presence of anions can be attributed to the alteration of electrical double layer surrounding mineral particles, thereby affecting the electrostatic interaction forces between particles. For example, the reduced zeta potential of mineral particles results in a reduction of repulsion forces between particles (Laskowski, 1970; Laskowski et al., 1991; G. Li et al., 2017). As a consequence, the decrease in repulsion forces can lead to the increase in particle aggregation via the operation of van der Waals attraction forces, ultimately an elevation in pulp viscosity (Ancey and Jorrot, 2001; Chen et al., 2019; G. Li et al., 2017). Ong et al. (2008) showed that the maximum yield stress of aluminium oxide dispersion was achieved at near PZC where the van der Waals attraction forces are present only while electrostatic repulsion is absent. Given the significant influence of mineral particle zeta potential on pulp viscosity, a detailed investigation and discussion on zeta potential were conducted in section 3.4.

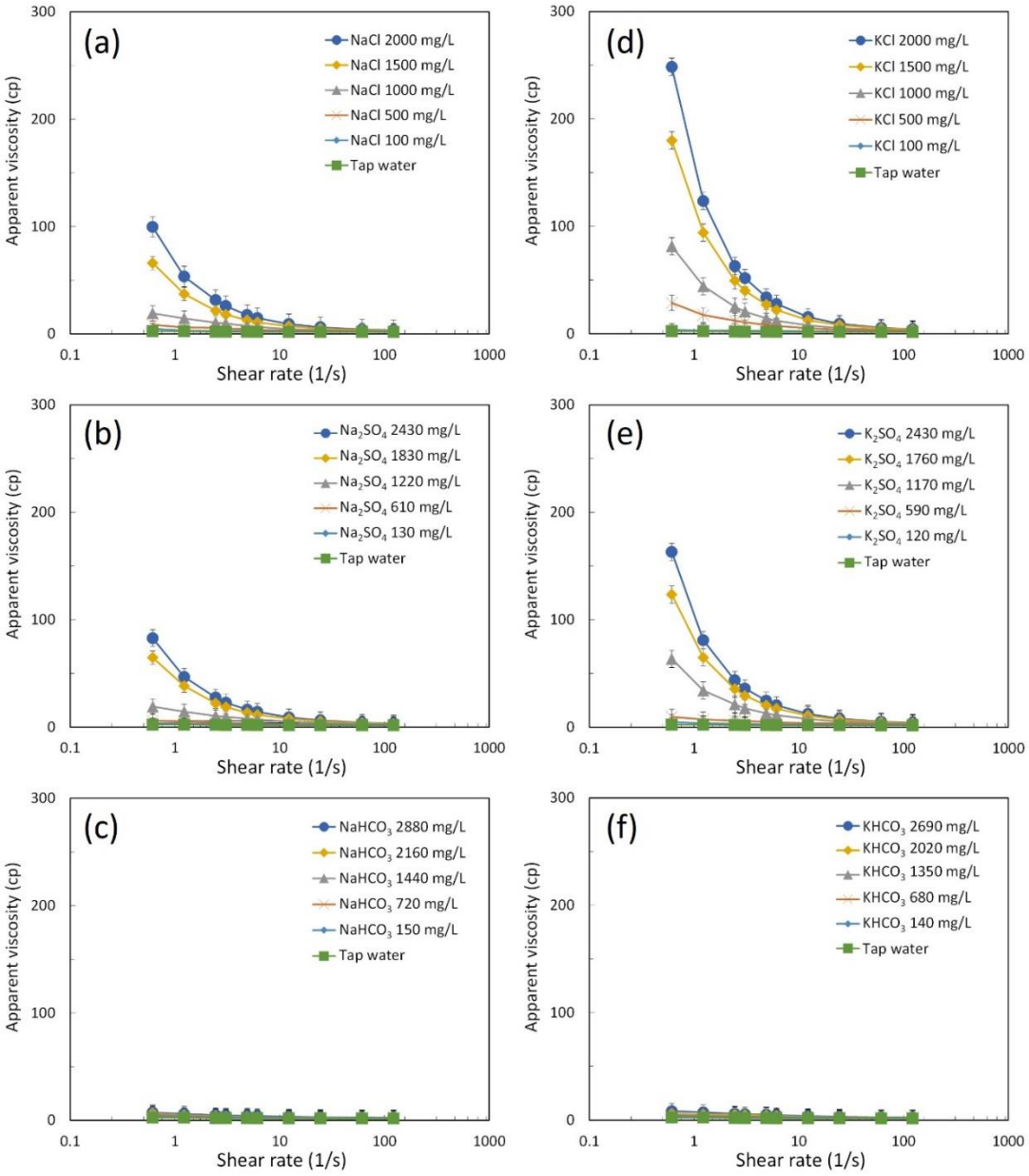

Figure 6−4. The effect of different concentrations of anions on the pulp viscosity.

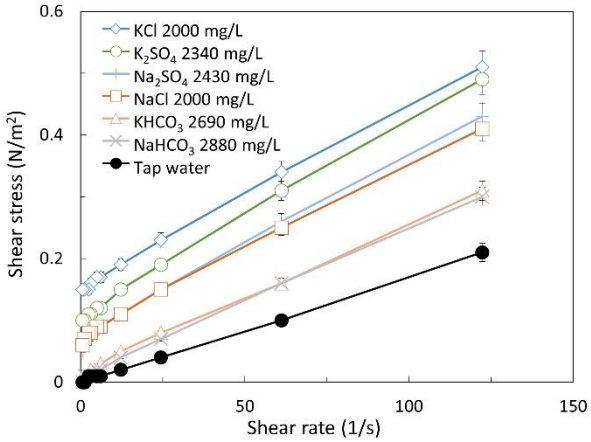

Figure 6−5. Rheogram of flotation pulp in the absence and presence of different types of anions.

The rheogram of the flotation pulp, both in the absence and presence of various anions, is shown in Figure 6−5. In the absence of anions and in the presence of HCO_3^-, the pulp exhibited Newtonian fluid characteristics, displaying a linear relationship between shear stress and shear rate without any yield stress. However, the introduction of Cl^- and SO_4^{2-} resulted in a transition from Newtonian behavior to Bingham plastic fluid properties, with the presence of yield stress observed. Notably, the yield stress was found to be higher in the presence of Cl^- compared to SO_4^{2-}. This change in fluid type from Newtonian to Bingham plastic has important implications for flotation efficiency, as it has been reported that such a transition can lead to an increase in non−selective gangue entrainment (W. Chen et al., 2017; Fu et al., 2018; Kirjavainen, 1992). Non−selective gangue entrainment can adversely affect the selectivity of the flotation process, reducing the efficiency of separating valuable minerals from unwanted gangue minerals.

6.2.3 Effect of anions on the entrainment

Figure 6−6 illustrates the impact of various anions on the degree of entrainment of mineral particles. The results indicate that the increase of entrainment was most pronounced when KCl was present, followed by K_2SO_4, NaCl, and Na_2SO_4. These findings align with the observed increase in pulp viscosity caused by these ions, where the magnitude of the viscosity increase followed the order of KCl > K_2SO_4 > NaCl > Na_2SO_4 (see Figure 6−4). However, the presence of high concentrations of HCO_3^- did not lead to a significant increase in the degree of entrainment. This observation can be

attributed to the fact that the pulp viscosity did not show a substantial increase when these ions were introduced into the flotation pulp, as depicted in Figure 6−4.

The correlation between pulp viscosity and entrainment suggests that the rise in pulp viscosity hindered the transportation of fine particles through the froth phase, resulting in a higher retention of particles within the froth and subsequent recovery. This is well agreed with literatures, showing that the increased pulp viscosity led to the increased entrainment of various minerals. For example, Kirjavainen et al. demonstrated that elevated yield stress in flotation pulp transformed the pulp into a Bingham plastic fluid, leading to increased gangue mineral entrainment (Kirjavainen, 1992). Fu et al. (2018) highlighted that higher pulp viscosity led to enhanced froth stability, thereby causing significant chlorite entrainment due to slower foam drainage. Similarly, Chen et al. (2017) observed that increased viscosity resulted in reduced copper mineral recovery due to increased entrainment of gangue minerals.

Fu et al. introduced an equation that combines the effects of gravity, capillary force, and viscous force to calculate the average velocity of fluidic cells present in the plateau border in froth, as shown in Eq. 6-2 (Fu et al., 2018).

$$u = \frac{1}{f\mu}\left(\rho g A + \left(\sqrt{3} - \frac{\pi}{2}\right)^{0.5} \frac{\gamma}{\sqrt{A}} \frac{\partial A}{\partial x}\right) \tag{6-2}$$

where f is a parameter related to the shape of the plateau border, μ is the pulp viscosity, ρ is the pulp density, g is the gravitational acceleration, A is the cross−sectional area of plateau border, γ is the tension of liquid surface, and x is the unit length of fluid cells.

In accordance with Eq (8), the higher pulp viscosity (μ) causes the slower average velocity of fluidic cells (u), thus the entrainment may be enhanced due to the slower rate of froth drainage.

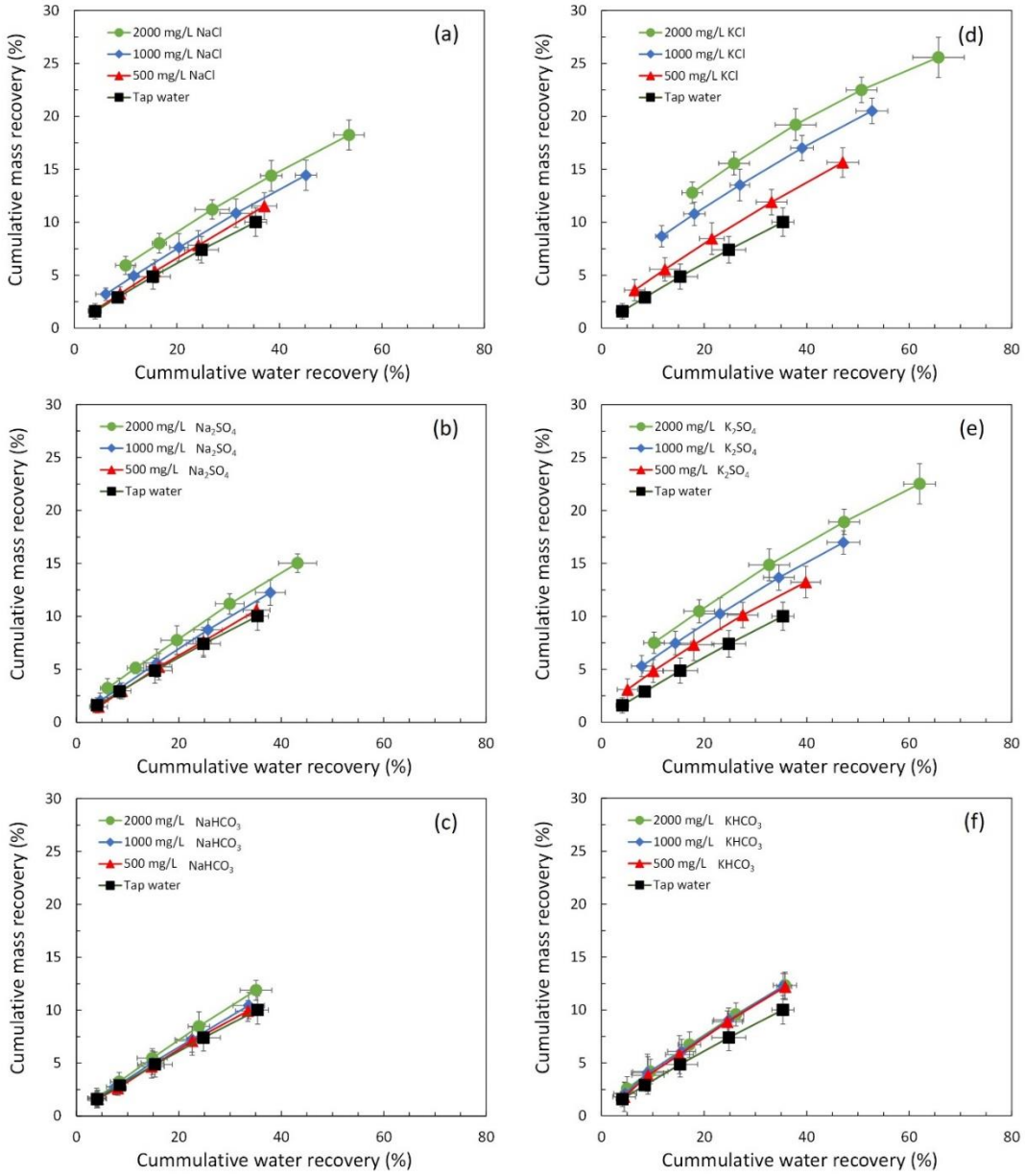

Figure 6−6. The degree of particle entrainment in the presence of (a) NaCl, (b) Na_2SO_4, (c) $NaHCO_3$, (d) KCl, (e) K_2SO_4 and (f) $KHCO_3$.

6.2.4 Effect of anions on zeta potential of mineral particles

The direct measurements of zeta potential of ore sample were found to be challenging due to the complex mineral composition of feed ore. To overcome the challenge, the zeta potential measurements were conducted using pure minerals such as monazite and

goethite. These minerals were selected as representatives of valuable and gangue minerals in the ore.

Figure 6−7 illustrates the results of zeta potential measurements conducted on pure monazite and goethite under various conditions, including both the absence and presence of different anions at pH 10. In distilled water at pH 10, the pure monazite and goethite minerals exhibited negative zeta potentials of −18.0 mV and −37.37 mV, respectively. The addition of sodium oleate and sodium silicate led to a more negative zeta potential of both minerals. This shift is attributed to the adsorption of anions such as OL^- and SiO_4^{2-} onto the surfaces of these minerals. When Cl^-, SO_4^{2-} and HCO_3^- were introduced in the solution, the shift of zeta potentials on both monazite and goethite minerals was also observed. The zeta potential decreased in the following order: $Cl^- > SO_4^{2-} > HCO_3^-$.

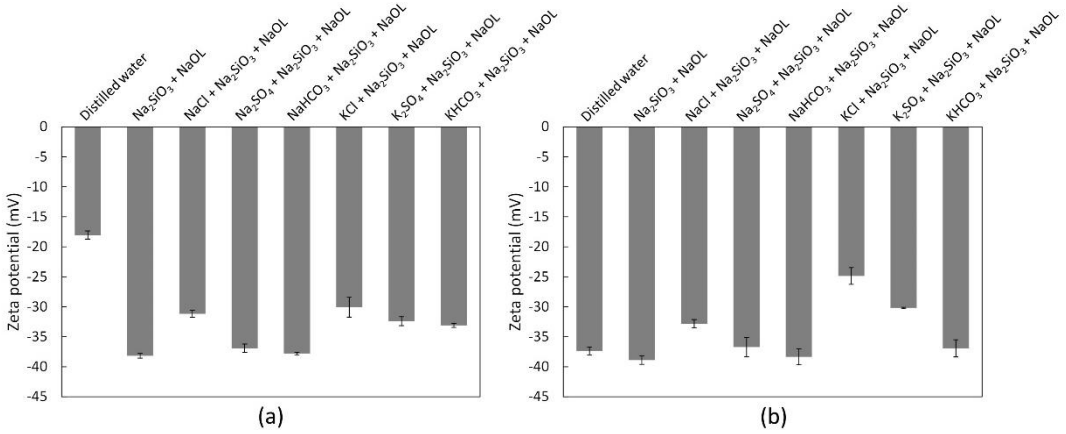

Figure 6−7. The zeta potential of (a) monazite and (b) goethite in the different condition at pH 10 ([Na_2SiO_3] = 3800 g/t and [NaOL] = 2200 g/t).

The introduction of Cl^- and SO_4^{2-} in the solution resulted in a significant shift of the zeta potential for both monazite and goethite to the less negative value. This observation may be attributed to the compression of the electrical double layer caused by the increased ionic strength in the solution, as reported in previous studies (Burns and Zydney, 2000; Zhao et al., 2005). Interestingly, it was noted that the shift in zeta potential was more pronounced in the presence of Cl^- compared to SO_4^{2-}. This finding contradicts the expected relationship between zeta potential and ionic strength, where higher ionic strength typically leads to a greater shift of zeta potential. In this study,

the ionic strength was higher in the presence of SO_4^{2-} than Cl^- , yet the shift in the zeta potential was greater for Cl^- (see Table 6−1). Similar observations were reported by Niriella et al. who found that the zeta potential of bentonite was more negative in the presence of 0.01 M Na_2SO_4 compared to 0.01 M NaCl, despite the higher ionic strength of Na_2SO_4 (Niriella and Carnahan, 2006). Additionally, Salgin et al. (2013) discovered that the zeta potential of polyethersulfone ultrafiltration membranes was more negative in the presence of 0.001 M K_2SO_4 compared to 0.001 M KCl within a pH range between 4 and 8. These results suggest that the zeta potential of mineral surfaces can be influenced not only by the ionic strength of a solution but also by type of anions. Tang and Wen (2019) proposed that SO_4^{2-} can adsorb through hydrogen bonding with hydroxyl ions on iron oxide mineral surfaces, whereas Cl^- tends to form outer−sphere complexes and remain highly hydrated within the diffusion ion swarm as seen in Figure 6−8. Therefore, the zeta potential in the presence of SO_4^{2-} was lower compared to that in the presence of Cl^-, which may be attributed to the adsorption of SO_4^{2-}.

Table 6−1. Ionic strength of solution in the presence of different salts.

	NaCl	KCl	Na_2SO_4	K_2SO_4	$NaHCO_3$	$KHCO_3$
Ionic strength	0.0342	0.0268	0.0513	0.0403	0.0288	0.0269

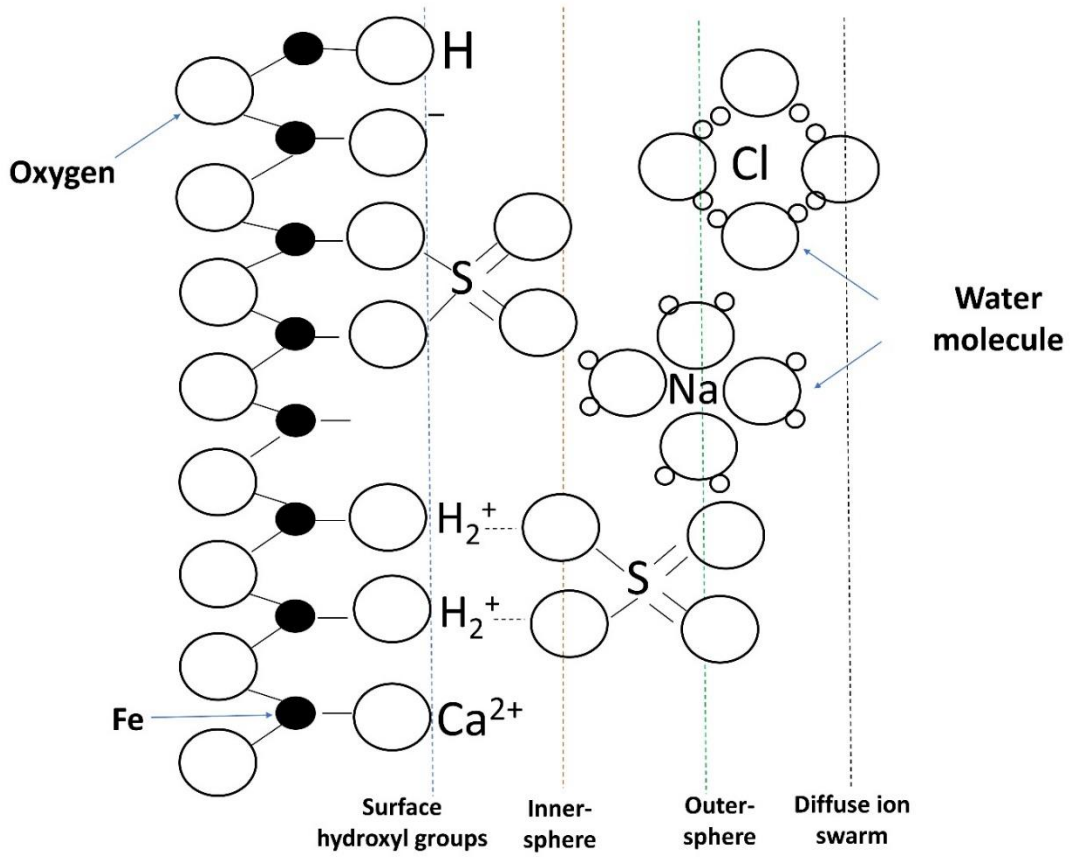

Figure 6−8. Schematic diagram of surface complex structure in hydrous iron oxide: surface hydroxyl groups, inner−sphere complexes, outer−sphere complexes, and diffuse Ion Swarm (Tang and Wen, 2019).

The impact of adding HCO_3^- to the solution had a lesser effect on the zeta potential of the minerals compared to Cl^- and SO_4^{2-}. This is likely due to the limited solubility of metallic carbonate compounds, as indicated in Table 6−2. Previous studies have reported that chemisorption occurs between CO_3^{2-} and lattice cations (such as Ce^{3+} and Fe^{2+}) on the mineral surfaces (Espiritu and Waters, 2018; D. Li et al., 2017). The reactions in Eq. 6-3 and Eq. 6-4 demonstrate that at pH 10, HCO_3^- exists in the form of HCO_3^- and CO_3^{2-}, as shown in Figure 6−9 (Castro, 2012). It was noted that CO_3^{2-} adsorb onto iron oxide surfaces (i.e., magnetite) through hydrogen bonding and form complexation with Fe ions (Roonasi and Holmgren, 2010).

$$H_2CO_3 \rightarrow H^+ + HCO_3^-,\ pK_{a1} = 6.352 \quad (6\text{-}3)$$

$$HCO_3^- \rightarrow H^+ + CO_3^{2-}, pK_{a2} = 10.329 \quad (6\text{-}4)$$

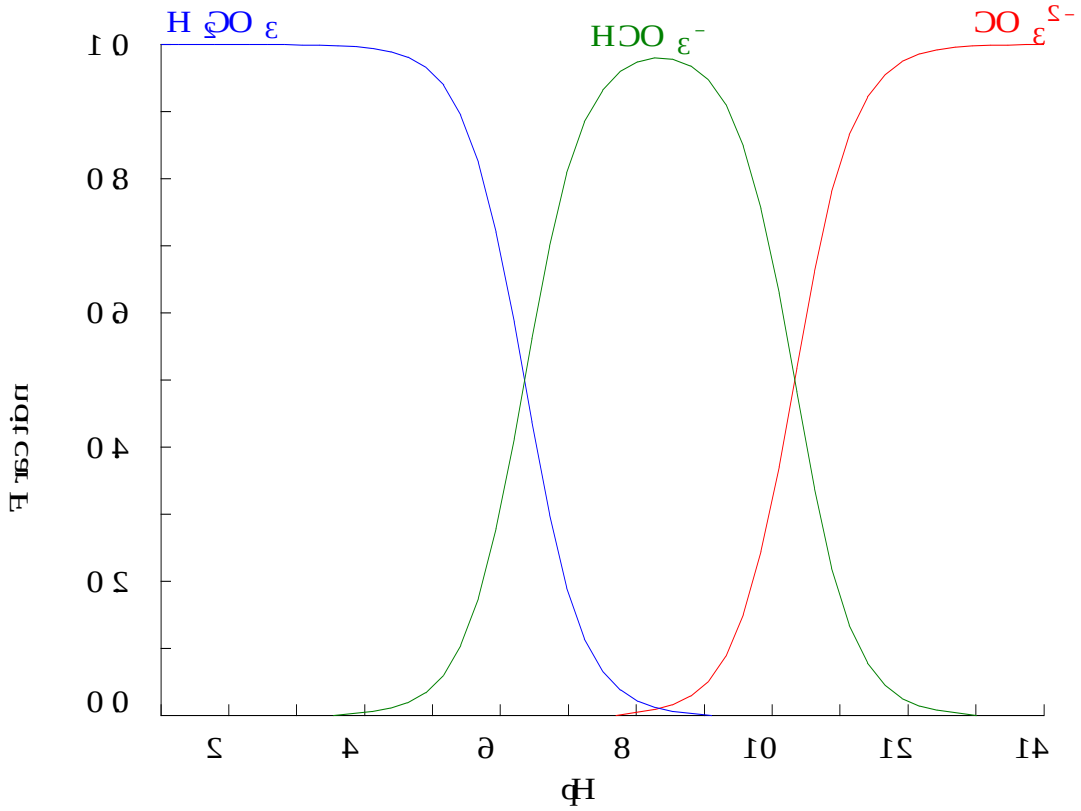

Figure 6−9. Species distribution diagram of carbonate species by pH.

Table 6−2. Chemical reactions and thermodynamic constants.

Chemical reaction	Equilibrium constant	References
$FeCO_{3(s)} \rightarrow Fe^{2+} + CO_3^{2-}$	$K_{sp} = 10^{-10.68}$	(D. Li et al., 2017)
$La_2(CO_3)_{3(s)} \rightarrow 2La^{3+} + 3CO_3^{2-}$	$K_{sp} = 10^{-29.91\pm0.05}$	(Firsching and Mohammadzadei, 1986)
$Ce_2(CO_3)_{3(s)} \rightarrow 2Ce^{3+} + 3CO_3^{2-}$	$K_{sp} = 10^{-21.80\pm0.05}$	(Ferri et al., 1983)

6.2.5 Effect of anions on settling behaviour of flotation pulp

Figure 6−10 presents the results of settling experiments conducted over 144 h in the presence and in the absence of anions (HCO_3^-, Cl^- and SO_4^{2-}). In the tap water, a large number of particles remained suspended, resulting in a significantly turbid flotation

pulp, as illustrated in Figure 6−11. However, when anions were present, the settling rate of particles was noticeably enhanced. The settling rates decreased in the following order: KCl > K_2SO_4 ≈ NaCl > Na_2SO_4 > $KHCO_3$ > $NaHCO_3$. This can be attributed to a decrease in the repulsive forces between particles due to the reduction in the zeta potential of mineral particles when these ions were present as seen in Figure 6−7. A few studies have shown that the presence of electrolyte ions can compress electrical double layers, which reduce the repulsive forces between mineral particles (Rattanakawin and Hogg, 2001; Wang and Peng, 2013). This phenomenon promotes the aggregation of particles in mineral suspensions, resulting in faster sedimentation rates. Figure 6−11 provides a visual demonstration of this effect, displaying photographs of flotation pulp taken over a period of 144 h. These photos provide clear evidence of the impact of anions on particle settlings, with a faster settling rate observed in the flotation pulp containing Cl^- and SO_4^{2-}, compared to those containing HCO_3^-.

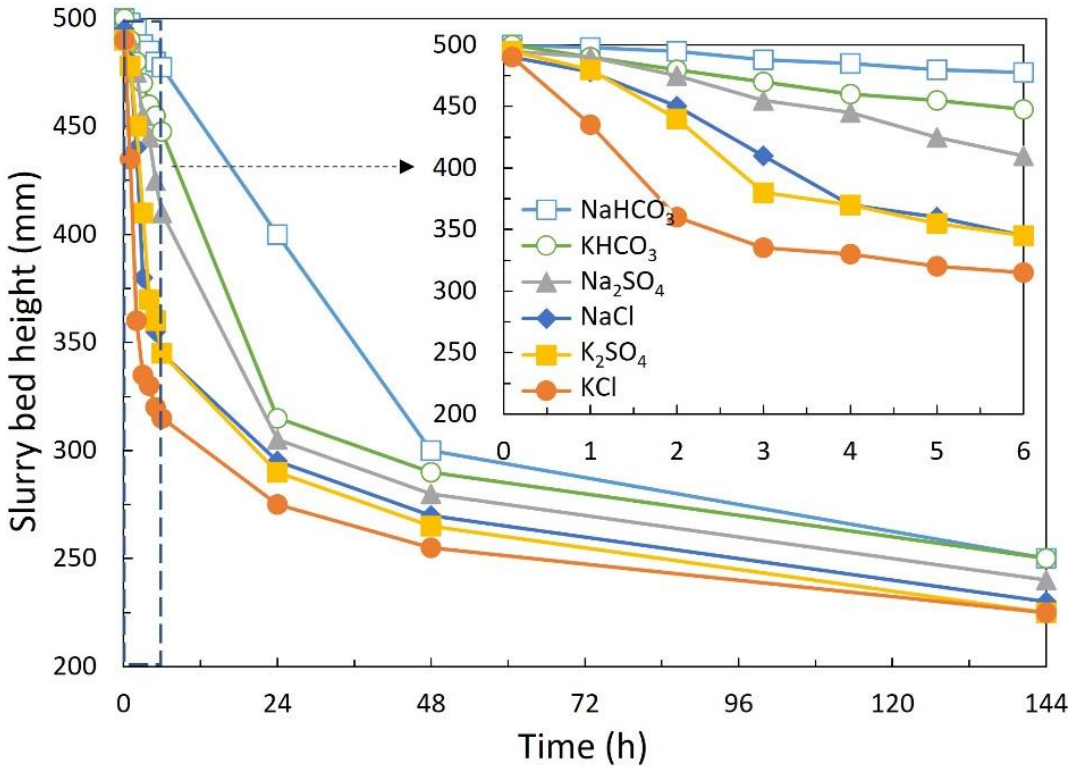

Figure 6−10. Settling behavior of flotation feed slurry in the presence of different anions.

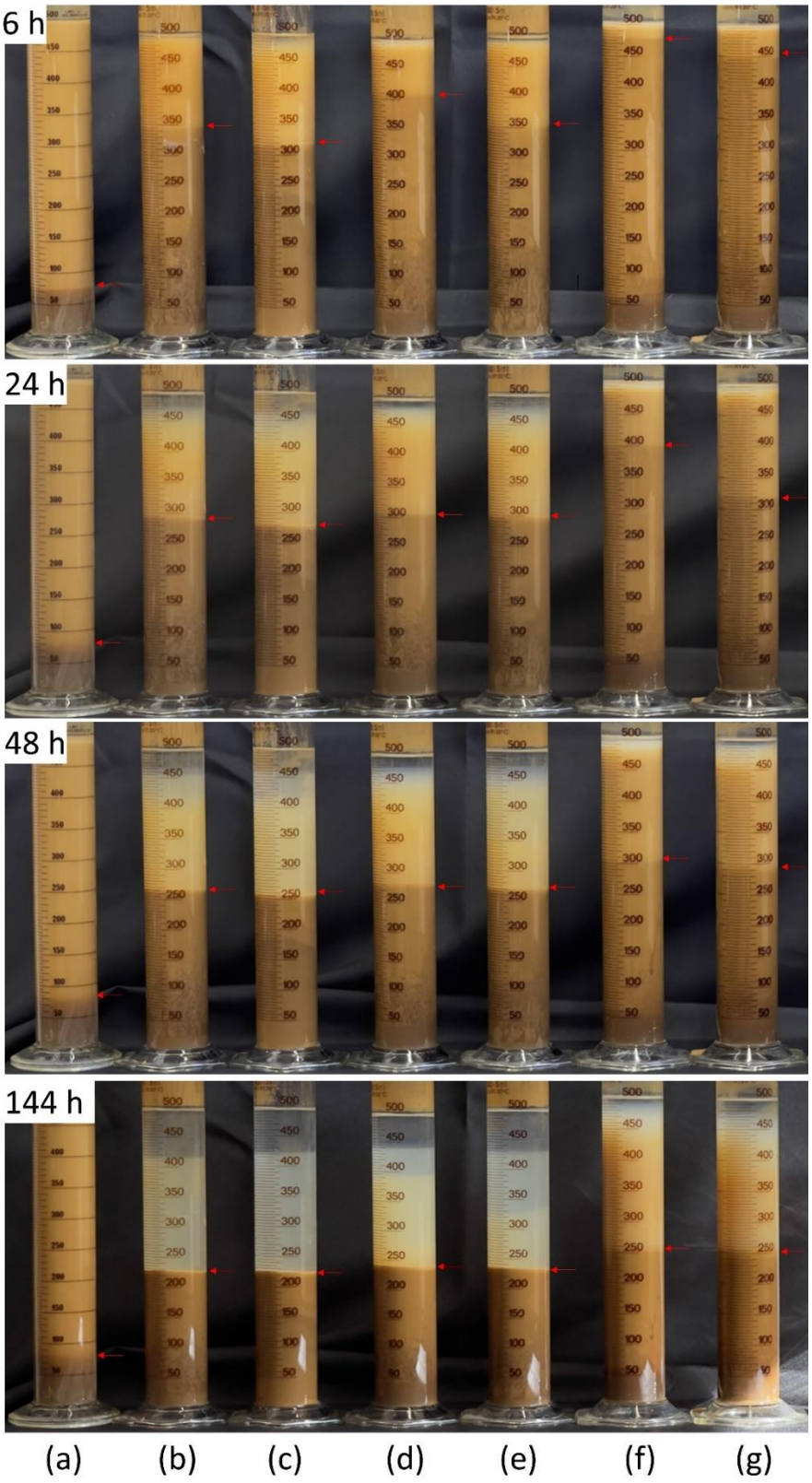

Figure 6−11. Photographs of flotation pulp after 6, 24, 48, and 144 h settling (a) in the absence of anions and in the presence of (b) NaCl, (c) KCl (d) Na_2SO_4, (e) K_2SO_4, (f) $NaHCO_3$ and (g) $KHCO_3$.

6.2.6 DLVO theory calculation

The total interaction energy between each mineral particles (i.e., monazite−monazite particles or goethite/goethite particles), based on the DLVO theory, is presented in Figure 6−12(a) and Figure 6−12(b), respectively. Figure 6−12 shows that the total interaction energy remains positive in the presence of SiO_3^{2-} and OL^- ions. This indicates that strong repulsive forces are the dominant force between the particles. Consequently, the settling of fine particles is slow, making the flotation pulp turbid even after 144 h, as illustrated in Figure 6−11(a).

When anions are added to the flotation pulp, there is a clear shift in interaction energy between particles. The total interaction energy between monazite particles decreases and becomes negative, indicating that attractive forces are dominant between these particles as shown in Figure 6−12(a). In the case of goethite particles, the total interaction energy decreases when Cl^- and SO_4^{2-} are present in the pulp; however, the addition of HCO_3^- resulted in repulsive interactions between these particles, making them suspended in the flotation pulp (see Figure 6−12(b)). In contrast, the presence of Cl^- and SO_4^{2-} increases the rate of particle settling, as seen in Figure 6−10.

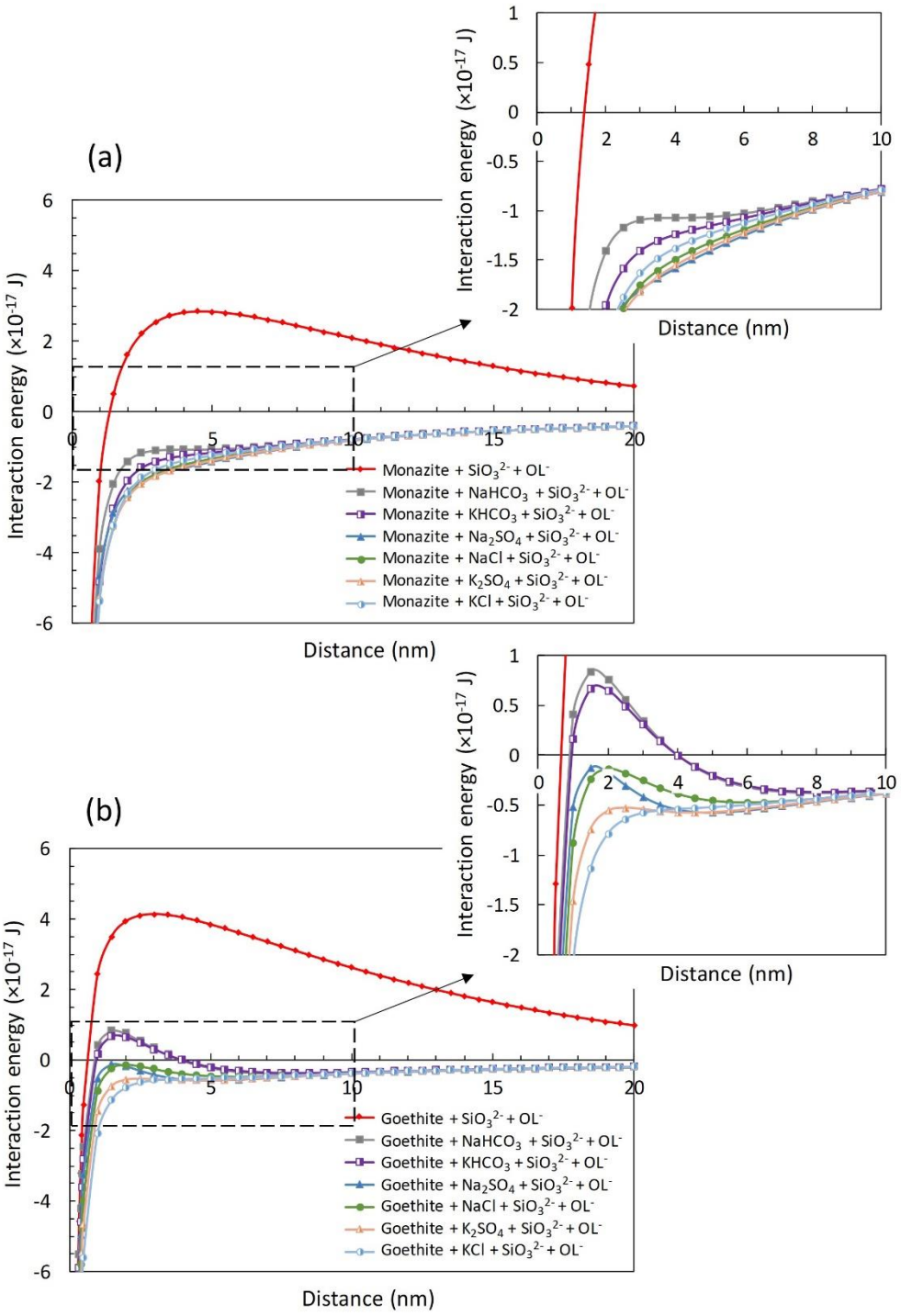

Figure 6−12. DLVO interaction energy between (a) monazite−monazite particles and (b) goethite−goethite particles.

6.3 Chapter summary

This chapter investigated the influence of anions, specifically Cl^-, SO_4^{2-}, and HCO_3^-, on the flotation performance of RE ore by integrating various techniques such as flotation experiments, rheology measurements, entrainment experiments, zeta potential measurements, settling experiments, and DLVO theory. The results revealed that an increased concentration of Cl^-, SO_4^{2-}, and HCO_3^- had an adverse effect on flotation efficiency, leading to a decrease in the recovery of RE minerals while increasing the recovery of FeO minerals. The presence of Cl^- had a particularly detrimental effect on the flotation of RE minerals, likely attributed to the significant increase in pulp viscosity. The reduction in zeta potential of fine particles in the presence of high concentrations of these ions appeared to be a critical factor contributing to the increase in pulp viscosity. The stronger the attractive forces between particles, the higher the pulp viscosity, leading to increased mechanical entrainment. These results were validated through settling experiments and calculations using the DLVO theory. This study emphasizes the importance of water quality in maximizing RE flotation efficiency.

Chapter 7. Fundamental study on the flotation behavior of goethite gangue mineral

7.1 Introduction

In Chapters 4, 5, and 6, comprehensive studies were undertaken to understand the impact of water quality on RE phosphate minerals using both monazite single minerals and RE ore samples. The primary findings revealed that the detrimental effects on monazite flotation were largely attributed to the presence of divalent cations, specifically Ca^{2+} and Mg^{2+}. These ions also played a role in reducing the recovery of RE minerals in bulk ore flotation experiments. Conversely, these ions led to an increase in the recovery of iron oxide gangue minerals, significantly affecting the selectivity towards RE minerals. While a mechanism was proposed for the increased recovery of iron oxide gangue minerals, the complex mineral composition in the mixed ore system made it challenging to definitively explain the flotation behavior of these iron oxide minerals. Therefore, there's a need to further investigate the flotation behavior of gangue minerals to quantify the effects of divalent cations such as Ca^{2+} and Mg^{2+}.

This chapter aimed to offer a focused analysis of the flotation behavior of goethite single minerals when exposed to divalent cations. Microflotation experiments were conducted to observe the flotation recovery of goethite minerals. To further comprehend the influence of divalent cations on goethite flotation, techniques such as zeta potential measurements, adsorption experiments, and XPS analysis were utilized.

7.2 Results and discussion

7.2.1 Flotation experiments of goethite

7.2.1.1 Effect of distilled water

Figure 7−1(a) illustrates the flotation recovery of goethite at varying pH levels, ranging from 2 to 12. The results indicate that the maximum recovery of goethite was achieved within the neutral to weakly alkaline pH range. According to the literature, the maximum recovery of goethite was observed at around pH 6 (Joseph-Soly et al., 2015), 8.5 (Rath et al., 2014), between 7 and 8 (Abeidu, 1976) when using sodium oleate

collector. The pH for optimal goethite recovery differed from these studies, likely due to variations in mineral history, surface characteristics, oleate dosage, and other factors. Since the surface of naturally occurring goethite is typically hydrophilic, recovery is intrinsically dependent on the adsorption of the collector. The species distribution diagram of oleate species reveals that the OL^-, $(OL)_2H^-$ and $(OL)_2^{2-}$ species become predominant within the neutral to alkaline pH range as presented in Figure 7−2. This supports the notion that goethite recovery is closely tied to the concentration of dissolved oleate species such as OL^-, $(OL)_2H^-$ and $(OL)_2^{2-}$ as reported in literature (Jung et al., 1987). Consequently, all experiments were conducted at pH 8, where dissolved oleate species, namely oleate ions (OL^-), dimers ($(OL)_2^{2-}$) and oleate acid soaps ($(OL)_2H^-$) were predominant.

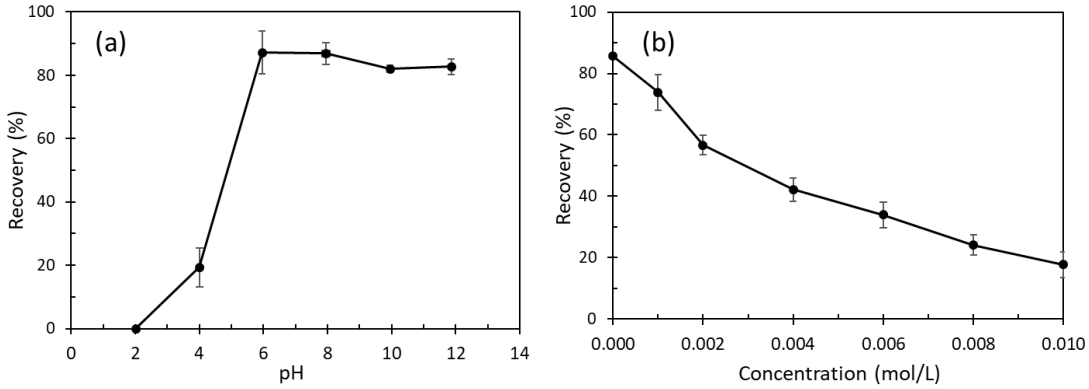

Figure 7−1. Effect of (a) pH and (b) sodium silicate at pH 8 on the recovery of goethite in the presence of 2×10^{-4} mol/L sodium oleate.

The effect of the concentration of sodium silicate on the flotation recovery of goethite was also investigated. Figure 7−1(b) showed that the recovery of goethite was gradually reduced with the increase of Na_2SiO_3 concentration, indicating that the more Na_2SiO_3 dosage can depress the more goethite recovery. However, it should be considered that the high dosage of sodium silicate can affect the recovery of the target minerals as well, thus the selectivity can be reduced (Abaka-Wood et al., 2019; Jung et al., 2022; Pavez and Peres, 1993; Zhang and Honaker, 2018). In the previous work, the recovery of monazite was depressed significantly in the presence of more than 0.006 mol/L Na_2SiO_3 dosage (Jung et al., 2022). Therefore, 0.006 mol/L of Na_2SiO_3 concentrate was used for all the experiments.

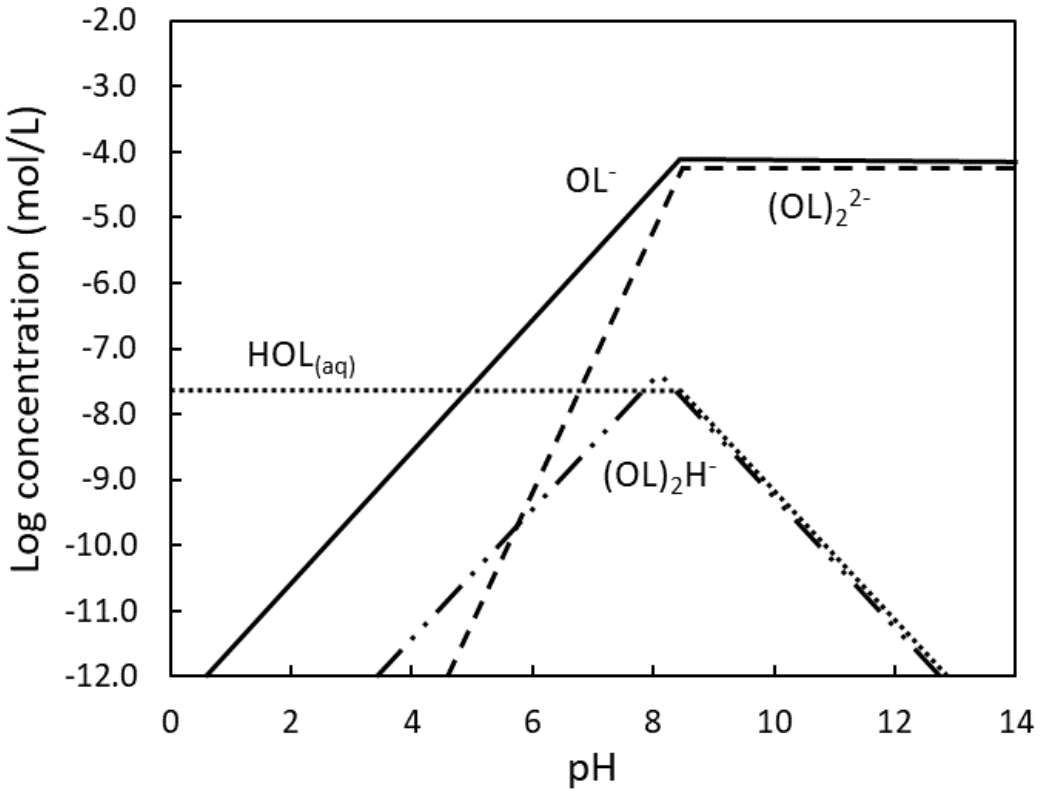

Figure 7−2. The species distribution diagram of oleate in the presence of 2×10^{-4} mol/L oleate.

7.2.1.2 Effect of Ca^{2+} and Mg^{2+} on goethite flotation

Figure 7−3 illustrates a goethite recovery with the increase in the concentrations of Ca^{2+} and Mg^{2+}. The results show that there was an increase in the recovery when 1×10^{-5} mol/L of Ca^{2+} and Mg^{2+} were added into the solution. This was probably due to the adsorption of these small number of ions on the mineral surface where the SiO_3^{2-} was adsorbed. Thus, this resulted in the increase in collector adsorption as seen in Figure 5−3 discussed in chapter 5.2.2.

When the concentration of Ca and Mg was higher than 1×10^{-5} mol/L, the flotation recovery of goethite decreased with the increase in the cation concentration. This is probably because the excessive number of dissolved cations in the solution may form insoluble precipitates with oleate collector. Thus, this resulted in the reduced adsorption of collector on the mineral surface as seen in Figure 7−4. It is also worth to note that the presence of Ca^{2+} resulted in a more significant decrease in goethite recovery than Mg^{2+}. This aligns with a study in the literature, which found that

hematite recovery was more adversely affected by Ca^{2+} than Mg^{2+} when sodium oleate was used (Li et al., 2017). This was due to the lesser solubility product of calcium oleate compared to magnesium oleate, resulting in a greater precipitation of calcium oleate than magnesium oleate.

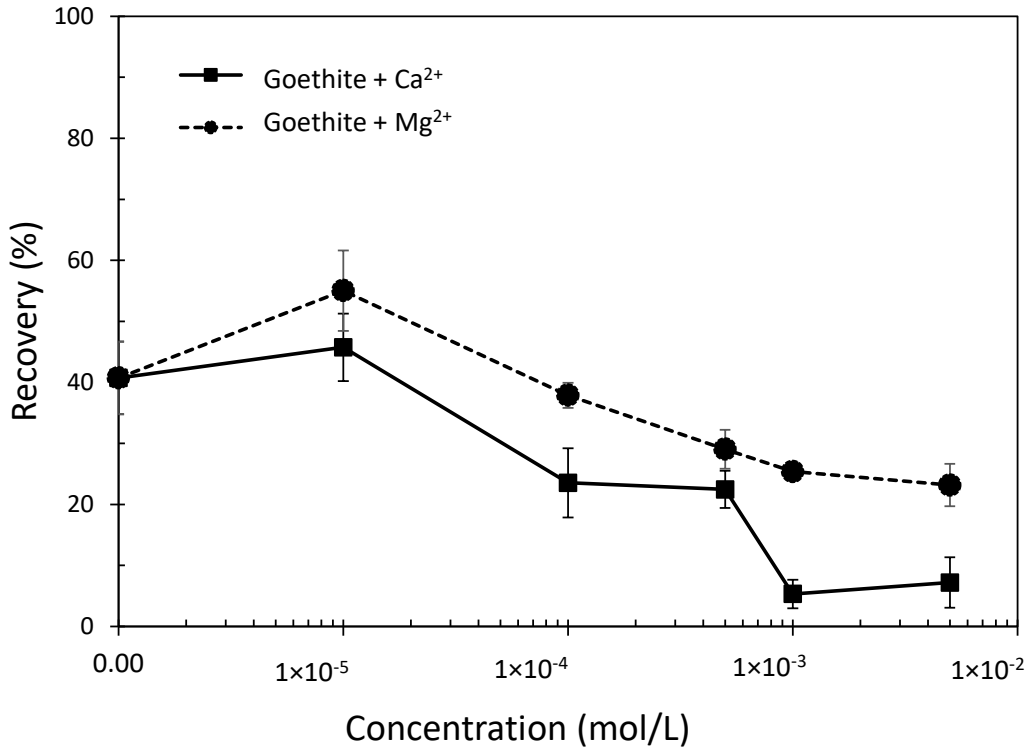

Figure 7−3. Effect of Ca^{2+} and Mg^{2+} on the recovery of goethite in the presence of 6×10^{-3} mol/L sodium silicate and 2×10^{-4} mol/L sodium oleate at pH 8.

7.2.2 Adsorption behavior of oleate in the presence of Ca^{2+} and Mg^{2+}

Figure 7−4 shows the influence of Ca^{2+} and Mg^{2+} on the adsorption density of oleate ions on goethite surfaces. This suggests that the adsorption density decreased as the concentration of Ca^{2+} increased, likely because of the formation of insoluble calcium oleate. A similar trend was observed with Mg^{2+}, which can be attributed to the precipitation of magnesium oleate. However, the adsorption density of oleate was notably lower in the presence of Ca^{2+} than Mg^{2+}. This is because more oleate precipitated with Ca^{2+} than with Mg^{2+}. The greater precipitation of oleate with Ca^{2+} can be attributed to the lower solubility product of calcium oleate (Ksp = $10^{-15.4}$) compared to magnesium oleate (Ksp = $10^{-13.8}$). This was validated by the free

formation energy calculation: $\Delta G^{\theta}_{CaOL2} = -35.46\ kJ\ mol^{-1}$ $\Delta G^{\theta}_{MgOL2} = -31.74\ kJ\ mol^{-1}$ at pH 10 (Jung et al., 2022). As a result, the recovery of goethite was lower in the presence of Ca^{2+} compared to Mg^{2+}. This observation is consistent with findings from studies on minerals such smithsonite (Araújo and Lima, 2017), hematite (Li et al., 2017), and monazite (Jung et al., 2022).

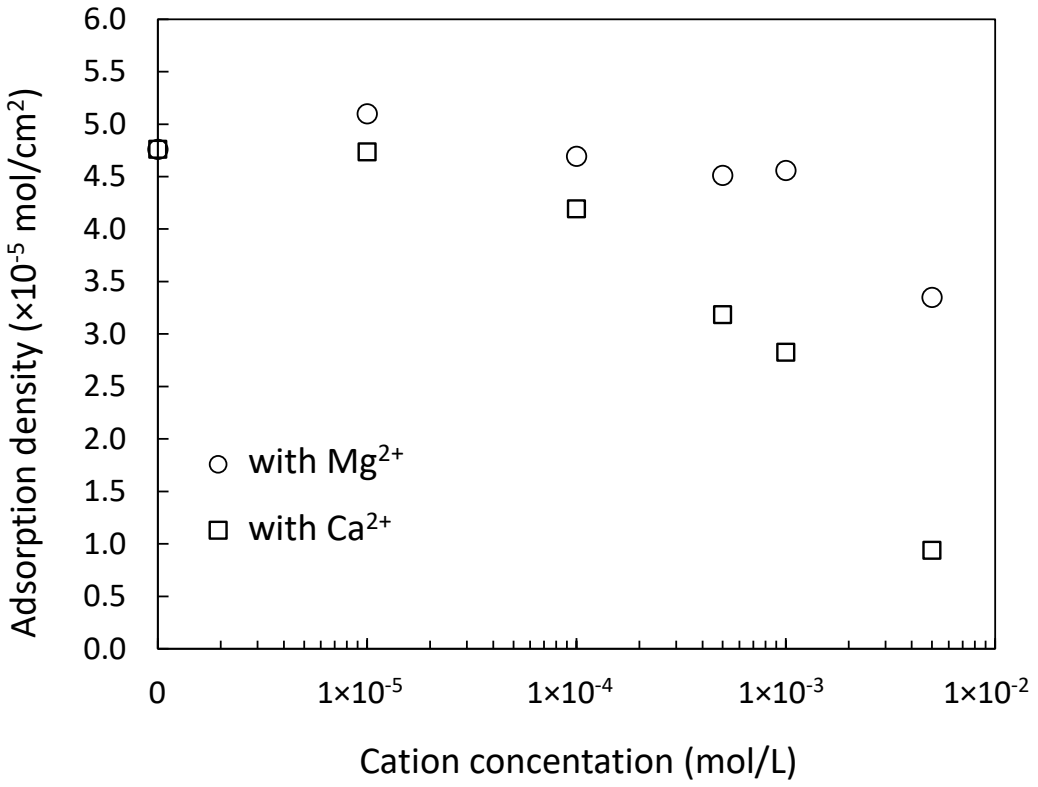

Figure 7−4. Adsorption density of oleate on the goethite surface in the presence of Ca^{2+} and Mg^{2+} using 2×10^{-4} mol/L sodium oleate and 6×10^{-3} mol/L sodium silicate.

7.2.3 Zeta potential of goethite

7.2.3.1 Effect of sodium oleate and sodium silicate

The zeta potential of goethite was measured at varying pH levels in the presence and absence of Na_2SiO_3 and NaOL, as shown in Figure 7−5. The results showed that the PZC of goethite in distilled water was approximately at pH 5.5. In the literature, the PZC values for goethite was reported to range between pH 6 and 8.5 (Uwadiale, 1992; Yenial et al., 2014; Zhang et al., 2007). The variation in PZC values can be ascribed

to several factors, including the origin of the mineral (whether naturally occurring or synthesized), the measurement technique, and the chemical composition on mineral surfaces.

In the presence of NaOL and Na_2SiO_3, the PZC was shifted to pH 2.5 and 4, respectively, indicating the adsorption of OL^- and SiO_3^{2-} on the goethite surface. At pH 8 where the flotation experiments were carried out, no significant change was observed when either silicate or oleate was present alone or together. It implies that the adsorption of SiO_3^{2-} can inhibit the adsorption of oleate ions at this pH. It was reported that the adsorption of SiO_3^{2-} on the hematite hindered the adsorption of dissolved organic matter (Li et al., 2019). Roonasi et al. (2010) also demonstrated that silicate ions adsorbed on the magnetite surface effectively reduced the adsorption of oleate ions from the solution, as evidenced by in−situ ATR−FTIR spectroscopy.

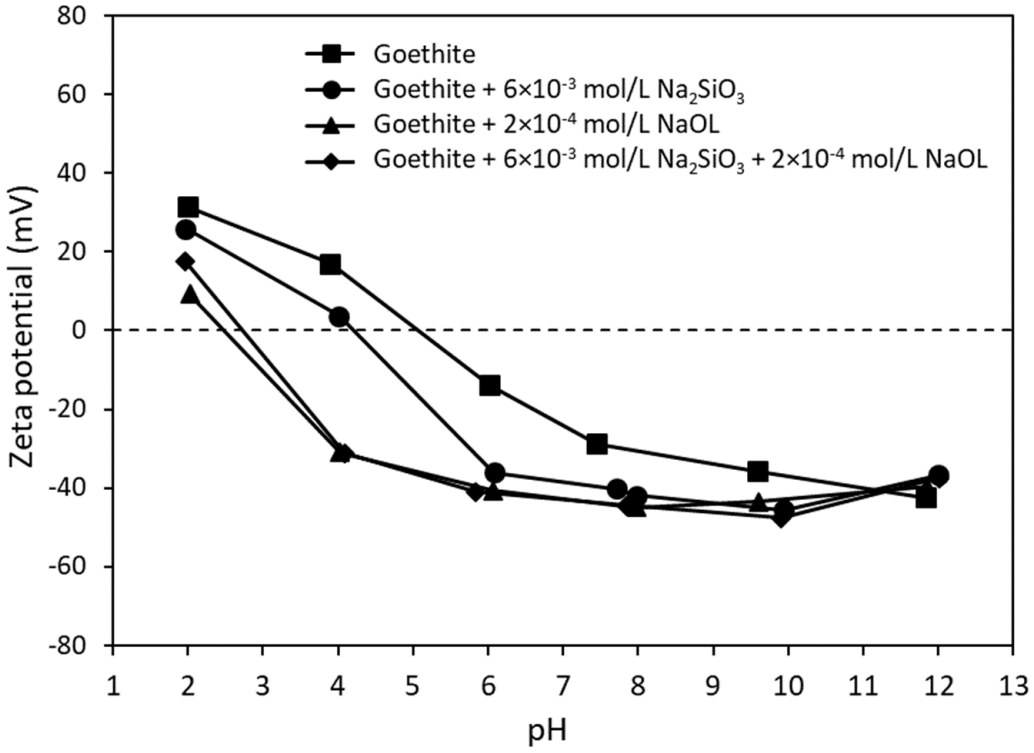

Figure 7−5. Zeta potential of goethite in the absence and presence of 2×10^{-4} mol/L NaOL and 6×10^{-3} mol/L Na_2SiO_3 as a function of pH.

7.2.3.2 Effect of Ca^{2+} and Mg^{2+}

Figure 7−6 and Figure 7−**7** show the influence of Ca^{2+} and Mg^{2+} on the zeta potential of goethite. As the concentration of Ca^{2+} and Mg^{2+} increased, the zeta potential of goethite shifted towards less negative values. This is likely due to the adsorption of positively charged species such as Ca^{2+}, $Ca(OH)^{+}$, Mg^{2+} and $Mg(OH)^{+}$. Metallic cation adsorption on the mineral surface can occur in the form of monodentate surface complex (Eq. 7-1) or bidentate surface complexes (Eq. 7-2), releasing H^{+} from the surface (Stumm and Morgan, 2012). In this study, it should be noted that silicate species were pre−adsorbed on the goethite surface, as represented by Eq. 7-3. Consequently, the adsorption of Ca^{2+} and Mg^{2+} likely occurred through electrostatic attraction to negatively charged sites on the goethite surface, where silicate ions were previously adsorbed as seen in Eq. 7-4.

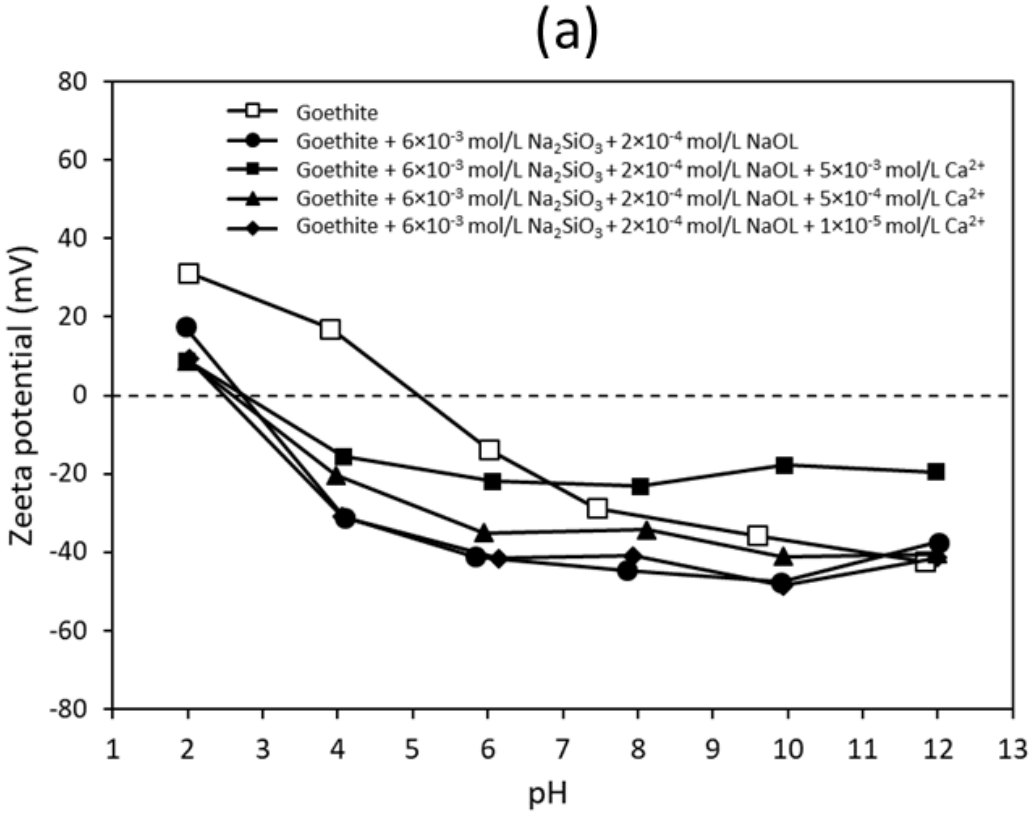

Figure 7−6. The influence of the different concentration of Ca^{2+} on the zeta potential of goethite.

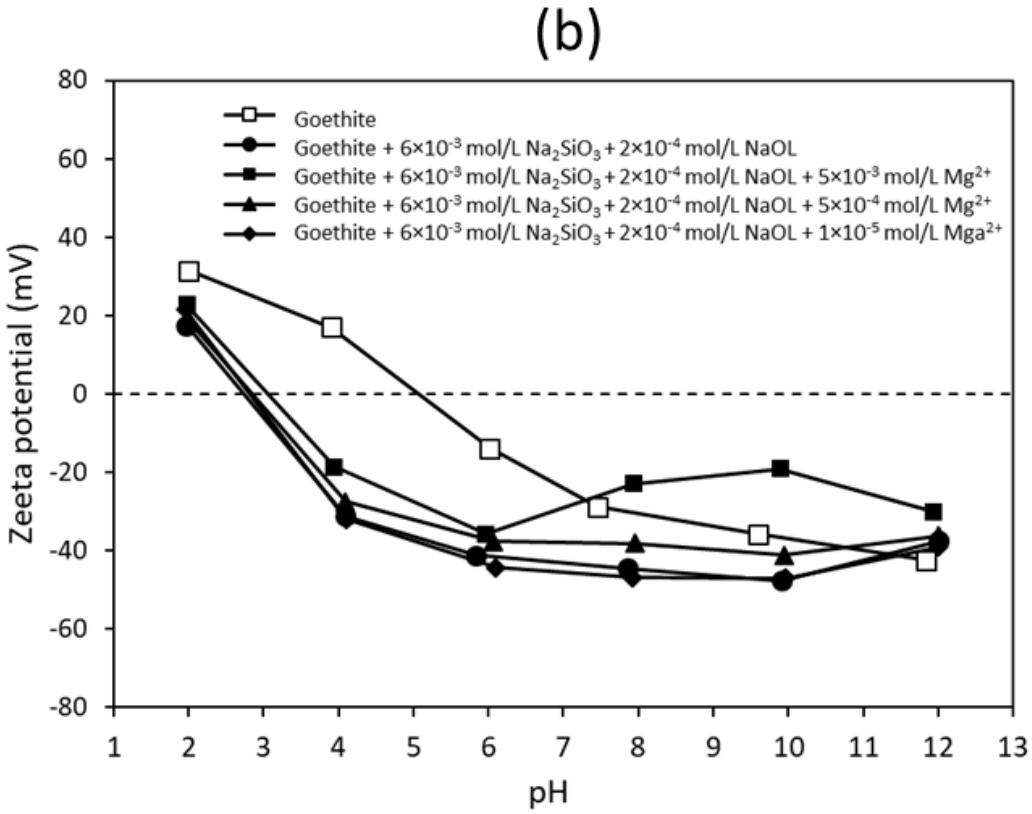

Figure 7−7. The influence of the different concentration of Mg^{2+} on the zeta potential of goethite.

Several studies reported the synergistic adsorption of Ca^{2+} and Mg^{2+} on the mineral surface in the presence of oxyanions such as PO_4^{3-} (Atouei et al., 2016; Gao and Mucci, 2003) and SiO_3^{2-} (Cao et al., 2022). Atouei et al. (2016) demonstrated that the presence of PO_4^{3-} led to an increased adsorption of Ca^{2+} and Mg^{2+} on goethite compared to when PO_4^{3-} was absent. The synergistic adsorption effect was attributed to the increased negative charge on the goethite surface due to PO_4^{3-} adsorption, thereby enhancing the electrostatic attraction between the negatively charged goethite surface and the positively charged Ca^{2+} and Mg^{2+}. Gao and Mucci (2003) also found that the adsorption of PO_4^{3-} on the goethite surface increased in the presence of Ca^{2+} and Mg^{2+} due to the formation of ternary surface complexes such as $Ca{-}PO_4$ and $Mg{-}PO_4$ on the mineral surface under alkaline condition. A similar result was observed in a study on bastnaesite flotation with Ca^{2+} and SiO_3^{2-}, which showed that a greater amount of SiO_3^{2-} was adsorbed on bastnaesite when its surface was preconditioned with Ca^{2+} (Cao et al., 2022). Based on the findings in the literature, the

zeta potential of goethite became less negatively with the presence of Ca^{2+} and Mg^{2+}, primarily due to the adsorption of Ca^{2+} and Mg^{2+} on the pre−adsorbed silicate reactive site on the goethite surface as Eq. 7-4.

$$\equiv FeOH + Me^{2+} \rightarrow FeOMe^{+} + H^{+} \quad (7\text{-}1)$$

$$\equiv 2FeOH + Me^{2+} \rightarrow (FeO)_2Me^{0} + 2H^{+} \quad (7\text{-}2)$$

$$\equiv FeOH + SiO(OH)_3^{-} \rightarrow FeO_2SiO(OH)_3^{-} + H^{+} \quad (7\text{-}3)$$

$$\equiv FeOH + SiO(OH)_3^{-} + Me^{2+} \rightarrow FeO_2SiO(OH)_3Me + H^{+} \quad (7\text{-}4)$$

7.2.4 XPS analysis of goethite surface

XPS analysis was conducted to examine the variations in elemental composition on the goethite surface when exposed to Ca^{2+} and Mg^{2+}. Table 7−1 presents the elemental composition on goethite surface. The data revealed that the C 1s content decreased after conditioning with Ca^{2+} and Mg^{2+} compared to before conditioning. While the C 1s peak is typically attributed to adventitious contamination from CO_2 in the air, it can also indicate the adsorption of the oleate ion, a long−chain hydrocarbon ($C_{18}H_{34}O_2$). Hence, the C 1s peak suggests reduced oleate adsorption in the presence of Ca^{2+} and Mg^{2+}. This diminished adsorption could be due to either the formation of insoluble precipitates with Ca^{2+} and Mg^{2+} consuming oleate ions or the adsorption of silicate ions inhibiting oleate ion adsorption. Furthermore, the C 1s peak was more reduced in the presence of Ca^{2+} than Mg^{2+}, aligning with the observation that goethite recovery was lower with Ca^{2+} than with Mg^{2+}.

It also shows the increased percentage of Ca and Mg composition, indicating the adsorption of Ca^{2+} and Mg^{2+} in the presence of theses ions. It is postulated that the adsorption of Ca^{2+} and Mg^{2+} took place on sites where silicate had previously adsorbed.

Table 7−1. Elemental composition on the surface of goethite by XPS.

	OL	OL + SiO_3^{2+} + Ca^{2+}	OL + SiO_3^{2+} + Mg^{2+}
O 1s	54.73	55.6	54.41
C 1s	21.49	19.87	20.91
Mg 1S	0.25	0.24	0.49
Fe 2p	9.09	8.26	8.58
Ca 2p	0.6	1.13	0.71
Si 2p	7.86	10.38	9.74

7.3 Chapter summary

This chapter examines the effects of divalent cations, specifically Ca^{2+} and Mg^{2+}, on the flotation of goethite using sodium oleate and sodium silicate. Microflotation and various surface characterization techniques, such as zeta potential, XPS, and UV adsorption, were utilized to understand these effects. The findings indicate that the presence of Ca^{2+} and Mg^{2+} substantially impedes goethite flotation. This negative impact arises from the formation of insoluble compounds when these divalent metallic cations interact with the sodium oleate collector. As a result, there's a reduced adsorption of oleate ions on the goethite surfaces, leading to a decline in goethite recovery. Notably, the presence of Ca^{2+} has a more pronounced effect on goethite recovery than Mg^{2+}.

Chapter 8. Conclusions and recommendations

8.1 Conclusions

This PhD research aimed to investigate the impact of water quality on the flotation efficiency of RE phosphate minerals and to identify the underlying mechanisms. To understand the fundamental mechanism of RE ore flotation, the flotation behaviours of both valuable and gangue single minerals were scrutinized. Furthermore, the study assessed the effect of water quality using ore samples, aiming to quantify its influence and understand the associated mechanisms in the mixed mineral system.

The investigation of the monazite flotation mechanism with an oleate collector in the presence of various ions (Ca^{2+}, Mg^{2+}, Na^{+}, and K^{+}) indicated that Ca^{2+} or Mg^{2+} were highly detrimental to monazite flotation. This is attributed to the formation of insoluble products with these divalent metal ions, leading to decreased adsorption of oleate ions on monazite surfaces and consequently, reduced flotation recovery. In contrast, the presence of Na^{+} or K^{+} had a minimal effect on the flotation recovery of monazite because these ions do not react with oleate ions. These findings were confirmed by adsorption experiments, XPS analysis, and zeta potential measurements.

The negative effects of Ca^{2+} and Mg^{2+} on the flotation of RE minerals using ore samples were also validated through multi−stage batch flotation experiments, adsorption tests, rheological measurements, and solution chemistry analyses. Both Ca^{2+} and Mg^{2+} adversely impacted the selectivity and recovery of RE minerals due to their chemical reactions with the collector and depressant. The formation of insoluble calcium and magnesium carboxylate compounds led to a decrease in the residual collector concentration and subsequently, a reduced RE mineral recovery. Additionally, these divalent cations were found to act as bridges between the oxygen atoms of the adsorbed SiO_3^{2-} and carboxylate ions, leading to increased adsorption of the fatty acid collector ions and a higher recovery of FeO. Notably, Mg^{2+} had a more pronounced negative effect on the flotation recovery of RE minerals than Ca^{2+}, possibly because magnesium has a stronger affinity for SiO_3^{2-}, while calcium prefers oleate. The presence of $CaCl_2$ or $MgCl_2$ also increased the viscosity of flotation pulp, likely due to the compression of the electrical double layer by these divalent cations.

The presence of anions, specifically Cl^{-}, SO_4^{2-}, and HCO_3^{-}, in the flotation pulp also negatively impacted flotation efficiency. This led to a reduced recovery of RE minerals

and an increased recovery of FeO minerals. Among these, Cl^- had the most detrimental effect on the flotation of RE minerals, likely due to a most significant increase in pulp viscosity. The reduction in zeta potential of fine particles in the presence of these ions seemed to be a key factor in increasing pulp viscosity. Stronger attractive forces between particles resulted in higher pulp viscosity, leading to increased mechanical entrainment. These observations were supported by settling experiments and DLVO theory calculations.

Lastly, the effect of Ca^{2+} and Mg^{2+} on the flotation of gangue minerals was examined using sodium oleate and sodium silicate. Their presence significantly hindered goethite flotation, primarily due to the formation of insoluble compounds with the sodium oleate collector. Consequently, there was decreased adsorption of oleate ions on goethite surfaces, leading to reduced goethite recovery. Additionally, the adverse effect on goethite recovery was more significant with Ca^{2+} than with Mg^{2+}.

8.2 Recommendation for future study

- This study aims to quantify the effects of water quality on the flotation of RE phosphate minerals and to uncover the underlying mechanisms. Having understood these impacts, future research should explore methods to mitigate the adverse effects of dissolved ions.
- The detrimental effects of Ca^{2+} and Mg^{2+} were identified as stemming from the formation of insoluble precipitates with the collector, which subsequently reduced the collector concentration. Future research should consider experiments that investigate the potential of masking reagents to prevent the formation of these insoluble precipitates.
- Anions were found to influence flotation pulp rheology due to increased attraction forces between mineral particles. Exploring the effects of dispersants, which can maintain mineral particles in a dispersed state, is recommended.
- Dissolved ions might alter bubble properties within the flotation pulp. Investigating the influence of ions on bubble characteristics, such as bubble size and the probability of particle attachment to bubbles, could offer valuable insights.

- Froth stability plays a crucial role in determining flotation efficiency, as it can directly influence the degree of entrainment. Research into the effects of various dissolved ions on froth stability is recommended.

References

Abaka-Wood, G.B., Addai-Mensah, J., Skinner, W., 2018a. A study of selective flotation recovery of rare earth oxides from hematite and quartz using hydroxamic acid as a collector. Adv. Powder Technol. 29, 1886–1899.

Abaka-Wood, G.B., Addai-Mensah, J., Skinner, W., 2017a. A study of flotation characteristics of monazite, hematite, and quartz using anionic collectors. Int. J. Miner. Process. 158, 55–62.

Abaka-Wood, G.B., Addai-Mensah, J., Skinner, W., 2017b. Selective flotation of rare earth oxides from hematite and quartz mixtures using oleic acid as a collector. Int. J. Miner. Process. 169, 60–69.

Abaka-Wood, G.B., Fosu, S., Addai-Mensah, J., Skinner, W., 2019. Flotation recovery of rare earth oxides from hematite–quartz mixture using sodium oleate as a collector. Miner. Eng. 141, 105847.

Abaka-Wood, G.B., Zanin, M., Addai-Mensah, J., Skinner, W., 2018b. The upgrading of rare earth oxides from iron-oxide silicate rich tailings: Flotation performance using sodium oleate and hydroxamic acid as collectors. Adv. Powder Technol. 29, 3163–3172.

Abeidu, A.M., 1976. Reagents influencing the selective soap flotation of hematite and goethite. Indian Journal of Technology 14, 249–253.

Abeidu, A.M., 1972. The separation of monazite from zircon by flotation. J. Less Common Met. 29, 113–119.

Abu-Jdayil, B., 2011. Rheology of sodium and calcium bentonite–water dispersions: Effect of electrolytes and aging time. Int. J. Miner. Process. 98, 208–213.

Agrawal, Y.K., 1980. Hydroxamic acids and their analytical applications. Rev. Anal. Chem. 5, 3–28.

Agulhon, P., Markova, V., Robitzer, M., Quignard, F., Mineva, T., 2012. Structure of Alginate Gels: Interaction of Diuronate Units with Divalent Cations from Density Functional Calculations. Biomacromolecules 13, 1899–1907.

Aktas, Z., Cilliers, J.J., Banford, A.W., 2008. Dynamic froth stability: Particle size, airflow rate and conditioning time effects. Int. J. Miner. Process. 87, 65–71.

Albijanic, B., Ozdemir, O., Nguyen, A.V., Bradshaw, D., 2010. A review of induction and attachment times of wetting thin films between air bubbles and particles and its relevance in the separation of particles by flotation. Adv. Colloid Interface Sci. 159, 1–21.

Alonso, E., Sherman, A.M., Wallington, T.J., Everson, M.P., Field, F.R., Roth, R., Kirchain, R.E., 2012. Evaluating rare earth element availability: A case with revolutionary demand from clean technologies. Environ. Sci. Technol. 46, 3406–3414.

Ananthapadmanabhan, K.P., Somasundaran, P., 1988. Acid-soap formation in aqueous oleate solutions. J. Colloid Interface Sci. 122, 104–109.

Ancey, C., Jorrot, H., 2001. Yield stress for particle suspensions within a clay dispersion. J. Rheol. 45, 297–319.

Anderson, C.D., Taylor, P.R., Anderson, C.G., 2016. Rare earth flotation fundamentals: A review. In IMPC 2016 Proceedings of the XXVIII International Mineral Processing Congress.

Arantes, R.S., Lima, R.M.F., 2013. Influence of sodium silicate modulus on iron ore flotation with sodium oleate. Int. J. Miner. Process. 125, 157–160.

Araújo, A.C.A., Lima, R.M.F., 2017. Influence of cations Ca2+, Mg2+ and Zn2+ on the flotation and surface charge of smithsonite and dolomite with sodium oleate and sodium silicate. Int. J. Miner. Process. 167, 35–41.

Arnold, B.J., Aplan, F.F., 1986. The effect of clay slimes on coal flotation, part II: The role of water quality. Int. J. Miner. Process. 17, 243–260.

Ata, S., 2008. Coalescence of bubbles covered by particles. Langmuir 24, 6085–6091.

Atouei, M.T., Rahnemaie, R., Kalanpa, E.G., Davoodi, M.H., 2016. Competitive adsorption of magnesium and calcium with phosphate at the goethite water interface: Kinetics, equilibrium and CD-MUSIC modeling. Chem. Geol. 437, 19–29.

Azizi, D., Sarvaramini, A., Larachi, F., 2017. Liquid-liquid mineral separation via ionic-liquid complexation of monazite and bastnäsite—An alternate route for rare-earth mineral beneficiation. Colloids Surf. A: Physicochem. Eng. Asp. 520, 301–323.

Bai, J., Xu, X., Duan, Y., Zhang, G., Wang, Z., Wang, L., Zheng, C., 2022. Evaluation of resource and environmental carrying capacity in rare earth mining areas in China. Sci. Rep. 12, 6105.

Balaram, V., 2019. Rare earth elements: A review of applications, occurrence, exploration, analysis, recycling, and environmental impact. Geosci. Front. 10, 1285–1303.

Baldassarre, F., Cacciola, M., Ciccarella, G., 2015. A predictive model of iron oxide nanoparticles flocculation tuning Z-potential in aqueous environment for biological application. J. Nanoparticle Res. 17, 377.

Basilio, C.I., Kartio, I.J., Yoon, R.-H., 1996. Lead activation of sphalerite during galena flotation. Miner. Eng. 9, 869–879.

Basnayaka, L., Subasinghe, N., Albijanic, B., 2017. Influence of clays on the slurry rheology and flotation of a pyritic gold ore. Appl. Clay Sci. 136, 230–238.

Becker, M., Yorath, G., Ndlovu, B., Harris, M., Deglon, D., Franzidis, J.-P., 2013. A rheological investigation of the behaviour of two Southern African platinum ores. Miner. Eng. 49, 92–97.

Behkish, A., Lemoine, R., Sehabiague, L., Oukaci, R., Morsi, B.I., 2007. Gas holdup and bubble size behavior in a large-scale slurry bubble column reactor operating with an organic liquid under elevated pressures and temperatures. Chem. Eng. J. 128, 69–84.

Ben-Naim, A., 1974. Water and Aqueous Solutions. Springer New York, NY.

Blake, T.D., Kitchener, J.A., 1972. Stability of aqueous films on hydrophobic methylated silica. J. Chem. Soc., Faraday Trans. 1: Phys. Chem. Condens. Phases 68, 1435–1442.

Boger, D.V., 2009. Rheology and the resource industries. Chem. Eng. Sci. 64, 4525–4536.

Boulton, A., Fornasiero, D., Ralston, J., 2005. Effect of iron content in sphalerite on flotation. Miner. Eng. 18, 1120–1122.

Bradshaw, D.J., Harris, P.J., O'Connor, C.T., 1998. Synergistic interactions between reagents in sulphide flotation. The Journal of The South African Institute of Mining and Metallurgy 98, 189–193.

Broman, P.G., 1980. Water reuse at sulfide ore concentrators in Sweden: Practice, experience and current developments. Complex sulphide ores 28–39.

Bulatovic, S.M., 2010. Handbook of Flotation Reagents: Chemistry, Theory and Practice 111–125.

Burns, D.B., Zydney, A.L., 2000. Buffer effects on the zeta potential of ultrafiltration membranes. J. Membr. Sci. 172, 39–48.

Cao, Z., Cheng, Z., Wang, J., Cao, Y., 2022. Synergistic depression mechanism of Ca2+ ions and sodium silicate on bastnaesite flotation. J. Rare Earths 40, 988–995.

Castro, S., 2012. Challenges in flotation of Cu-Mo sulfide ores in sea water, in: Water in Mineral Processing. SME, pp. 29–40.

Castro, S., Laskowski, J.S., 2011. Froth Flotation in Saline Water. KONA Powder Part. J. 29, 4–15.

Castro, S., Ramos, O., Cancino, J.P., Laskowski, J.S., 2012. Frothing in the flotation of copper sulfide ores in sea water. Society for Mining, Metallurgy, and Exploration, Colorado, USA.

Celik, M.S., Somasundaran, P., 1986. The effect of multivalent ions on the flotation of coal. Sep. Sci. Technol. 21, 393–402.

Chelgani, S.C., Rudolph, M., Leistner, T., Gutzmer, J., Peuker, U.A., 2015a. A review of rare earth minerals flotation: Monazite and xenotime. Int. J. Min. Sci. Technol. 25, 877–883.

Chelgani, S.C., Rudolph, M., Leistner, T., Gutzmer, J., Peuker, U.A., 2015b. A review of rare earth minerals flotation: Monazite and xenotime. Int. J. Min. Sci. Technol. 25, 877–883.

Chen, G.L., Tao, D., 2005. Reverse Flotation of Magnesite by Dodecyl Phosphate from Dolomite in the Presence of Sodium Silicate. Sep. Sci. Technol. 39, 377–390.

Chen, J., Liu, R., Sun, W., Qiu, G., 2009. Effect of mineral processing wastewater on flotation of sulfide minerals. Trans. Nonferrous Met. Soc. China 19, 454–457.

Chen, W., Chen, F., Bu, X., Zhang, G., Zhang, C., Song, Y., 2019. A significant improvement of fine scheelite flotation through rheological control of flotation pulp by using garnet. Miner. Eng. 138, 257–266.

Chen, W., Honghui, H., Bai, T., Jiang, S., 2017. Geochemistry of Monazite within Carbonatite Related REE Deposits. Resources 6, 51.

Chen, X., Hadde, E., Liu, S., Peng, Y., 2017. The effect of amorphous silica on pulp rheology and copper flotation. Miner. Eng. 113, 41–46.

Chen, Z., 2011. Global rare earth resources and scenarios of future rare earth industry. J. Rare Earths 29, 1–6.

Cheng, S., Li, W., Han, Y., Sun, Y., Gao, P., Zhang, X., 2023. Recent process developments in beneficiation and metallurgy of rare earths: A review. J. Rare Earths.

Cheng, T.W., 2000. The point of zero charge of monazite and xenotime. Miner. Eng. 13, 105–109.

Cheng, T.-W., Holtham, P.N., Tran, T., 1993. Froth flotation of monazite and xenotime. Miner. Eng. 6, 341–351.

Coetzer, R., Preez, D., Bredenhann, H.S., 2003. Influence of water resources and metal ions on galena flotation of Rosh Pinah ore. Journal of the Southern African Institute of Mining and Metallurgy 103, 193–207.

Cook, N.J., Ciobanu, C.L., Wade, B.P., Gilbert, S.E., Alford, R., 2023. Mineralogy and Distribution of REE in Oxidised Ores of the Mount Weld Laterite Deposit, Western Australia. Minerals 13, 656.

Corin, K.C., Reddy, A., Miyen, L., Wiese, J.G., Harris, P.J., 2011. The effect of ionic strength of plant water on valuable mineral and gangue recovery in a platinum bearing ore from the Merensky reef. Miner. Eng. 24, 131–137.

Craig, V.S.J., Ninham, B.W., Pashley, R.M., 1993. Effect of electrolytes on bubble coalescence. Nature 364, 317–319.

Crawford, C. B., and Quinn, B., *Microplastic pollutants*. Elsevier, 2016.

Dai, Z., Fornasiero, D., Ralston, J., 1999. Particle–Bubble Attachment in Mineral Flotation. J. Colloid Interface Sci. 217, 70–76.

Dang, D.H., Thompson, K.A., Ma, L., Nguyen, H.Q., Luu, S.T., Duong, M.T.N., Kernaghan, A., 2021. Toward the Circular Economy of Rare Earth Elements: A Review of Abundance, Extraction, Applications, and Environmental Impacts. Arch. Environ. Contam. Toxicol. 81, 521–530.

Davis, C.C., Chen, H.-W., Edwards, M., 2002. Modeling Silica Sorption to Iron Hydroxide. Environ. Sci. Technol. 36, 582–587.

Deglon, D.A., 2005. The effect of agitation on the flotation of platinum ores. Miner. Eng. 18, 839–844.

Dehaine, Q., Filippov, L.O., 2015. Rare earth (La, Ce, Nd) and rare metals (Sn, Nb, W) as by-product of kaolin production, Cornwall: Part1: Selection and characterisation of the valuable stream. Miner. Eng. 76, 141–153.

Dehaine, Q., Filippov, L.O., Glass, H.J., Rollinson, G., 2019. Rare-metal granites as a potential source of critical metals: A geometallurgical case study. Ore Geol. Rev. 104, 384–402.

Derjaguin, B.V., 1955. The definition and magnitude of disjoining pressure and its role in the statics and dynamics of thin fluid films. Kolloid Zh 17, 207–214.

Dietzel, M., 2011. Water-Rock Interaction. Water Sci. Technol. Libr. 207–235.

Dixit, Biswas, and A.K., 1969. pH-Dependence of the flotation and adsorption properties of some beach sand minerals. Trans Soc Mining Eng AIME 244, 173–178.

Dixon, D.R., 1985. Interaction of alkaline-earth-metal ions with magnetite. Colloids Surf. 13, 273–286.

Drzymala, J., 1994. Characterization of materials by Hallimond tube flotation. Part 1: maximum size of entrained particles. Int. J. Miner. Process. 42, 139–152.

Lynas Rare Earths, 2022. 2022 Annual Report. Lynas Rare Earths.

Espinosa-Gomez, R., Finch, J.A., Laplante, A.R., 1987. Effects of the type of water on the selective flotation of pyrochlore from niobec. Colloids Surf. 26, 333–350.

Espiritu, E.R.L., Naseri, S., Waters, K.E., 2018a. Surface chemistry and flotation behavior of dolomite, monazite and bastnäsite in the presence of benzohydroxamate, sodium oleate and phosphoric acid ester collectors. Colloids Surf. A: Physicochem. Eng. Asp. 546, 254–265.

Espiritu, Eileen Ross L., Naseri, S., Waters, K.E., 2018. Surface chemistry and flotation behavior of dolomite, monazite and bastnäsite in the presence of benzohydroxamate, sodium oleate and phosphoric acid ester collectors. Colloids Surf. A: Physicochem. Eng. Asp. 546, 254–265.

Espiritu, E.R.L., Silva, G.R. da, Azizi, D., Larachi, F., Waters, K.E., 2019. Flotation behavior and electronic simulations of rare earth minerals in the presence of dolomite supernatant using sodium oleate collector. J. Rare Earths 37, 101–112.

Espiritu, E.R.L., Silva, G.R. da, Azizi, D., Larachi, F., Waters, K.E., 2018b. The effect of dissolved mineral species on bastnäsite, monazite and dolomite flotation using benzohydroxamate collector. Colloids Surf. A: Physicochem. Eng. Asp. 539, 319–334.

Espiritu, E.R.L., Waters, K.E., 2018. Flotation studies of monazite and dolomite. Miner. Eng. 116, 101–106.

Fan, H.-R., Yang, K.-F., Hu, F.-F., Liu, S., Wang, K.-Y., 2016. The giant Bayan Obo REE-Nb-Fe deposit, China: Controversy and ore genesis. Geosci. Front. 7, 335–344.

Fan, X., Waters, K.E., Rowson, N.A., Parker, D.J., 2009. Modification of ilmenite surface chemistry for enhancing surfactants adsorption and bubble attachment. J. Colloid Interface Sci. 329, 167–172.

Fang, S., Xu, L., Wu, H., Xu, Y., Wang, Z., Shu, K., Hu, Y., 2020. Influence of surface dissolution on sodium oleate adsorption on ilmenite and its gangue minerals by ultrasonic treatment. Appl. Surf. Sci. 500, 144038.

Farrokhpay, S., 2012. The importance of rheology in mineral flotation: A review. Miner. Eng. 36, 272–278.

Farrokhpay, S., 2011. The significance of froth stability in mineral flotation — A review. Adv. Colloid Interface Sci. 166, 1–7.

Farrokhpay, S., Bradshaw, D., Dunne, R., 2013. Rheological investigation of the flotation performance of a high clay containing gold ore from Carlin trend, in: 5th World Gold 2013 Conference. Brisbane, QLD, Australia, pp. 333–340.

Farrokhpay, S., Zanin, M., 2012. An investigation into the effect of water quality on froth stability. Adv. Powder Technol. 23, 493–497.

Feinstein, M.E., Rosano, H.L., 1967. The determination of the apparent binding of counterions to micelles by electromotive force measurements. J. Colloid Interface Sci. 24, 73–79.

Ferri, D., Grenthe, I., Hietanen, S., Salvatore, F., Powell, D.L., Suchi, R., 1983. Studies on Metal Carbonate Equilibria. 5. The Cerium(III) Carbonate Complexes in Aqueous Perchlorate Media. Acta Chem. Scand. 37a, 359–365.

Ferron, C.J., Bulatovic, S.M., Salter, R.S., 1991. Beneficiation of Rare Earth Oxide Minerals. Mater. Sci. Forum 70–72, 251–270.

Filippov, L.O., Filippova, I.V., Lafhaj, Z., Fornasiero, D., 2019. The role of a fatty alcohol in improving calcium minerals flotation with oleate. Colloids Surf. A: Physicochem. Eng. Asp. 560, 410–417.

Finch, J.A., 1995. Column flotation: A selected review— part IV: Novel flotation devices. Miner. Eng. 8, 587–602.

Finch, J.A., Dobby, G.S., 1990. Column flotation. Flotation Science and Engineering 291–329.

Firouzi, M., Howes, T., Nguyen, A.V., 2015. A quantitative review of the transition salt concentration for inhibiting bubble coalescence. Adv. Colloid Interface Sci. 222, 305–318.

Firsching, F.H., Mohammadzadei, J., 1986. Solubility products of the rare-earth carbonates. J. Chem. Eng. Data 31, 40–42.

Fornasiero, D., Ralston, J., 2006. Effect of surface oxide/hydroxide products on the collectorless flotation of copper-activated sphalerite. Int. J. Miner. Process. 78, 231–237.

Frank, H.S., Evans, M.W., 1945. Free Volume and Entropy in Condensed Systems III. Entropy in Binary Liquid Mixtures; Partial Molal Entropy in Dilute Solutions; Structure and Thermodynamics in Aqueous Electrolytes. J. Chem. Phys. 13, 507–532.

Frank, H.S., Wen, W.-Y., 1957. Ion-solvent interaction. Structural aspects of ion-solvent interaction in aqueous solutions: a suggested picture of water structure. Discuss. Faraday Soc. 24, 133–140.

Franks, F., 1979. Water: A Comprehensive Treatise. Springer New York, NY.

Free, M.L., Miller, J.D., 1996. The significance of collector colloid adsorption phenomena in the fluorite/oleate flotation system as revealed by FTIR/IRS and solution chemistry analysis. Int. J. Miner. Process. 48, 197–216.

Friend, J.P., Hunter, R.J., 1971. Plastic flow behavior of coagulated suspensions treated as a repeptization phenomenon. J. Colloid Interface Sci. 37, 548–556.

Fu, Y., Yin, W., Yang, B., Li, C., Zhu, Z., Li, D., 2018. Effect of sodium alginate on reverse flotation of hematite and its mechanism. Int. J. Miner., Met., Mater. 25, 1113–1122.

Fuerstenau, D.W., Pradip, 2005. Zeta potentials in the flotation of oxide and silicate minerals. Adv. Colloid Interface Sci. 114, 9–26.

Fuerstenau, M.C., Miller, J.D., Kuhn, M.C., 1985. Chemistry of flotation. American Institute of Mining, Metallurgical, and Petroleum Engineers 156–177.

Gao, Y., Mucci, A., 2003. Individual and competitive adsorption of phosphate and arsenate on goethite in artificial seawater. Chem. Geol. 199, 91–109.

Gence, N., 2006. Wetting behavior of magnesite and dolomite surfaces. Appl. Surf. Sci. 252, 3744–3750.

Geneyton, A., Filippov, L.O., Heinig, T., Buaron, N., Menad, N.E., 2021. Towards the efficient flotation of monazite from silicate-rich tailings with fatty acids collectors using a lanthanum salt as a selective phosphate activator. Miner. Eng. 160, 106704.

Gibbs, W., 1878. Collected Works. Vol. I. Thermodynamics. VII. Electrochemical Thermodynamics. Yale Universiity Press, New Haven Connecticut.

Golev, A., Scott, M., Erskine, P.D., Ali, S.H., Ballantyne, G.R., 2014. Rare earths supply chains: Current status, constraints and opportunities. Resour. Polic. 41, 52–59.

Golikova, E.V., Burdina, N.M., Vysokovskaya, N.A., 2002. Aggregation Stability of SiO2, FeOOH, ZrO2, CeO2, and Natural Diamond Sols and Their Binary Mixtures: 1. The Photometric Study of Sols in KCl and BaCl2 Solutions. Colloid J. 64, 135–141.

Gregory, G.R.E.C., 1966. The determination of residual anionic surface-active reagents in mineral flotation liquors. Analyst 91, 251–257.

Gulgonul, I., 2019. Zeta potential of Teflon in presence of monvalent and divalent ions. Physicochemical Problems of Mineral Processing 55, 792–801.

Gupta, A., Yan, D.S., 2016. Mineral processing design and operations: an introduction. Elsevier.

Gupta, C.K., Krishnamurthy, N., 2005. Extractive Metallurgy of Rare Earths. CRC PRESS.

Gurney, Ronald.W., 1953. Ionic processes in solution. McGraw-Hill Book Company, Inc.

Hallimond, A.F., 1944. Laboratory apparatus for flotation tests. Min. Mag. 70, 87–91.

Hancer, M., Celik, M.S., Miller, J.D., 2001. The Significance of Interfacial Water Structure in Soluble Salt Flotation Systems. J. Colloid Interface Sci. 235, 150–161.

Hansen, H.C.B., Wetche, T.P., Raulund-Rasmussen, K., Borggaard, O.K., 1994. Stability constants for silicate adsorbed to ferrihydrite. Clay Miner. 29, 341–350.

Hao, H., Cao, Y., Li, L., Fan, G., Liu, J., 2021. Dispersion and depression mechanism of sodium silicate on quartz: Combined molecular dynamics simulations and density functional theory calculations. Appl. Surf. Sci. 537, 147926.

Hao, H., Li, L., Yuan, Z., Liu, J., 2018. Molecular arrangement of starch, Ca2+ and oleate ions in the siderite-hematite-quartz flotation system. J. Mol. Liq. 254, 349–356.

Haque, N., Hughes, A., Lim, S., Vernon, C., 2014. Rare Earth Elements: Overview of Mining, Mineralogy, Uses, Sustainability and Environmental Impact. Resources 3, 614–635.

Haxel, G.B., Hedrick, J.B., Orris, and G.J., 2002. Rare earth elements-critical resources for high technology (No. Fact Sheet 087-02). U.S. Geological Survey.

Hogarth, G., Onwudiwe, D.C., 2021. Copper Dithiocarbamates: Coordination Chemistry and Applications in Materials Science, Biosciences and Beyond. Inorganics 9, 70.

Horn, R.G., Castillo, L.A.D., Ohnishi, S., 2011. Coalescence map for bubbles in surfactant-free aqueous electrolyte solutions. Adv. colloid interface Sci. 168, 85–92.

Houot, R., Cuif, J.-P., Mottot, Y., Samama, J.-C., 1991. Recovery of Rare Earth Minerals, with Emphasis on Flotation Process. Mater. Sci. Forum 70–72, 301–324.

Humphries, M., 2012. Rare earth elements the global supply chain. CRS Report for Congress.

Ikumapayi, F., Makitalo, M., Johansson, B., Rao, K.H., 2012. Recycling of process water in sulphide flotation: Effect of calcium and sulphate ions on flotation of galena. Miner. Eng. 39, 77–88.

Ikumapayi, F., Rao, K.H., 2015. Recycling Process Water in Complex Sulfide Ore Flotation: Effect of Calcium and Sulfate on Sulfide Minerals Recovery. Miner. Process. Extr. Met. Rev. 36, 45–64.

Ito, S., Yotsumoto, H., Sakamoto, H., 1991. Magnetic Separation of Monazite and Xenotime. Mater. Sci. Forum 70–72, 279–300.

Iveson, S.M., Holt, S., Biggs, S., 2000. Contact angle measurements of iron ore powders. Colloids Surf. A: Physicochem. Eng. Asp. 166, 203–214.

Iwasaki, I., Cooke, S.R.B., Colombo, A.F., n.d. Flotation characteristics of goethite. [Washington, D.C.] : U.S. Dept. of the Interior, Bureau of Mines, 1960.

Jaireth, S., Hoatson, D.M., Miezitis, Y., 2014. Geological setting and resources of the major rare-earth-element deposits in Australia. Ore Geol. Rev. 62, 72–128.

Jeldres, R.I., Forbes, L., Cisternas, L.A., 2016. Effect of Seawater on Sulfide Ore Flotation: A Review. Miner. Process. Extr. Met. Rev. 37, 369–384.

Johansson, G., Pugh, R.J., 1992. The influence of particle size and hydrophobicity on the stability of mineralized froths. Int. J. Miner. Process. 34, 1–21.

Johnson, N.W., 1972. The flotation behavior of some chalcopyrite ores. Ph.D. thesis, University of Queensland, Brisbane, Australia.

Jordan, N., Marmier, N., Lomenech, C., Giffaut, E., Ehrhardt, J.-J., 2007. Sorption of silicates on goethite, hematite, and magnetite: Experiments and modelling. J. Colloid Interface Sci. 312, 224–229.

Jordens, A., Cheng, Y.P., Waters, K.E., 2013. A review of the beneficiation of rare earth element bearing minerals. Miner. Eng. 41, 97–114.

Joseph-Soly, S., Quast, K., Connor, J.N., 2015. Effects of Eh and pH on the oleate flotation of iron oxides. Miner. Eng. 83, 97–104.

Jung, M., Tadesse, B., Dick, C., Logan, A., Dyer, L., Albijanic, B., 2022. Influence of monovalent and divalent cations on monazite flotation. Colloids Surf. A: Physicochem. Eng. Asp. 653, 129975.

Jung, R.F., James, R.O., Healy, T.W., 1987. Adsorption, precipitation, and electrokinetic processes in the iron oxide (Goethite)—oleic acid—oleate system. J. Colloid Interface Sci. 118, 463–472.

Kanazawa, Y., Kamitani, M., 2006. Rare earth minerals and resources in the world. J. Alloy. Compd. 408, 1339–1343.

Kang, B., Tang, H., Zhao, Z., Song, S., 2020. Hofmeister Series: Insights of Ion Specificity from Amphiphilic Assembly and Interface Property. ACS Omega 5, 6229–6239.

Kirjavainen, V.M., 1992. Mathematical model for the entrainment of hydrophilic particles in froth flotation. Int. J. Miner. Process. 35, 1–11.

Klassen, V.I., Mokrousov, V.A., 1963. An introduction to the theory of flotation. Butterworths, London.

Klimpel, A.A., 1984. The effect of chemical reagents on the flotation recovery of minerals. Chemical Engineering 91.

Kou, J., Tao, D., Xu, G., 2010. Fatty acid collectors for phosphate flotation and their adsorption behavior using QCM-D. Int. J. Miner. Process. 95, 1–9.

Kurniawan, A.U., Ozdemir, O., Nguyen, A.V., Ofori, P., Firth, B., 2011. Flotation of coal particles in MgCl2, NaCl, and NaClO3 solutions in the absence and presence of Dowfroth 250. Int. J. Miner. Process. 98, 137–144.

Lascelles, D., Finch, J.A., Sui, C., 2003. Depressant Action of Ca and Mg on Flotation of Cu Activated Sphalerite. Can. Met. Q. 42, 133–140.

Laskowski, 1970. Role of capillary effects in bubble-particle collision in flotation. Transactions Institution of Mining and Metallurgy 79, C6–C10.

Laskowski, J., Castro, S., 2015. Flotation in concentrated electrolyte solutions. Int. J. Miner. Process. 144, 50–55.

Laskowski, J., Iskra, J., 1970. Role of capillary effects in bubble-particle collision in flotation. Transactions Institution of Mining and Metallurgy 79, C6–C10.

Laskowski, J.S., Castro, S., Ramos, O., 2013. Effect of seawater main components on frothability in the flotation of Cu-Mo sulfide ore. Physicochem. Probl. Miner. Process 50, 17–29.

Laskowski, J.S., Xu, Z., Yoon, R.-H., 1991. Energy barrier in particle−bubble attachment and its effect on flotation kinetics, in: Proc. 17th Int. Mineral Processing Congress. Dresden, pp. 237–249.

Lenormand, J., Salman, T., Yoon, R.H., 1979. Hydroxamate Flotation of Malachite. Can. Met. Q. 18, 125–129.

Lessard, R.R., Zieminski, S.A., 1971. Bubble Coalescence and Gas Transfer in Aqueous Electrolytic Solutions. Ind. Eng. Chem. Fundam. 10, 260–269.

Levay, G., Smart, R.St.C., Skinner, W.M., 2001. The impact of water quality on flotation performance. Journal of the Southern African Institute of Mining and Metallurgy 101, 69–75.

Li, B., Trueman, B.F., Rahman, M.S., Gao, Y., Park, Y., Gagnon, G.A., 2019. Understanding the impacts of sodium silicate on water quality and iron oxide particles. Environ. Sci.: Water Res. Technol. 5, 1360–1370.

Li, D., Yin, W., Xue, J., Yao, J., Fu, Y., Liu, Q., 2017. Solution chemistry of carbonate minerals and its effects on the flotation of hematite with sodium oleate. Int. J. Miner., Met., Mater. 24, 736–744.

Li, G., Deng, L., Cao, Y., Wang, B., Ran, J., Zhang, H., 2017. Effect of sodium chloride on fine coal flotation and discussion based on froth stability and particle coagulation. Int. J. Miner. Process. 169, 47–52.

Li, R., Marion, C., Espiritu, E.R.L., Multani, R., Sun, X., Waters, K.E., 2021. Investigating the use of an ionic liquid for rare earth mineral flotation. J. Rare Earths 39, 866–874.

Li, Yubiao, Lartey, C., Song, S., Li, Yingjie, Gerson, A.R., 2018. The fundamental roles of monovalent and divalent cations with sulfates on molybdenite flotation in the absence of flotation reagents. RSC Adv. 8, 23364–23371.

Liu, D., Peng, Y., 2014. Reducing the entrainment of clay minerals in flotation using tap and saline water. Powder Technol. 253, 216–222.

Liu, L., Rao, S.R., Finch, J.A., 1993. Technical note laboratory study of effect of recycle water on flotation of a Cu/Zn sulphide ore. Miner. Eng. 6, 1183–1190.

Liu, S., Chen, X., Lauten, R.A., Peng, Y., Liu, Q., 2018. Mitigating the negative effects of clay minerals on gold flotation by a lignosulfonate-based biopolymer. Miner. Eng. 126, 9–15.

Liu, W., Moran, C.J., Vink, S., 2013. A review of the effect of water quality on flotation. Miner. Eng. 53, 91–100.

Liu, W., Wang, X., Miller, J.D., 2019. Collector Chemistry for Bastnaesite Flotation – Recent Developments. Miner. Process. Extr. Met. Rev. 40, 370–379.

Liu, W., Zhang, S., Wang, W., Zhang, J., Yan, W., Deng, J., Feng, Q., Huang, Y., 2015. The effects of Ca(II) and Mg(II) ions on the flotation of spodumene using NaOL. Miner. Eng. 79, 40–46.

Long, K.R., Gosen, B.S.V., Foley, N.K., Cordier, D., 2012. Non-Renewable Resource Issues, Geoscientific and Societal Challenges. pp. 131–155.

Luukkanen, S., Tanhua, A., Zhang, Z., Canales, R.M., Auranen, I., 2022. Towards waterless operations from mine to mill. Miner. Eng. 187, 107793.

Ma, M., McCall, W.J.B., David, 2012. Role of Water Structure-Making/Breaking Ions in the Cationic Flotation of Kaolinite: Implications for Iron Ore Processing. Int. J. Min. Eng. Miner. Process. 1, 17–20.

Magee, R.J., Hill, J.O., 1985. The Analytical Chemistry of Metal Dithiocarbamate Complexes. Rev. Anal. Chem. 8, 5–72.

Manono, M., Corin, K., Wiese, J., 2019. The Effect of the Ionic Strength of Process Water on the Interaction of Talc and CMC: Implications of Recirculated Water on Floatable Gangue Depression. Minerals 9, 231.

Marangoni, C., 1871. Ueber die Ausbreitung der Tropfen einer Flüssigkeit auf der Oberfläche einer anderen. Ann. Phys. 219, 337–354.

Marcus, Y., 2009. Effect of Ions on the Structure of Water: Structure Making and Breaking. Chem. Rev. 109, 1346–1370.

Mariano, A.N., Mariano, A., 2012. Rare Earth Mining and Exploration in North America. Elements 8, 369–376.

Marinakis, K.I., Shergold, H.L., 1985. Influence of sodium silicate addition on the adsorption of oleic acid by fluorite, calcite and barite. Int. J. Miner. Process. 14, 177–193.

Marion, C., Jordens, A., Li, R., Rudolph, M., Waters, K.E., 2017. An evaluation of hydroxamate collectors for malachite flotation. Sep. Purif. Technol. 183, 258–269.

Marion, C., Li, R., Waters, K.E., 2020. A review of reagents applied to rare-earth mineral flotation. Adv. Colloid Interface Sci. 279, 102142.

Marrucci, G., Nicodemo, L., 1967. Coalescence of gas bubbles in aqueous solutions of inorganic electrolytes. Chem. Eng. Sci. 22, 1257–1265.

Mesa, D., Brito-Parada, P.R., 2019. Scale-up in froth flotation: A state-of-the-art review. Sep. Purif. Technol. 210, 950–962.

Mewis, J., Wagner, N.J., 2012. Colloidal Suspension Rheology. Cambridge University Press, New York, NY, USA.

Mielczarski, E., Donato, Ph. de, Mielczarski, J.A., Cases, J.M., Barres, O., Bouquet, E., 2000. Solution Chemistry in Adsorption Layer Formation of Oleate on Fluorite. J. Colloid Interface Sci. 226, 269–276.

Moon, K.S., Fuerstenau, D.W., 2003. Surface crystal chemistry in selective flotation of spodumene (LiAl[SiO3]2) from other aluminosilicates. Int. J. Miner. Process. 72, 11–24.

Morales, J.E., 1975. Flotation of the Andacollo's ore in pilot plant by using seawater. Minerals 30, 16–22.

Moudgil, B.M., 1993. Correlation between froth viscosity and flotation efficiency. Min., Met. Explor. 10, 100–101.

Moudgil, B.M., Chanchani, R., 1985. Flotation of Apatite and Dolomite Using Sodium Oleate as the Collector. Min., Met. Explor. 2, 13–19.

Mueller, S., Llewellin, E.W., Mader, H.M., 2010. The rheology of suspensions of solid particles. Proc. R. Soc. A: Math., Phys. Eng. Sci. 466, 1201–1228.

Muzinda, I., Schreithofer, N., 2018. Water quality effects on flotation: Impacts and control of residual xanthates. Miner. Eng. 125, 34–41.

Nativ, P., Leifman, O., Lahav, O., Epsztein, R., 2021. Desalinated brackish water with improved mineral composition using monovalent-selective nanofiltration followed by reverse osmosis. Desalination 520, 115364.

Nied, D., Enemark-Rasmussen, K., L'Hopital, E., Skibsted, J., Lothenbach, B., 2016. Properties of magnesium silicate hydrates (M-S-H). Cem. Concr. Res. 79, 323–332.

Niriella, D., Carnahan, R.P., 2006. Comparison Study of Zeta Potential Values of Bentonite in Salt Solutions. J. Dispers. Sci. Technol. 27, 123–131.

Nowosielska, A.M., Nikoloski, A.N., Parsons, D.F., 2023. The effects of saline water on the recovery of lead and zinc sulfide during froth flotation. Miner. Eng. 202, 108236.

Nuri, O.S., Mehdilo, A., Irannajad, M., 2014. Influence of microwave irradiation on ilmenite surface properties. Appl. Surf. Sci. 311, 27–32.

Oldroyd, J.G., 1955. The effect of interfacial stabilizing films on the elastic and viscous properties of emulsions. Proc. R. Soc. Lond. Ser. A Math. Phys. Sci. 232, 567–577.

Ong, B.C., Leong, Y.K., Chen, S.B., 2008. Yield stress-zeta potential relationship of oxide dispersions with adsorbed polyacrylate — Steric effect and zeta potential at the flocculated-dispersed transition state. Powder Technol. 186, 176–183.

Oolman, T.O., Blanch, H.W., 1986. Bubble coalescence in stagnant liquids. Chem. Eng. Commun. 43, 237–261.

Otsuki, A., Dodbiba, G., Fujita, T., 2007. Two-Liquid Flotation: Heterocoagulation of Fine Particles in Polar Organic Solvent. Mater. Trans. 48, 1095–1104.

Özcan, Ö., Çelik, M.S., Nickolov, Z.S., Miller, J.D., 2003. Effect of thermal stability on the flotation response of sodium carbonate salts. Miner. Eng. 16, 353–358.

Ozdemir, O., Çelik, M.S., Nickolov, Z.S., Miller, J.D., 2007. Water structure and its influence on the flotation of carbonate and bicarbonate salts. J. Colloid Interface Sci. 314, 545–551.

Ozdemir, O., Taran, E., Hampton, M.A., Karakashev, S.I., Nguyen, A.V., 2009. Surface chemistry aspects of coal flotation in bore water. Int. J. Miner. Process. 92, 177–183.

Parfitt, C.D., Rochester, G.D., 1983. Adsorption from Solution at the Solid/Liquid Interface. Academic Press, New York.

Partridge, A.C., Smith, G.W., 1971. Flotation and adsorption characteristics of the hematite-dodecylamine-starch system. Can. Met. Q. 10, 229–234.

Patra, P., Bhambhani, T., Nagaraj, D.R., Somasundaran, P., 2012. Impact of pulp rheological behavior on selective separation of Ni minerals from fibrous serpentine ores. Colloids Surf. A: Physicochem. Eng. Asp. 411, 24–26.

Pavez, O., Brandao, P.R.G., Peres, A.E.C., 1996. Adsorption of oleate and octyl-hydroxamate on to rare-earths minerals. Miner. Eng. 9, 357–366.

Pavez, O., Peres, A.E.C., 1993. Effect of sodium metasilicate and sodium sulphide on the floatability of monazite-zircon-rutile with oleate and hydroxamates. Miner. Eng. 6, 69–78.

Peng, Y., Bradshaw, D., 2012. Mechanisms for the improved flotation of ultrafine pentlandite and its separation from lizardite in saline water. Miner. Eng. 36, 284–290.

Peng, Y., Li, Y., Li, W., Fang, X., Liu, C., Fan, R., 2020. Elimination of adverse effects of seawater on molybdenite flotation using sodium silicate. Miner. Eng. 146, 106108.

Peng, Y., Seaman, D., 2011. The flotation of slime–fine fractions of Mt. Keith pentlandite ore in de-ionised and saline water. Miner. Eng. 24, 479–481.

Peppersack, C., Wermbter, K., Kwade, A., Garnweitner, G., Breitung-Faes, S., 2022. Top-Down Formulation of Goethite Nanosuspensions for the Production of Transparent, Inorganic Glass Coatings. Coatings 12, 330.

Philippe, R., Dixon, R., Pozzo, S.D., 2010. Sal or desal: sea water supply options for the mining industry, in: II International Congress on Water Management in the Mining Industry.

Plateau, J., 1873. Statique expérimentale et théorique des liquides soumis aux seules forces moléculaires. Gauthier-Villars, Paris.

Poling, G.W., Leja, J., 1963. Infrared study of xanthate adsorption on vacuum deposited films of lead sulfide and metallic copper under conditions of controlled oxidation. J. Phys. Chem 67, 2121.

Potapova, E., Grahn, M., Holmgren, A., Hedlund, J., 2010. The effect of calcium ions and sodium silicate on the adsorption of a model anionic flotation collector on magnetite studied by ATR-FTIR spectroscopy. J. Colloid Interface Sci. 345, 96–102.

Pradip, 1981. The surface properties and flotation of rare−earth minerals, phd thesis. University of California.

Pradip, Fuerstenau, D.W., 2013. Design and development of novel flotation reagents for the beneficiation of Mountain Pass rare-earth ore. Min., Met. Explor. 30, 1–9.

Pradip, Fuerstenau, D.W., 1991. The role of inorganic and organic reagents in the flotation separation of rare-earth ores. Int. J. Miner. Process. 32, 1–22.

Predali, J.J., 1969. Flotation of carbonates with salts of fatty acids; role of pH and the alkyl chain. Trans IMM 78, C140–C147.

Prosser, I., Wolf, L., Littleboy, A., 2011. Water in mining and industry. Water: Science and Solutions for Australia 135–146.

Qi, G.W., Klauber, C., Warren, L.J., 1993. Mechanism of action of sodium silicate in the flotation of apatite from hematite. Int. J. Miner. Process. 39, 251–273.

Quinn, J.J., Kracht, W., Gomez, C.O., Gagnon, C., Finch, J.A., 2007. Comparing the effect of salts and frother (MIBC) on gas dispersion and froth properties. Miner. Eng. 20, 1296–1302.

Ralston, J., Fornasiero, D., Grano, S., Duan, J., Akroyd, T., 2007. Reducing uncertainty in mineral flotation—flotation rate constant prediction for particles in an operating plant ore. Int. J. Miner. Process. 84, 89–98.

Ramos, O., Castro, S., Laskowski, J.S., 2013. Copper–molybdenum ores flotation in sea water: Floatability and frothability. Miner. Eng. 53, 108–112.

Rao, K.H., Antti, B.-M., Forssberg, E., 1989. Flotation of phosphatic material containing carbonatic gangue using sodium oleate as collector and sodium silicate as modifier. Int. J. Miner. Process. 26, 123–140.

Rao, S.R., 2013. Surface Chemistry of Froth Flotation, Volume 1: Fundamentals. Springer Science & Business Media.

Rao, S.R., Finch, J.A., 1989. A review of water re-use in flotation. Miner. Eng. 2, 65–85.

Rath, S.S., Sinha, N., Sahoo, H., Das, B., Mishra, B.K., 2014. Molecular modeling studies of oleate adsorption on iron oxides. Appl. Surf. Sci. 295, 115–122.

Rattanakawin, C., Hogg, R., 2001. Aggregate size distributions in flocculation. Colloids Surf. A: Physicochem. Eng. Asp. 177, 87–98.

Ren, L., Qiu, H., Zhang, Y., Nguyen, A.V., Zhang, M., Wei, P., Long, Q., 2018. Effects of alkyl ether amine and calcium ions on fine quartz flotation and its guidance for upgrading vanadium from stone coal. Powder Technol. 338, 180–189.

Rey, M., Raffinot, P., 1966. FLOTATION OF ORES IN SEA WATER--HIGH FROTHING., SOLUBLE XANTHATE COLLECTING. World Mining 19, 18–21.

Roonasi, P., Holmgren, A., 2010. An ATR–FTIR study of carbonate sorption onto magnetite. Surf. Interface Anal. 42, 1118–1121.

Roonasi, P., Yang, X., Holmgren, A., 2010. Competition between sodium oleate and sodium silicate for a silicate/oleate modified magnetite surface studied by in situ ATR-FTIR spectroscopy. J. Colloid Interface Sci. 343, 546–552.

Sajjad, M., Otsuki, A., 2022. Coupling Flotation Rate Constant and Viscosity Models. Metals 12, 409.

Salgin, S., Salgin, U., Soyer, N., 2013. Streaming Potential Measurements of Polyethersulfone Ultrafiltration Membranes to Determine Salt Effects on Membrane Zeta Potential. Int. J. Electrochem. Sci. 8, 4073–4084.

Schulz, 1970. Separation Efficiency, Society of Mining Engineer. In AMIE 247, 81–87.

Schwarz, S., Grano, S., 2005. Effect of particle hydrophobicity on particle and water transport across a flotation froth. Colloids Surf. A: Physicochem. Eng. Asp. 256, 157–164.

Senior, G.D., Thomas, S.A., 2005. Development and implementation of a new flowsheet for the flotation of a low grade nickel ore. Int. J. Miner. Process. 78, 49–61.

Shabalala, N.Z.P., Harris, M., Filho, L.S.L., Deglon, D.A., 2011. Effect of slurry rheology on gas dispersion in a pilot-scale mechanical flotation cell. Miner. Eng. 24, 1448–1453.

Shen, Z., 2021. Principles and Technologies of Flotation Machines. Springer Singapore, Singapore.

Shi, Q., Feng, Q., Zhang, G., Deng, H., 2012. Electrokinetic properties of smithsonite and its floatability with anionic collector. Colloids Surf. A: Physicochem. Eng. Asp. 410, 178–183.

Shimazaki, H., Yang, Z., Miyawaki, R., Shigeoka, M., 2008. Scandium-Bearing Minerals in the Bayan Obo Nb-REE-Fe Deposit, Inner Mongolia, China. Resour. Geol. 58, 80–86.

Sjoeberg, S., Oehman, L.O., 1986. ChemInform Abstract: Equilibrium and Structural Studies of Silicon(IV) and Aluminium(III) in Aqueous Solution. Part 13. A Potentiometric and 27Al NMR Study of Speciation and Equilibria in the Aluminium(III)-Oxalic Acid-Hydroxide System. Chem. Informationsdienst 17, no-no.

Smith, P.G., Warren, L.J., 1989. Entrainment of Particles into Flotation Froths. Miner. Process. Extr. Met. Rev. 5, 123–145.

Snow, R., Zhang, J. “Patrick”, Miller, J.D., 2004. Froth modification for reduced fuel oil usage in phosphate flotation. Int. J. Miner. Process. 74, 91–99.

Somasundaran, P., Wang, D., 2006. Solution Chemistry: Minerals and Reagents. Elsevier.

Somasundaran, P., Xiao, L., Wang, D., 1991. Solution chemistry of flotation of sparingly soluble minerals. Min., Met. Explor. 8, 115–121.

Sørensen, Lundgaard, and T., 1966. Selective flotation of steenstrupine and monazite from Kvanefjeld Lujavrite (No. 133). Danish Atomic Energy Commission, Research Establishment Risö.

Stark, T., Silin, I., Wotruba, H., 2017. Mineral Processing of Eudialyte Ore from Norra Kärr. J. Sustain. Met. 3, 32–38.

Stern, O., 1924. Theory of the electrical double layer. Electrochemistry 30, 508–516.

Stubenrauch, C., Klitzing, R. von, 2003. Disjoining pressure in thin liquid foam and emulsion films—new concepts and perspectives. J. Phys.: Condens. Matter 15, R1197.

Stumm, Morgan, J.J., 2012. Aquatic Chemistry: Chemical Equilibria and Rates in Natural Waters, 3rd Edition. ed. John Wiley & Sons, New York.

Subrahmanyam, T.V., Forssberg, E., 1988. Froth characteristics and grade-recovery relationships in the flotation of lead-zinc and copper ores. Miner. Eng. 1, 41–52.

Sun, J., Zhu, X., Chen, Y., Fang, N., 2013. Iron isotopic constraints on the genesis of Bayan Obo ore deposit, Inner Mongolia, China. Precambrian Res. 235, 88–106.

U.S. Geological Survey, 2023. Mineral commodity summaries 2023. U. S. Geological Survey.

U.S. Geological Survey, 2022. Mineral commodity summaries 2022. U. S. Geological Survey.

U.S. Geological Survey, 2021. Mineral commodity summaries 2021. U. S. Geological Survey.

U.S. Geological Survey, 2020. Mineral commodity summaries 2020. U. S. Geological Survey.

U.S. Geological Survey, 2019. Mineral commodity summaries 2019. U.S. Geological Survey.

Swedlund, P.J., Webster, J.G., 1999. Adsorption and polymerisation of silicic acid on ferrihydrite, and its effect on arsenic adsorption. Water Res. 33, 3413–3422.

Tadros, T.F., 2011. Rheology of dispersions: principles and applications. John Wiley & Sons.

Taggart, A.F., Hassialis, M.D., 1946. Solubility product and bubble attachment in flotation. Transactions of the American Institute of Mining and Metallurgical Engineers 169, 259–265.

Tang, M., Wen, S., 2019. Effects of Cations/Anions in Recycled Tailing Water on Cationic Reverse Flotation of Iron Oxides. Minerals 9, 161.

Triffett, B.B., Cilliers, J.J., 2004. Measuring froth stability. International Patent Application Number: PCT/AU2004/000331.

Trifonov, D.N., 1963. The Rare-Earth Elements. A Pergamon Press Book.

Uwadiale, G.G.O.O., 1992. Flotation of Iron Oxides and Quartz—A Review. Miner. Process. Extr. Met. Rev. 11, 129–161.

Verrelli, D.I., Albijanic, B., 2015. A comparison of methods for measuring the induction time for bubble–particle attachment. Miner. Eng. 80, 8–13.

Vlachy, N., Jagoda-Cwiklik, B., Vácha, R., Touraud, D., Jungwirth, P., Kunz, W., 2009. Hofmeister series and specific interactions of charged headgroups with aqueous ions. Adv. Colloid Interface Sci. 146, 42–47.

Voncken, J.H.L., 2015. The Rare Earth Elements, An Introduction. SpringerBriefs Earth Sci. 53–72.

Wang, B., Peng, Y., 2013. The behaviour of mineral matter in fine coal flotation using saline water. Fuel 109, 309–315.

Wang, D., 2016. Flotation Reagents: Applied Surface Chemistry on Minerals Flotation and Energy Resources Beneficiation 115–123.

Wang, L., Li, C., 2020. A Brief Review of Pulp and Froth Rheology in Mineral Flotation. J. Chem. 2020, 1–16.

Wang, L., Peng, Y., Runge, K., Bradshaw, D., 2015. A review of entrainment: Mechanisms, contributing factors and modelling in flotation. Miner. Eng. 70, 77–91.

Wang, Y., Peng, Y., Nicholson, T., Lauten, R.A., 2015. The different effects of bentonite and kaolin on copper flotation. Appl. Clay Sci. 114, 48–52.

Wang, Y., Yu, F., 2007. Effects of metallic ions on the flotation of spodumene and beryl. J. China Univ. Min. Technol. 17, 35–39.

Wang, Z., Wang, L., Zheng, Y., Xiao, J., 2019. Role of calcium dioleate in the flotation of powellite particles using oleate. Miner. Eng. 138, 95–100.

Wang, Z., Wu, H., Xu, Y., Shu, K., Fang, S., Xu, L., 2020a. The effect of dissolved calcite species on the flotation of bastnaesite using sodium oleate. Miner. Eng. 145, 106095.

Wang, Z., Wu, H., Xu, Y., Shu, K., Yang, J., Luo, L., Xu, L., 2020b. Effect of dissolved fluorite and barite species on the flotation and adsorption behavior of bastnaesite. Sep. Purif. Technol. 237, 116387.

Wilhelm, E., Battino, R., Wilcock, R.J., 1977. Low-pressure solubility of gases in liquid water. Chem. Rev. 77, 219–262.

Wills, B.A., 1988. Mineral Processing Technology (Fourth Edition) 377–419.

Xu, L., Hu, Y., Tian, J., Wu, H., Yang, Y., Zeng, X., Wang, Z., Wang, J., 2016. Selective flotation separation of spodumene from feldspar using new mixed anionic/cationic collectors. Miner. Eng. 89, 84–92.

Xu, Z., Liu, J., Choung, J.W., Zhou, Z., 2003. Electrokinetic study of clay interactions with coal in flotation. Int. J. Miner. Process. 68, 183–196.

Yaminsky, V.V., Ohnishi, S., Vogler, E.A., Horn, R.G., 2010. Stability of Aqueous Films between Bubbles. Part 1. The Effect of Speed on Bubble Coalescence in Purified Water and Simple Electrolyte Solutions. Langmuir 26, 8061–8074.

Yang, X., Roonasi, P., Holmgren, A., 2008. A study of sodium silicate in aqueous solution and sorbed by synthetic magnetite using in situ ATR-FTIR spectroscopy. J. Colloid Interface Sci. 328, 41–47.

Yang, X.J., Lin, A., Li, X.-L., Wu, Y., Zhou, W., Chen, Z., 2013. China's ion-adsorption rare earth resources, mining consequences and preservation. Environ. Dev. 8, 131–136.

Yenial, Ü., Bulut, G., Sirkeci, A.A., 2014. Arsenic Removal by Adsorptive Flotation Methods. CLEAN Soil, Air, Water 42, 1567–1572.

Yianatos, J.B., Bergh, L.G., Cortés, G.A., 1998. Froth zone modelling of an industrial flotation column. Miner. Eng. 11, 423–435.

Yianatos, J.B., Espinosa-Gomez, R., Finch, J.A., Laplante, A.B., Dobby, G.S., 1988. Effect of column height on flotation column performance. Miner. Met. Process. 5, 11–14.

Yoon, R.H., Luttrell, G.H., 1989. The Effect of Bubble Size on Fine Particle Flotation. Miner. Process. Extr. Met. Rev. 5, 101–122.

Yoon, R.-H., Yordan, J.L., 1991. Induction time measurements for the quartz—amine flotation system. J. Colloid Interface Sci. 141, 374–383.

Yu, F., Wang, Y., Zhang, L., Zhu, G., 2015. Role of oleic acid ionic−molecular complexes in the flotation of spodumene. Miner. Eng. 71, 7–12.

Yuehua, H., Chi, R., Xu, Z., 2003. Solution Chemistry Study of Salt-type Mineral Flotation Systems: Role of Inorganic Dispersants. Ind. Eng. Chem. Res. 42, 1641–1647.

Zhan, Y.-X., Li, X.-C., Wu, B., Yang, K.-F., Fan, H.-R., Li, X.-H., 2023. The occurrence and genesis of HREE-rich minerals from the giant Bayan Obo deposit, China. Ore Geol. Rev. 157, 105438.

Zhang, J.S., Stanforth, R.S., Pehkonen, S.O., 2007. Effect of replacing a hydroxyl group with a methyl group on arsenic (V) species adsorption on goethite (α-FeOOH). J. Colloid Interface Sci. 306, 16–21.

Zhang, W., Honaker, R.Q., 2018. Flotation of monazite in the presence of calcite part II: Enhanced separation performance using sodium silicate and EDTA. Miner. Eng. 127, 318–328.

Zhang, W., Honaker, R.Q., Groppo, J.G., 2017. Flotation of monazite in the presence of calcite part I: Calcium ion effects on the adsorption of hydroxamic acid. Miner. Eng. 100, 40–48.

Zhao, S., Peng, Y., 2014. Effect of electrolytes on the flotation of copper minerals in the presence of clay minerals. Miner. Eng. 66, 152–156.

Zhao, Y., Sun, X., Meng, D., Liu, X., Zhong, Q., Feng, Z., 2023. Effect of phase transition during roasting of Mountain Pass rare earth concentrate on leaching efficiency of rare earths. J. Rare Earths.

Zhao, Y., Xing, W., Xu, N., Wong, F.-S., 2005. Effects of inorganic electrolytes on zeta potentials of ceramic microfiltration membranes. Sep. Purif. Technol. 42, 117–121.

Appendix: Copyright Agreement to Use Copyright Materials

Appendix 1.

This is a License Agreement between Moonchul Jung / Curtin University ("User") and Copyright Clearance Center, Inc. ("CCC") on behalf of the Rightsholder identified in the order details below. The license consists of the order details, the Marketplace Permissions General Terms and Conditions below, and any Rightsholder Terms and Conditions which are included below.

Order Date: 09-Feb-2024

Order License ID: 1448763-1

ISSN: 0927-7757

Type of Use: Republish in a thesis/dissertation

Publisher: ELSEVIER BV

Portion: Chapter/article

LICENSED CONTENT

Publication Title: Colloids and surfaces. A, Physicochemical and engineering aspects

Article Title: Influence of monovalent and divalent cations on monazite flotation

Date: 01/01/1993

Language: English

Country: Netherlands

Rightsholder: Elsevier Science & Technology Journals

Publication Type: Journal

Start Page: 129975

Volume: 653

REQUEST DETAILS

Portion Type: Chapter/article

Page Range(s): 1-9

Total Number of Pages: 9

Format (select all that apply): Print, Electronic

Who Will Republish the Content?: Academic institution

Duration of Use: Life of current edition

Lifetime Unit Quantity: Up to 9,999

Rights Requested: Main product

Distribution: Worldwide

Translation: Original language of publication

Copies for the Disabled?: No

Minor Editing Privileges?: No

Incidental Promotional Use?: No

NEW WORK DETAILS

Title: The Effects of Water Quality on Rare Earth Phosphate Mineral Flotation

Instructor Name: Moonchul Jung

Institution Name: Curtin University

Expected Presentation Date: 2024-03-09

ADDITIONAL DETAILS

Order Reference Number: N/A

The Requesting Person / Organization to Appear on the License: Moonchul Jung / Curtin University

REQUESTED CONTENT DETAILS

Title, Description or Numeric Reference of the Portion(s): Influence of monovalent and divalent cations on monazite flotation

Editor of Portion(s): Jung, Moonchul; Tadesse, Bogale; Dick, Craig; Logan, Alex; Dyer, Laurence; Albijanic, Boris

Volume / Edition: 653

Page or Page Range of Portion: 129975

Title of the Article / Chapter the Portion Is From: Influence of monovalent and divalent cations on monazite flotation

Author of Portion(s): Jung, Moonchul; Tadesse, Bogale; Dick, Craig; Logan, Alex; Dyer, Laurence; Albijanic, Boris

Issue, if Republishing an Article From a Serial: N/A

Publication Date of Portion: 2022-11-20

Appendix 2.

This is a License Agreement between Moonchul Jung (“User”) and Copyright Clearance Center, Inc. (“CCC”) on behalf of the Rightsholder identified in the order details below. The license consists of the order details, the Marketplace Permissions General Terms and Conditions below, and any Rightsholder Terms and Conditions which are included below.

Order Date: 09-Feb-2024

Order License ID: 1448765-1

ISSN: 0892-6875

Type of Use: Republish in a thesis/dissertation

Publisher: PERGAMON

Portion: Chapter/article

LICENSED CONTENT

Publication Title: Minerals engineering

Article Title: Understanding the role of water quality in separation of rare earth minerals from iron oxide minerals in a flotation circuit

Date: 01/01/1988

Language: English

Country: United Kingdom of Great Britain and Northern Ireland

Rightsholde: rElsevier Science & Technology Journals

Publication Type: Journal

Start Page: 108461

Volume: 205

REQUEST DETAILS

Portion Type: Chapter/article

Page Range(s): 1-12

Total Number of Pages: 12

Format (select all that apply) : Print, Electronic

Who Will Republish the Content? : Academic institution

Duration of Use: Life of current edition

Lifetime Unit Quantity: Up to 9,999

Rights Requested: Main product

Distribution: Worldwide

Translation: Original language of publication

Copies for the Disabled?: No

Minor Editing Privileges?: No

Incidental Promotional Use?: No

NEW WORK DETAILS

Title: The Effects of Water Quality on Rare Earth Phosphate Mineral Flotation

Instructor Name: Moonchul Jung

Institution Name: Curtin University

Expected Presentation Date: 2024-03-09

ADDITIONAL DETAILS

Order Reference Number: N/A

The Requesting Person / Organization to Appear on the License: Moonchul Jung

REQUESTED CONTENT DETAILS

Title, Description or Numeric Reference of the Portion(s) : Chapter 5. Influence of cations on the rare earth phosphate mineral flotation

Editor of Portion(s) : Jung, Moonchul; Tadesse, Bogale; Dick, Craig; Logan, Alex; Dyer, Laurence; Albijanic, Boris

Volume / Edition: 205

Page or Page Range of Portion: 108461

Title of the Article / Chapter the Portion Is From: Understanding the role of water quality in separation of rare earth minerals from iron oxide minerals in a flotation circuit

Author of Portion(s): Jung, Moonchul; Tadesse, Bogale; Dick, Craig; Logan, Alex; Dyer, Laurence; Albijanic, Boris

Issue, if Republishing an Article From a Serial: N/A

Publication Date of Portion: 2024-01-01

Appendix 3.

This is a License Agreement between Moonchul Jung (“User”) and Copyright Clearance Center, Inc. (“CCC”) on behalf of the Rightsholder identified in the order details below. The license consists of the order details, the Marketplace Permissions General Terms and Conditions below, and any Rightsholder Terms and Conditions which are included below.

Order Date: 09-Feb-2024

Order License ID: 1448821-1

ISSN: 1002-0721

Type of Use: Republish in a thesis/dissertation

Publisher: INTERNATIONAL ACADEMIC PUBLISHERS,

Portion: Chapter/article

LICENSED CONTENT

Publication Title: JOURNAL OF RARE EARTHS

Article Title: Rheological properties of rare earth minerals flotation pulp in the presence of anions

Author/Editor: CHUNG-KUO HSI TU HSUEH HUI.

Date: 01/01/1991

Language: English

Country: China

Rightsholder: Elsevier Science & Technology Journals

Publication Type: Journal

REQUEST DETAILS

Portion Type: Chapter/article

Page Range(s): 3-36

Total Number of Pages: 37

Format (select all that apply): Print, Electronic

Who Will Republish the Content?: Academic institution

Duration of Use: Life of current edition

Lifetime Unit Quantity: Up to 9,999

Rights Requested: Main product

Distribution: Worldwide

Translation: Original language of publication

Copies for the Disabled?: No

Minor Editing Privileges?: No

Incidental Promotional Use?: No

NEW WORK DETAILS

Title: The Effects of Water Quality on Rare Earth Phosphate Mineral Flotation

Instructor Name: Moonchul Jung

Institution Name: Curtin University

Expected Presentation Date: 2024-03-09

ADDITIONAL DETAILS

Order Reference Number: N/A

The Requesting Person / Organization to Appear on the License: Moonchul Jung

REQUESTED CONTENT DETAILS

Title, Description or Numeric Reference of the Portion(s): Chapter 6. Influence of anions on the rare earth phosphate mineral flotation

Editor of Portion(s): Jung, Moonchul; Tadesse, Bogale; Dick, Craig; Logan, Alex; Dyer, Laurence; Albijanic, Boris

Volume / Edition: N/A

Page or Page Range of Portion: 3-36

Title of the Article / Chapter the Portion Is From: Rheological properties of rare earth minerals flotation pulp in the presence of anions

Author of Portion(s): Jung, Moonchul; Tadesse, Bogale; Dick, Craig; Logan, Alex; Dyer, Laurence; Albijanic, Boris

Issue, if Republishing an Article From a Serial: N/A

Publication Date of Portion: 2023-10-11